KfK 4433
FPA-88-2
September 1988

Possibilities for Breakeven and Ignition of D-^{3}He Fusion Fuel in a Near Term Tokamak

Final Report

G. A. Emmert, L. El-Guebaly, R. Klingelhöfer,
G. L. Kulcinski, J. F. Santarius, J. E. Scharer,
I. N. Sviatoslavsky, P. L. Walstrom, J. L. Wittenberg
Projekt Kernfusion
Fusion Power Associates

Kernforschungszentrum Karlsruhe

KERNFORSCHUNGSZENTRUM KARLSRUHE

Projekt Kernfusion

FUSION POWER ASSOCIATES

KfK 4433

FPA-88-2

POSSIBILITIES FOR BREAKEVEN AND IGNITION OF D-^{3}He FUSION FUEL IN A NEAR TERM TOKAMAK

FINAL REPORT

by

G.A. Emmert*, L. El-Guebaly*, R. Klingelhöfer**,
G.L. Kulcinski*, J.F. Santarius*, J.E. Scharer*,
I.N. Sviatoslavsky*, P.L. Walstrom*, J.L. Wittenberg

* University of Madison, Wisconsin, USA
** Institut für Kernverfahrenstechnik

Kernforschungszentrum Karlsruhe GmbH, Karlsruhe

Kernforschungszentrum Karlsruhe GmbH
Postfach 3640, 7500 Karlsruhe 1

ISSN 0303-4003

Über die Möglichkeiten in einem Tokamak der nächsten Generation mit einem D-^{3}He-Gemisch "breakeven"- und Zündbedingungen herzustellen

ZUSAMMENFASSUNG

Nachdem kürzlich bekannt wurde, daß auf dem Mond relativ große Mengen des Isotops ^{3}He lagern, entstand erneutes Interesse am d-^{3}He-Prozeß. In der vorliegenden Studie wird geprüft, ob sich ein d-^{3}He-Plasma in einem Tokamak der NET/INTOR-Klasse unter Reaktorbedingungen untersuchen läßt. Es stellt sich heraus, daß sich, je nachdem, welche Skalierungsregel man für die Energieeinschlußzeit zugrunde legt, "breakeven"-Bedingungen herstellen lassen, ohne signifikante Änderungen am NET-Entwurf vorzunehmen. Die besten Resultate erhält man, wenn man von der optimistischen "H-mode"-Skalierung ausgeht. Mit der pessimistischeren Kaye-Goldston-Skalierung für die Energieeinschlußzeit, versehen mit einem Faktor > 1, der den H-mode-Betrieb berücksichtigt, ist es schwieriger, breakeven-Bedingungen zu erreichen.

Die reduzierte Neutronenproduktion beim d-^{3}He-Prozeß, verglichen mit d-t, gestattet es, den Q-Wert (Q = Fusionsleistung/injizierte Leistung) deutlich zu erhöhen und damit den Spielraum zu vergrößern, in dem die Zündung herbeigeführt werden kann. Zunächst kann man auf den Brutmantel für das Tritium verzichten und die Abschirmung der Spulen gegen die Neutronen verkleinern auf eine für das gegenüber dem d-t-Betrieb veränderte Neutronenspektrum optimierte Stärke. Auf diese Weise kann man den großen Radius R des Plasmas verkleinern und damit das Plasma auf der Innenseite näher an die Spulen zur Erzeugung des toroidalen Magnetfelds heranrücken. Dabei wird das Aspektverhältnis R/a (a = kleiner Plasmaradius) des Plasmas verkleinert und die magnetische Flußdichte am Ort des Plasmas erhöht, ohne die Flußdichte am Ort der Spulen zu ändern. Durch diese Maßnahme läßt sich der Wert von β ~ thermische Energiedichte des Plasmas/Energiedichte des Magnetfeldes vergrößern und der Q-Wert wächst ungefähr auf drei.

In dem Bericht werden die Auswirkungen, die sich durch den d-^{3}He-Betrieb für die Verluste schneller Ionen, die Neutronenabschirmung, die Wärmebelastung der ersten Wand und des Divertors, für die Plasmanachfüllung, die Änderungen des poloidalen Spulensystems und für das Abpumpen des Heliums aus dem Vakuumbehälter ergeben, berücksichtigt.

Possibilities for Breakeven and Ignition of D-^{3}He Fusion Fuel in a Near Term Tokamak

ABSTRACT

The recent realization that the moon contains a large amount of the isotope ^{3}He has rekindled interest in the D-^{3}He fuel cycle. In this study we consider the feasibility of investigating D-^{3}He reactor plasma conditions in a tokamak of the NET/INTOR class. We have found that, depending on the energy confinement scaling law, energy breakeven may be achieved without significant modification to the NET design. The best results are for the more optimistic ASDEX H-mode scaling law. Kaye-Goldston scaling with a modest improvement due to the H-mode is more pessimistic and makes achieving breakeven more difficult. Significant improvement in Q (ratio of the fusion power to the injected power), or the ignition margin, can be achieved by taking advantage of the much reduced neutron production of the D-^{3}He fuel cycle. Removal of the tritium producing blanket and replacing the inboard neutron shield by a thinner shield optimized for the neutron spectrum in D-^{3}He allows the plasma to be increased without changing the magnetic field at the toroidal field magnet. This allows the plasma to achieve higher beta and Q values up to about 3. The implications of D-^{3}He operation for fast ion loss, neutron shielding, heat loads on the first wall and divertor, plasma refuelling, changes to the poloidal field coil system, and pumping of the helium from the vacuum chamber are considered in the report.

TABLE OF CONTENTS

TABLE OF CONTENTS
(continued)

Überblick zu der d-^{3}He-Studie

1. Gründe für die Untersuchung der d-^{3}He-Reaktion

Fig. 3.1-1. auf S. 3-2 zeigt die Temperaturabhängigkeit des Reaktionskoeffizienten $<\sigma \cdot v>$ (die Reaktionsrate ist proportional zu $<\sigma v>$, σ = Wirkungsquerschnitt für den jeweiligen Fusionsprozeß, v = Relativgeschwindigkeit der Reaktionspartner; die Klammern bedeuten, daß $\sigma \cdot v$ über alle im Plasma vorkommenden Relativgeschwindigkeiten, gewichtet mit der Maxwell'schen Verteilung gemittelt wurde). Man entnimmt dem Diagramm, daß der Steilanstieg der Reaktionsrate, die mit zunehmender Temperatur infolge steigender Überwindbarkeit der Coulombabstoßung der Reaktionspartner zunächst wächst, bei der d-t-Reaktion in dem mit Abstand niedrigsten Temperaturbereich durchlaufen wird. Die mittlere Temperatur in einem gezündeten d-t-Plasma muß bekanntlich bereits bei 10^8 K liegen. Außerdem muß, um eine für die Zündung ausreichende thermische Isolierung des Plasmas zu erreichen, eine Energieeinschlußzeit τ des Plasmas im Magnetfeld von ca. 2 s erreicht werden. Beides zusammen ist nach bald 40-jähriger Entwicklungsarbeit noch nicht gelungen. Man kann deshalb ahnen, mit welchen Schwierigkeiten man bei den anderen Fusionsreaktionen rechnen muß. Dennoch wird der d-^{3}He-Prozeß seit langem[1] als eventuell noch kerntechnisch nutzbar angesehen. Da aber ^{3}He nur selten auf der Erde vorkommt, wurde bisher in diesem Zusammenhang an die Produktion von Tritium mit künftigen d-t-Reaktoren gedacht, die, ausgelegt für möglichst hohen Brutfaktor über den β-Zerfall des Tritiums in ^{3}He zusammen mit dem überall verfügbaren Deuterium den Brennstoff für d-^{3}He-Reaktoren liefern sollten.

Das Interesse an der d-^{3}He-Reaktion beruht darauf, daß sie neutronenfrei abläuft, und, daß keines der beteiligten Teilchen radioaktiv ist (s. S. 3-1). Über den d-d-Prozeß ist zwar eine störende Produktion von Tritium und von Neutronen vorhanden, jedoch ist, wie u.a. diese Studie zeigt, der Anteil der neutronischen Leistung nur ca. 10 % der Gesamtleistung eines d-^{3}He-Reaktors. 90 % der Leistung werden von schnellen Protonen und Heliumkernen getragen.

Nachdem im Jahre 1986 in Madison bekannt wurde, daß in der Oberfläche des Mondes erhebliche Mengen von ^{3}He lagern[2] mit einem Äquivalent von 10^7 GWa elektrischer Energie unter der Annahme einer Verbrennung mit Deuterium in Fusionsreaktoren mit einem Wirkungsgrad von 50 % ist das Interesse am d-^{3}He-Prozeß vor allem in den USA mit ihrem Raumfahrtprogramm deutlich gestiegen.

Insbesondere wegen der durch die Neutronen verursachten Werkstoffschäden und der Aktivierung eines d-t-Reaktors und außerdem wegen der radiologischen Probleme infolge des Tritiums besteht natürlich ein allgemeines Interesse daran, zu wissen, welche Schwierigkeiten nach gelungener Zündung eines d-t-Plasmas in einer vermutlich weiteren langfristigen Entwicklungsarbeit überwunden werden müßten, um wenigstens den nächst schwierigeren Prozeß, die d-^{3}He-Fusion und deren Vorteile nutzen zu können.

2. Abwicklung der d-^{3}He-Studie

Im KfK wurde deshalb zunächst in einer kurzen Vorstudie geprüft, welche Extrapolation der plasmaphysikalischen Parameter ungefähr notwendig ist, um die Zündung eines d-^{3}He-Gemischs nach heutigem Kenntnisstand herbeiführen zu können. Das vorläufige Ergebnis war, daß die Temperatur und die Energieeinschlußzeit gegenüber den für d-t in NET vorgesehenen Werten ($kT \approx 10$ kilo eV, $\tau_E \approx 2$ s) um etwa das 3fache und 7fache respektive weiter gesteigert werden müssen. (Der Stand der Technik liegt bei $kT \approx 10$ kilo eV und $\tau_E \approx 0{,}6$ s in JET). Ferner würde die Leistungsdichte im Plasma, die im d-t-Betrieb die Größenordnung 1 W/cm^3 hat auf etwa 1/4 W/cm^3 sinken.

Vor diesem Hintergrund wurde im KfK beschlossen, die vorliegende Studie, d.h. vorwiegend den plasmaphysikalischen Teil der d-^{3}He-Fusion in Madison in Auftrag zu geben in enger Zusammenarbeit mit Fachleuten des KfK, um sicherzustellen, daß die technischen Randbedingungen inbesondere bezüglich der Werkstoffbelastung der ersten Wand und des Divertors und bei der Auslegung der supraleitenden Spulen sowie beim "plasma exhaust" eingehalten werden. Die Studie wurde über KfK in engem Kontakt mit dem NET-Team abgewickelt.

Die Hauptaufgaben der Studie sollten sein, das Feld der plasmaphysikalischen Parameter um etwa $Q = 1$ (Q = thermonukleare Leistung/injizierte Leistung) d. h. etwa für breakeven quantitativ insbesondere daraufhinzu untersuchen, ob in NET sinnvolle Experimente mit einem d-^{3}He-Gemisch durchgeführt werden können.

Darüberhinaus sollte in parametrischer Darstellung dargestellt werden, wie ein Tokamakreaktor im Vergleich zu NET konzipiert werden muß, d. h. u. a. wie die Zündung eines d-^{3}He-Gemischs unter Extrapolation des heutigen plasmaphysikalen Kenntnisstands erreicht werden kann.

Insbesondere sollte untersucht werden, inwieweit sich der zunächst klare Vorteil, daß die thermnukleare Leistung bei d-^{3}He über die kinetische Energie geladener, nicht radioaktiver Teilchen anfällt zum Nachteil geraten kann, wenn es nicht gelingt, die Reaktionsprodukte im Plasma zu thermalisieren. Dann würde die Zündung erschwert und außerdem möglicherweise durch lokale Belastung der ersten Wand über die gefürchtete "ripple diffusion" schneller Teilchen ein neues, schwierig zu beherrschendes Problem herbeigeführt ("ripple" = Inhomogenität $\Delta B/B$ des Magnetfeldes zwischen den Toriodalfeldspulen).

3. Die Hauptergebnisse der Studie

d-^{3}He-Experimente in NET

Die Studie ergibt, daß sich in NET ohne wesentliche Änderungen*) des NET-Entwurfs für d-t breakeven-Bedingungen erreichen lassen (Q = 1), wenn die sogenannte H-mode-Skalierung für die Energieeinschlußzeit gilt (H-mode bedeutet, daß die Energieeinschlußzeit unabhängig von der Injektionsleistung ist, was im Tokamak ASDEX bis zu ca. 3,5 MW Injektionsleistung beobachtet wird).

Sollte das in Tokamaks ohne Divertor grundsätzlich beobachtete Absinken von τ mit steigender Injektionsleistung gelten (Kaye-Goldston-Skalierung), dann würde man nur Q = 0,4 erreichen mit einer injizierten Leistung von 120 MW gegenüber der für d-t-Betrieb zunächst geplanten Leistung von 70 MW.

Man kann daher sagen, daß Experimente mit d-^{3}He in einem praktisch unveränderten NET durchgeführt werden könnten zum Studium der Thermalisierung der geladenen-Reaktionskprodukte und zur eingangs erwähnten möglichen lokalen Wandbelastung durch "ripple-diffusion". Solche Experimente wären auch für den d-t-Betrieb von Interesse im Hinblick auf das Funktionieren der α-Teilchenheizung.

Es wäre zu empfehlen, solche Experimente in der Anfangsphase des NET-Betriebs, soll heißen, solange die Maschine noch nicht aktiviert ist, durchzuführen.

---

*) Da man bei d-^{3}He auf das Tritium-Brutblanket verzichten kann, läßt sich die thermische Isolierung des Plasmas durch Vergrößerung des kleinen Plasmaradius und damit die Energieeinschlußzeit steigern. Siehe auch die Erhöhung von β im nächsten Abschnitt.

d-^{3}He-Zündbedingung

Bei der Auslegung des Plasmas eines Tokamakreaktors ist eine der zu beachtenden Randbedingungen, daß die thermische Energiedichte bei vorgegebener magnetischer Flußdichte begrenzt ist, ausgedrückt durch

$$\beta = \frac{2\,nkT}{\frac{B^2}{2\,\mu o}} = \frac{2/3\ thermische\ Energiedichte}{Energiedichte\ des\ Magntfeldes} \leq \beta_{max} \sim \frac{a}{R}$$

Übersteigt β den Wert β_{max}, so wird der magnetische Einschluß zerstört.

a = kleiner Plasmaradius
R = großer Plasmaradius.

Man versucht deshalb, ein möglichst "fettes" Tokamakplasma (d. h. a/R so nahe wie möglich dem Wert eins) zu konzipieren.

(Beispiel: a/R = 0,42 in JET und a/R = 0,26 in NET).

Die praktische Bedeutung des maximal möglichen β-Wertes zeigt die Parameterabhängigkeit der Plasmaleistungsdichte

$$p \sim n_1 \cdot n_2 \cdot <\sigma v> \cdot Q_p \sim n^2 <\sigma v> \cdot Q_p$$

n_1, n_2 = Dichten der beiden Reaktionspartner, die beide proportional zu n, d. h. ein bestimmter Anteil der Gesamtionendichte n des Plasmas sind.

Q_p = im Plasma pro Reaktion deponierte Energie, d. h. die Energie der geladenen Teilchen. Q_p = 3,5 MeV und 18,3 MeV für d-t und d-^{3}He respektive.

Eliminiert man

$$n^2 \sim \beta^2 \cdot \frac{B^4}{T^2}\ in\ p,\ so\ erhält\ man$$

$$p \sim \beta^2 \cdot B^4 \frac{<\sigma v>}{T^2} Q_p \leq \beta^2_{max} \cdot B^4 \frac{<\sigma v>}{T^2} \cdot Q_p$$

Da β_{max} durch a/R und B aus technischen Gründen begrenzt sind, bleibt als einziger freier Parameter die Temperatur T. Auf S. 3-4 des Berichts ist deswegen die wichtige Größe $<\sigma v>/T^2$ in Fig. 3.-1-2. in Abhängigkeit von der Temperatur dargestellt. Man sieht, daß selbst bei Wahl der jeweils optimalen Temperatur entsprechend der Lage des Maximums von $<\sigma v>/T^2$ (kT = 13 kilo eV und kT = 55 kilo eV für d-t und d-^{3}He respektive) die Leistungsdichte eines vorgegebenen Reaktors, wenn man ihn mit d-^{3}He füllte um mehr als eine Zehnerpotenz kleiner würde als im d-t-Betrieb. Dabei ist vorausgesetzt, daß der Vorteil der d-^{3}He-Reaktion, nur geladene Reaktionsprodukte zu haben, voll zum Tragen kommt, d.h. die α-Teilchen und die Protonen auch vollständig im Plasma thermalisiert werden. Durch den Einfluß von $<\sigma v>/T^2$ allein sinkt die Leistungsdichte um einen Faktor 55, ein Nachteil, der bei allen anderen Fusionsreaktionen wegen der höheren Temperaturen und in der Tendenz abfallenden $<\sigma v>$-Werte immer stärker zu Buche schlägt. Man kann deshalb und, weil man bei d-t bereits bei nur etwa 1 W/cm^3 liegt, mutmaßen, daß, wenn überhaupt, der d-^{3}He-Prozess der einzige ist, der nach d-t für eine Nutzung noch in Frage kommen könnte, weil bei allen übrigen Reaktionen die Leistungsdichten auf Werte absinken, die aus ökonomischen Gründen nicht akzeptiert würden. Auch wird wegen der mit der Temperatur ansteigenden Strahlungsverluste irgendwann die Zündung des Brennstoffgemischs unmöglich.

Da man bei d-^{3}He keinen Brutmantel braucht und auch die Abschrimung für die supraleitenden Spulen wegen des stark reduzierten Neutronenflusses und wegen des etwas günstigeren Neutronenspektrums mit dem Plasma näher zur Achse des Tokamaks rücken kann, läßt sich der Wert von a/R und damit von β_{max} für ein d-^{3}He-Gemisch gegenüber d-t anheben und damit die Leistungsdichte etwas vergrößern (s. Fig. 4.2-2a. und 4.2-2b. auf S. 4-4 und S. 4-5). Die Studie ergibt, daß selbst mit diesen Maßnahmen in einem sonst völlig unverändertem NET auch unter den optimistischsten Annahmen über die Skalierung der Einschlußzeit (H-mode) und unter Benutzung der NET-EP-Auslegung (s. S. 2-2; expanded plasma) eine Zündung nicht möglich ist (s. Tab. 3.4-1., S. 3-45 ignition cases D-1 and D-2). Sowohl die zugrunde gelegten Werte der Plasmaelongation von 2,7 bzw. 2,38 als auch ein Wert von 13 Tesla an der Spule liegen außerhalb der von NET und KfK z.Zt. akzeptierten Auslegungskritieren. Das heißt nicht, daß die Zündung eines d-^{3}He-Plasmas prinzipiell unmöglich ist, der Tokamak müßte nur von vornherein anders ausgelegt werden. Die im übrigen interessierenden Daten wie z. B. Fusionsleistung, Neutronenleistung, Wandbelastung, Einschlußzeit usw.

entnimmt man Tab. 3.4-1., S. 3-45 und in Tab. 2-1., S. 2.2 sind die Vergleichsdaten für d-t-Betrieb in NET angegeben.

Es sei noch eine andere Schwierigkeit erwähnt, die in Plasmen mit Temperaturen oberhalb 10^8 K in zunehmendem Maße auftritt, die weiter vorn schon erwähnt wurde, der Leistungsverlust durch Synchrotronstrahlung. Schon in NET (s. S. 2-2) würde von den Elektronen des d-t-Plasmas Synchrotronstrahlung mit einer Leistungsdichte von 2,2 MW/m^3 (das ist mehr als die Fusionsleistung!) emittiert aber im Plasma praktisch sofort wieder absorbiert werden. Die vom kalten Plasmarand emittierte Synchrotronstrahlungsleistung wäre verschwindend klein, so daß dieser Verlustmechanismus beim d-t-Prozeß noch nicht berücksichtigt werden muß. Die Wiederabsorption im Plasma nimmt jedoch rapid ab mit zunehmender Temperatur, denn die Transparenz steigt mit $Te^{3/2}$! und die Zündung wird unmöglich, sobald die Verlustleistung durch Strahlung gleich der thermonuklearen Leistung im Plasma ist. Es kommt deshalb schon bei d-^{3}He (s. Tab. 3.4-1., S. 3-45 $<kTe>$ = 34 kilo eV in den cases D) sehr darauf an, wie groß das Reflexionsvermögen der ersten Wand für die Synchrotronstrahlung ist. Bei Frequenzen von ca. 140 GHz und deren ersten Oberwellen, was etwa dem Frequenzbereich der Synchrotronstrahlung des untersuchten d-^{3}He-Plasmas entspricht, ist das Reflexionsvermögen an polierten Metalloberflächen größer als 99 %, d. h. polierte Metalle sind praktisch ideale Spiegel. Weil das Reflexionsvermögen bei diesen Frequenzen jedoch für die erste Wand eines Tokamakreaktors nicht bekannt ist, wurde es im Rahmen dieser Studie im KfK gemessen. Sowohl Graphitziegel als auch Stahlplatten, die den Plasmen in JET als auch in ASDEX respektive für die Dauer von mehreren Monaten Betriebsphase ausgesetzt waren, ergab sich gemittelt über die ungleichmäßig beschädigten Oberflächen ein Reflexionsvermögen von R = 0,95.

Den vorliegenden Ergebnissen liegt die Annahme zugrunde, daß 19 % der Oberfläche der ersten Wand nicht reflektieren, weil dort Öffnungen sind z. B. für die Injektion oder für den Divertor und, daß die übrigen 81 % der Oberfläche mit R = 0,95 reflektieren. In Tab. 8.2-1., S. 8-11 sieht man das Ergebnis: 54 MW + 92 MW Transport durch Synchrotron- und Bremsstrahlung in case D-1, d. h. ungefähr 61 % der im Plasma produzierten Leistung (s. Tab. 3.4.-1., S. 3-45). Die Folge ist, daß durch Wärmeleitung nur eine entsprechend kleine Leistung transportiert werden darf, weil die Zündung sonst nicht möglich ist. Das Resultat ist eine erhöhte Forderung an die thermische Isolierung gegen Wärmeleitung, weshalb statt 2 s für d-t 14 s Energieeinschlußzeit für d-^{3}He erforderlich sind.

Belastung der ersten Wand durch schnelle Reaktionsprodukte.

Diese sehr komplexe Frage konnte im Rahmen der Studie noch nicht beantwortet werden, weil experimentelle Ergebnisse und Rechnungen für d-^{3}He noch nicht vorliegen. Die Studie beschränkt sich auf die Ergebnisse von Rechnungen einer japanischen und einer amerikanischen Gruppe für Tokamaks ohne Divertor und d-t. Die Rechenprogramme sind sehr komplex und außerdem verschieden aufgebaut, so daß die beiden Gruppen zu verschiedenen Ergebnissen gelangen.

Zur endgültigen Klärung der Frage, ob die Wandbelastung infolge von "ripple diffusion" ein ernstes Problem ist oder nicht sind unbedingt Experimente erforderlich, z. B. die für die Anfangsphase von NET vorgeschlagenen.

Plasmanachfüllung

Ein ebenfalls noch offenes Problem ist die Nachfüllung des verbrannten und des abdiffundierten Brennstoffs. Für den d-t-Betrieb sind mechanisch beschleunigte Kugeln aus festem Deuterium und Tritium vorgesehen, die beim Eindringen in das Plasma vorwiegend durch das Bombardement der Plasmaelektronen nach und nach abgetragen werden.

Das Konzept funktioniert nicht beim Helium, das sich nur unter relativ hohem Druck verfestigen läßt.

In der Studie wird die Injektion von Plama aus Plasmakanonen vorgeschlagen. Auch hierfür fehlen noch Versuche. Die vorliegende experimentelle Basis ist noch nicht breit genug, um garantieren zu können, daß solche sogenannten Plasmoide genügend tief in ein magnetisch eingeschlossenes Hochtemperaturplasma eindringen können.

Literatur zum Überblick für die d-^{3}He-Studie

1) McNally, J. Rand, Nucl. Fusion **18** (1978), 133.

2) Wittenberg, L.J., Santarius, S.F. and Kulcinski, G.L., Fusion Technology, Vol. 102 (1986), 167.

1. INTRODUCTION

There has been renewed worldwide interest in the advanced fusion fuels which produce relatively low levels of radioactivity.[1-4] The major emphasis of this recent research has been on the D-^{3}He cycle for which neither the fuel nor reaction products are radioactive. Of course, side reactions of the deuterium fuel produce some neutrons, but the neutron production and the total induced radiation damage and radioactivity are reduced by 1 to 2 orders of magnitude from the DT case, depending on the fuel mixture.

Contrary to conventional thinking of the 1970's and early 1980's, achievement of breakeven conditions for the D-^{3}He cycle by the end of this century is quite possible. The achievement of similar conditions for the DT cycle (breakeven in the early 1990's) will allow scientists to enter the 21st century with similar plasma conditions for the traditional DT cycle and the more environmentally attractive D-^{3}He cycle.

The purpose of this report is to show that such exciting near term D-^{3}He results could be obtained in a tokamak of the NET/INTOR class. This report will concentrate on the physics results as opposed to the technological advantages of this fuel cycle, some of which are covered in other papers.[1,2,5] The approach taken here is to use the latest documented (1985) design of NET[6] as a base case to illustrate the physics results that could be obtained in a hot D-^{3}He plasma without significant activation of the vacuum vessel and diagnostics. In this study, we examine three variations of a base case as described below.

Case	Objective	Impact on Base Cost for NET
A	Little or no change from current NET design; use D-^{3}He fuel in place of DT	none
B	Inboard shield modifications of NET to achieve high Q in D-^{3}He plasma	< 1%
C	Significant TF coil modification of NET to achieve high Q operation	< 9%
D	Major modification of NET to achieve ignition	< 11%

Cases B and C are alternative variations on the base case, A, with the objective of high Q in a driven mode of operation. Case D is an attempt to see what modifications to NET are required for ignition in a D-^{3}He plasma.

Throughout this study, it was assumed that the main goal of NET will continue to be the ignition of DT fuel and the demonstration of a controlled DT burn. These goals will have to be accomplished regardless of the success obtained with the D-^{3}He cycle. However, because of the difficulty in working with a radioactive device like NET, even after 1 hour of DT operation, it is assumed that the D-^{3}He tests would be conducted early in the life of NET after the initial "shakedown" phase using hydrogen or deuterium plasmas. The physics results obtained by the slowing down of the high energy proton (14.7 MeV) and helium (3.6 MeV) ions, and their impact on the plasma power balance, confinement, and MHD equilibrium without significant activation of the vacuum vessel and diagnostics, is certainly an attractive bonus for the physics community.

References for Chapter 1

1. L.J. Wittenberg, J.F. Santarius and G.L. Kulcinski, Fusion Technology, 10, 167 (1986).

2. G.L. Kulcinski, J.F. Santarius and L.J. Wittenberg, "Clean Nuclear Power From the Moon," Proceedings of the 1st Lunar Development Symposium, Atlantic City, NJ, September 1986, S. 1-8.

3. J.F. Santarius, Nuclear Fusion, 27, 167 (1987).

4. J.F. Santarius, G.L. Kulcinski, H. Attaya, M.L. Corradini, L.A. El-Guebaly, J.W. Johnson, C.W. Maynard, M.E. Sawan, I.N. Sviatoslavsky, W.F. Vogelsang, P.L. Walstrom, L.J. Wittenberg and T.E. Luzzi, "SOAR - Space Orbiting Advanced Fusion Power Reactor," Space Nuclear Power Systems, Orbit Publishers (1987).

5. G.L. Kulcinski and H.H. Schmitt, Proceedings of 11th Int. Scientific Forum on Fueling the 21st Century, Moscow, September 1987.

6. F. Engelmann, "Concept and Parameters of NET", NET Report 64, EUR-FU/XII-80/86/64, Commission of the European Communities (1986).

2. NET DT REFERENCE DESIGN

The study of D-^{3}He operation is, by necessity, based on the NET design developed for D-T operation by the NET team. Since this design continues to evolve, we present here a summary of the NET design parameters on which our study is based. These are taken from NET reports.[1,2]

The NET team has considered both single-null and double-null poloidal divertor configurations. We have adopted the parameters for the double-null configuration to use as a starting point for this study. In addition to the reference double-null case for DT operation, the NET team has studied an enhanced plasma size case with an double-null divertor. The enhanced plasma has a larger major and minor radius with a corresponding increase in the plasma current, but no change in the toroidal field at the TF magnet. The enhanced plasma case is of interest to us for D-^{3}He operation since the larger size and plasma current lead to an increased Q-value (energy multiplication). In order to distinguish between these two reference cases, we refer to the first reference case as NET-DT and the enhanced plasma size case as NET-EP. Shown in Table 2-1 are the major parameters for the NET-DT and NET-EP designs. These parameters are for D-T operation; in later sections of this report we will consider possible changes for D-^{3}He operation. The cross-section of plasma, blanket, shield, and toroidal field magnet of NET-DT is shown in Fig. 2-1.

References for Chapter 2

1. The NET Team, "NET Status Report 1985", NET Report 51, Commission of the European Communities (1985).

2. F. Engelmann, "Concept and Parameters of NET", NET Report 64, EUR-FU/XII-80/86/64, Commission of the European Communities (1986).

Table 2-1. Main Configurational and Plasma Parameters of the NET Reference Options NET-DT and NET-EP

		NET-DT	NET-EP
Plasma major radius	R (m)	5.18	5.41
Plasma minor radius	a (m)	1.35	1.68
Plasma elongation	b/a	2.18	2.17
Plasma triangularity	γ	0.65	.61
Aspect ratio	A=R/a	3.8	3.2
Plasma volume	V_p (m^3)	390	600
Total radial machine size	2 R_t (m)	21.40	(21.40)[a]
Total machine height	H_t (m)	14.00	(14.00)
Magnetic field on axis maximum on coils	B (T) B_m (T)	5.0 10.4	4.8 (10.4)
Toroidal field ripple	δ (%)	± 1.2	± 3.4
Plasma current	I_p (MA)	10.8	14.8
Safety factor	q_I	2.1	2.2
Average burn temperature	$\bar{T}$ (keV)	10	10
Average DT density	$\bar{n}_{DT}(10^{20}/m^3)$	1.20	1.26
Average electron density	$\bar{n}_e(10^{20}/m^3)$	1.56	1.64
Murakami parameter	$M(10^{19}/m^2T)$	16	18.5
Beta scaling factor	g	3.5	3.5
Total beta	β_{tot} (%)	5.6	6.4
DT beta	β_{DT} (%)	4.2	4.8
Poloidal beta	β_I	1.42	1.2
Fusion power	P_{fus} (MW)	600	1000
α-particle power	P_α (MW)	120	200
Fusion power density	p_{fus} (MW/m^3)	1.53	1.7
Average neutron wall loading	Q_n (MW/m^2)	1	1.4
Confinement capability	$C=P_\alpha/P_{loss}$	2.9	4.4
Confinement time during burn	τ_E(s)	2	
Burn time (minimum)	τ_b(s)	200	

(a) The items in ( ) are assumed to be the same as in NET-DT.

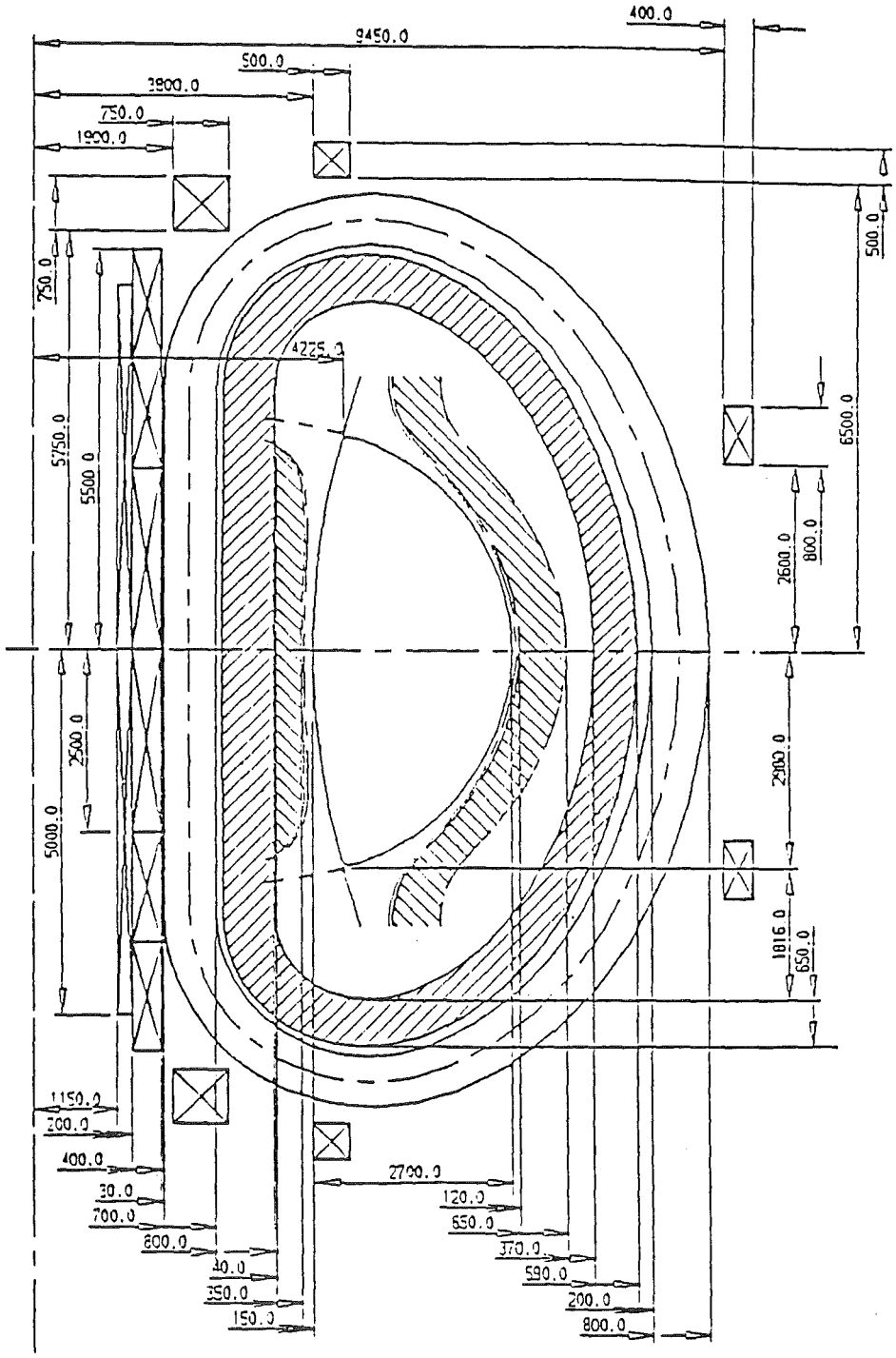

Fig. 2-1. Cross-section of the NET-DT device.

3. PLASMA PERFORMANCE MODELLING

3.1 General Considerations

Before considering the detailed plasma physics calculations, it is worthwhile to compare D-^{3}He fusion with D-T fusion from the point of view of basic physics principles. This comparison is helpful in understanding the more detailed physics calculations.

The basic fusion reactions of interest are:

$$D + {}^3He \rightarrow {}^4He(3.6) + p(14.7) + 18.3\ MeV \qquad (3.1\text{-}1)$$

$$D + T \rightarrow {}^4He(3.5) + n(14.1) + 17.6\ MeV\ . \qquad (3.1\text{-}2)$$

The D-^{3}He reaction releases 18.3 MeV of energy per reaction event, while the D-T reaction releases 17.6 MeV. The energy of the alpha particle released in each reaction is almost the same, but the D-^{3}He reaction releases a 14.7 MeV proton instead of a 14.1 MeV neutron. It is important that 100% of the energy released in the D-^{3}He reaction is in the form of charged particles which deposit their energy in the plasma and help maintain the plasma energy balance. For the D-T reaction, only 20% of the energy released is in the alpha particle and is available for plasma heating. The neutron carries away 80% of the energy and deposits it in the blanket and shield. Because of the smaller mass of the proton, its gyroradius and banana widths are only twice that of a 3.6 MeV alpha particle. Hence finite orbit effects are not greatly increased over that of the D-T case. Fast ion losses due to trapping in the magnetic ripple is a concern for both D-^{3}He and D-T, but is larger in D-^{3}He because of the higher energy protons. This loss leads to bombardment of the first wall by fast ions and results in an increased local surface heat load. The severity of this heat load is a concern, but has not yet been established. Since all of the D-^{3}He fusion yield is in the form of charged particles and is deposited in the plasma, it is transferred to the first wall and divertor as surface heating. In a D-T plasma 80% of the fusion yield is in neutron energy which is deposited in the blanket and shield as volumetric heating. Consequently, the surface heat loads are higher in a D-^{3}He plasma for the same fusion power density in the plasma.

The Maxwellian-average $\langle\sigma v\rangle_f$ for the various fusion reactions are shown in Fig. 3.1-1. The $\langle\sigma v\rangle_f$ for the D-^{3}He is much lower than that for D-T and peaks at a much higher plasma temperature. Of more interest in a β limited system is the figure of merit, $\langle\sigma v\rangle_f/T^2$, which is a measure of the power produced for a given β (ratio of the volume-averaged plasma pressure to the magnetic pressure) and magnetic field

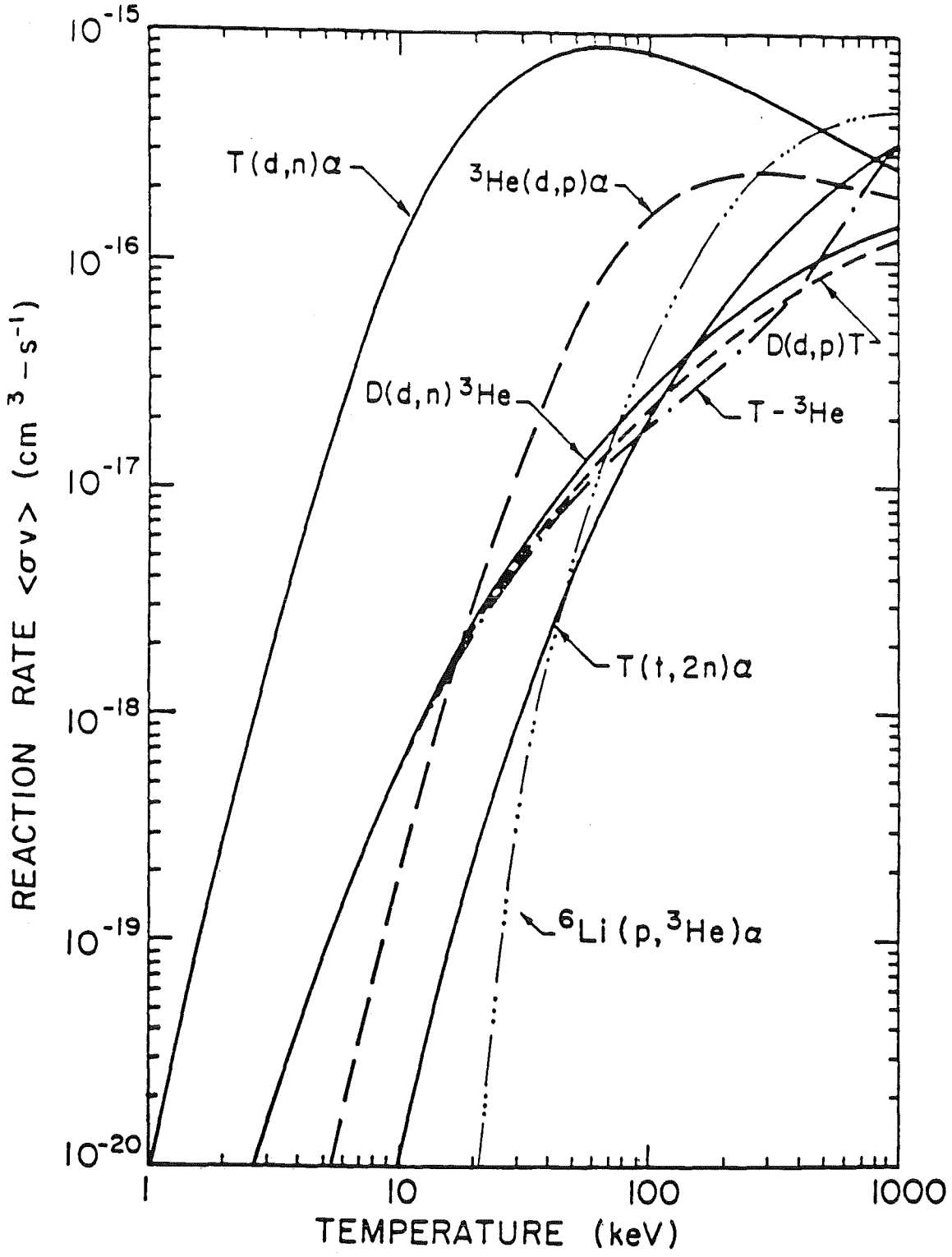

Fig. 3.1-1. The Maxwellian averaged reaction rate, $\langle\sigma v\rangle_f$, as a function of ion temperature for various fusion reactions.

strength. This is shown in Fig. 3.1-2. We see that $\langle\sigma v\rangle_f/T^2$ for D-^{3}He peaks at 55 keV compared with 13 keV for the D-T reaction. In addition, the peak value for the D-^{3}He reaction is about a factor of 50 smaller than that for the D-T reaction. Also shown for comparison is the $\langle\sigma v\rangle_f/T^2$ for the D-D reaction; this is about a factor of 2 lower than the D-^{3}He value. Other factors (e.g. confinement scaling, volume averaging, and radiation losses) can shift the optimum temperature from the 55 keV peak, but the optimum will still be in the 50-80 keV range and not at the very high values implied by the maximum of $\langle\sigma v\rangle_f$.

In addition to the fusion reactivity, a concern is the degree of plasma confinement required for ignition; the usual figure of merit for this is the product of the density and the energy confinement time required for the plasma to be self-sustaining against power losses (loosely referred to as the "Lawson criteria"). Shown in Fig. 3.1-3 is $n\tau$ required for ignition versus the ion temperature; this energy confinement time measures the loss of energy by diffusion across the confining magnetic field. Bremsstrahlung and synchrotron radiation losses are included separately. Synchrotron radiation loss depends not only on the magnetic field strength, density, and temperature, but also on the degree of reabsorption; the latter also introduces an additional magnetic field, density, temperature, size, and wall reflectivity dependence. Consequently, one cannot give a generic curve for $n\tau$ versus ion temperature. The density has been eliminated using the definition of beta (ratio of plasma pressure to magnetic field pressure), but the plasma minor radius has been chosen to be 2.5 m, the magnetic field at the plasma is 8 T, and the effective reflectivity is 0.8. These values are taken to be representative of a possible reactor. Also included in this $n\tau$ is the effect of the density and temperature profile in the plasma; both the density and temperature in Fig. 3.1-3 are volume-averaged. At low temperature bremsstrahlung dominates the losses; at higher temperature synchrotron radiation is more important. This is the reason for the beta dependence of the required $n\tau$ being larger at higher T_i. Reducing the reflectivity raises the required $n\tau$. At zero reflectivity the minimum in the beta = .1 curve is raised by a factor of about 2.5 and shifts the optimum temperature to a somewhat lower value. For beta = .1, the required $n\tau$ at the optimum ion temperature of 40 keV is about 1×10^{15} s/cm^3, which is about five times the required $n\tau$ for D-T fusion.

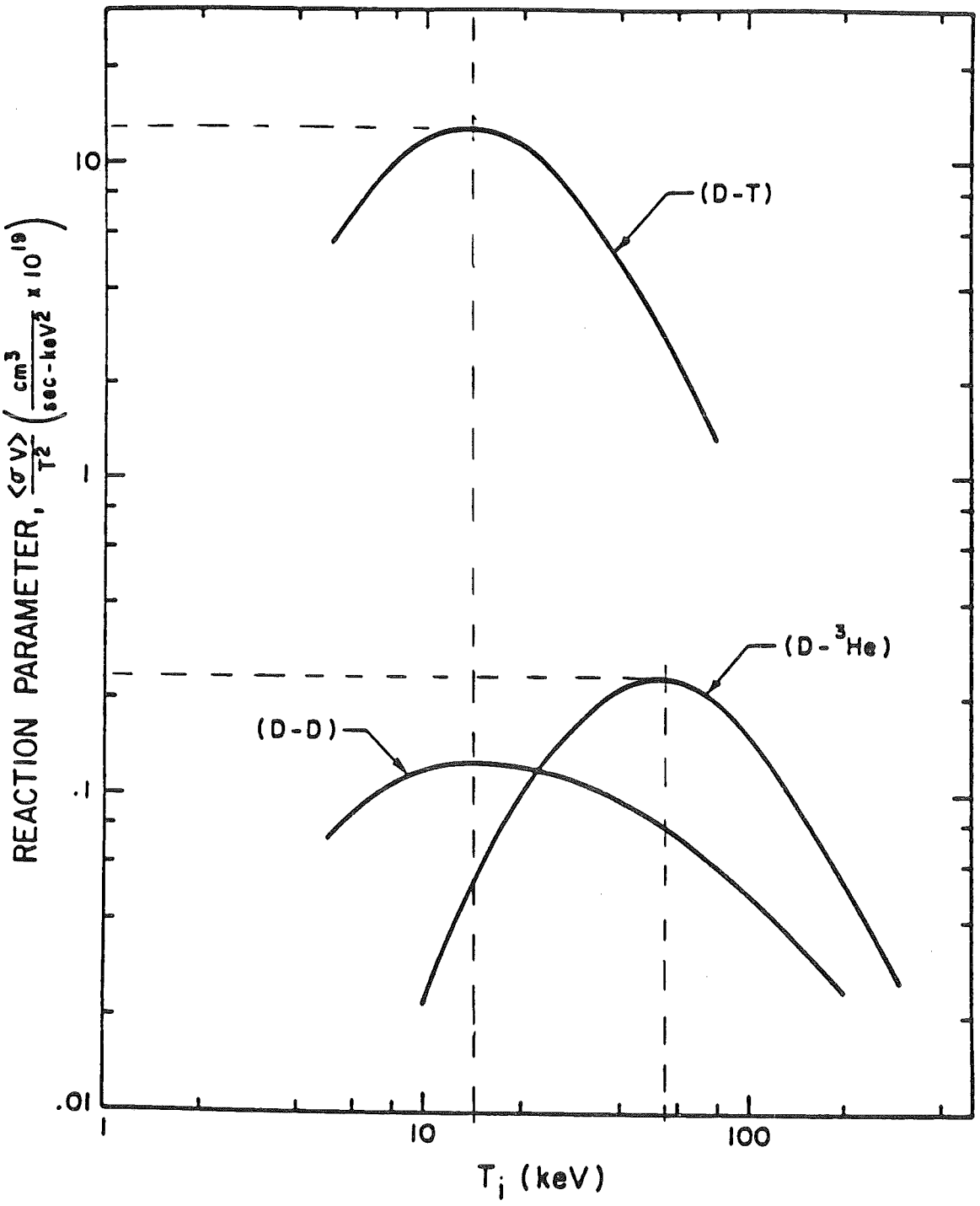

Fig. 3.1-2. The Maxwellian averaged reaction rate parameter, $\langle\sigma v\rangle/T^2$, as a function of ion temperature for several fusion fuel cycles.

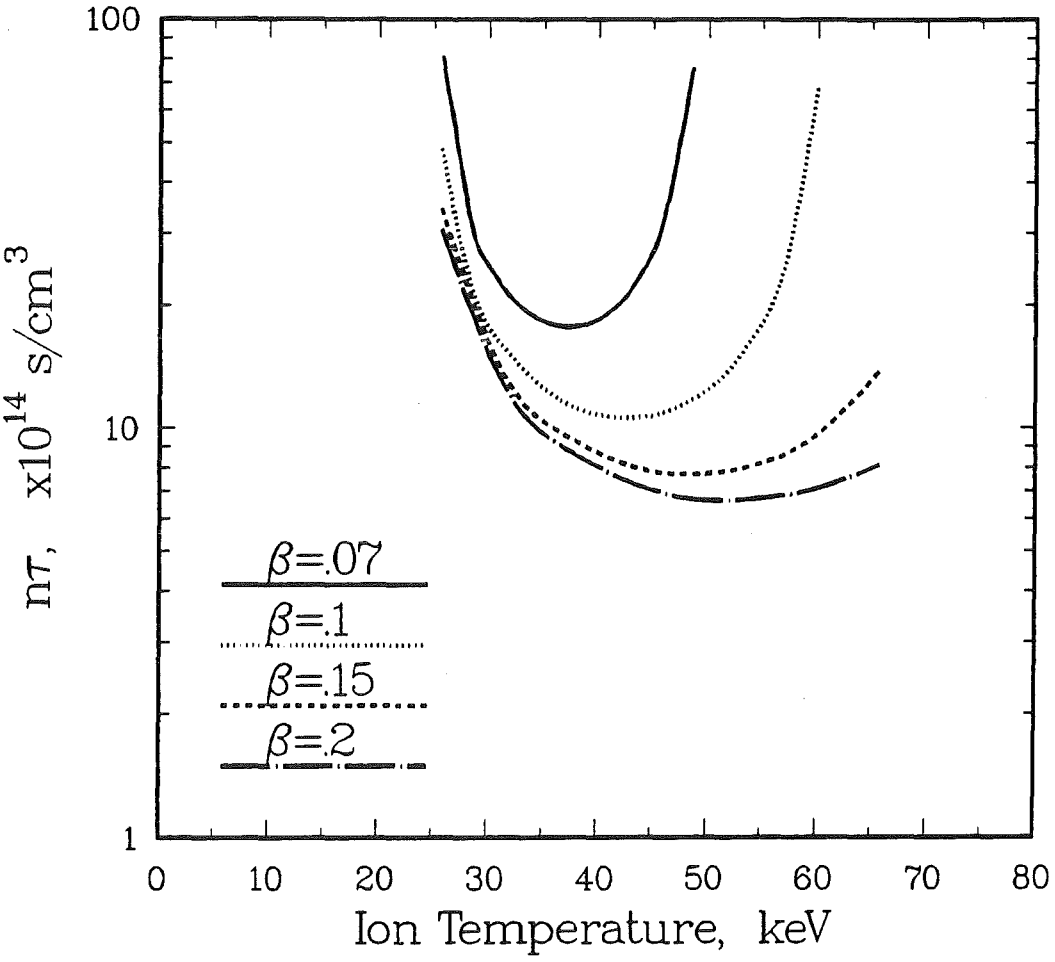

Fig. 3.1-3. Lawson parameter for D-^{3}He versus volume-averaged ion temperature.

Because the ^3He part of the fuel has Z = 2, the electron density is a larger fraction of the total charged particle density than in a D-T plasma. For a 50%-50% fuel mixture, the Z_{eff} is 1.67 without considering impurities or ash accumulation. This effect, coupled with the higher operating temperature for D-^3He, means that bremsstrahlung and synchrotron radiation play a larger role in the overall power balance than they do in the D-T plasma. In addition, the higher electron density reduces the allowed ion density for a given β and thereby reduces the fusion power density.

In a D-T plasma the optimum fuel mixture is 50% D and 50% T. In a D-^3He plasma, using a deuterium rich fuel mixture reduces the relative electron density and the radiation losses and improves the fusion power density. This is because, for every helium ion replaced by a deuterium ion, one electron is removed from the plasma. It turns out that the optimum fuel mixture is about 65% D and 35% ^3He.

Increasing the deuterium concentration in the fuel increases the neutron production rate. Neutrons are produced directly by the D-D reaction

$$D + D \rightarrow {}^3He + n \qquad (3.1\text{-}3)$$

and indirectly by the reaction chain

$$D + D \rightarrow T + p \qquad (3.1\text{-}4)$$

$$D + T \rightarrow {}^4He + n. \qquad (3.1\text{-}5)$$

Although this chain is a two-step process it is significant because of the large D-T cross-section. It is also significant because this neutron has an energy of 14 MeV while the neutron produced in reaction (3.1-3) has an energy of 2.45 MeV. The branching ratio between reactions (3.1-3) and (3.1-4) is about 50%. Ignoring escape of the tritium, the production rate of the low and high energy neutrons is the same. Some of the tritium, however, escapes from the plasma before being consumed in the D-T reaction. The escape probability depends on the confinement relative to the $\langle\sigma v\rangle_f$ for D-T. In subignited, driven systems the escape probability can be significant.

3.2 Plasma Power Balance Model

The performance of NET with D-^{3}He fuel can be calculated using power balance considerations to get the fusion power produced and the losses from the plasma. The fusion power produced can be calculated readily for a given plasma density and temperature profile. The loss mechanisms of concern are radiation losses by bremsstrahlung and synchrotron radiation, and transport across the confining magnetic field by conduction and convection. The plasma density and temperature that can be confined by the magnetic field are determined by MHD equilibrium and stability requirements. The plasma pressure, which is of concern for MHD, is determined not only by the fuel plasma, but also by the energetic ions generated by fusion reactions, and by the accumulation of ash and impurities. The energy of the charged particles generated by the fusion reactions also helps to maintain the energy of the reacting plasma. Folding all these effects together provides a mechanism for estimating the performance of NET using D-^{3}He fuel.

A computer code, called DHE3TOK, has been developed in order to estimate the performance of a NET-like tokamak operating with D-^{3}He. The basic physics assumptions built into this code are the same as one uses in the DT version of NET. We have built into the code the same level of conservatism or optimism as is implied in the analysis of NET by the NET design team. In particular, the following assumptions are made:

1. The beta, ratio of plasma pressure to magnetic pressure, is determined by the Troyon formula, which is an empirical fit to numerical MHD calculations.
2. The energy confinement time is given by empirical scalings. The NET team uses the so-called ASDEX H-mode scaling law which is based on H-mode confinement in ASDEX. The Kaye-Goldston scaling law was used in the U.S. TIBER study. It is based on a larger set of data from a variety of tokamaks and was developed for so-called L-mode operation. The effect of H-mode operation is generally included by multiplying the confinement time by a factor which represents the improved confinement of the H-mode.

The code is basically a zero-dimensional power balance code which calculates the ignition margin, M,

$$M = \frac{\text{Fusion Power}}{\text{Total Losses}}$$

and the energy multiplication, Q,

$$Q = \frac{\text{Fusion Power}}{\text{Injected Power}} = \frac{M}{1-M}$$

for a given set of plasma conditions. The injected power is the power required to sustain the plasma conditions. At ignition, the injected power is zero, $Q = \infty$ and $M = 1$. At scientific breakeven $Q = 1$; the fusion power produced is equal to the injected power. Note that $Q = 1$ in a D-^{3}He plasma is a stronger condition than $Q = 1$ in D-T because in the D-T case 80% of the power produced is in the form of neutron energy. The $Q = .2$ case in D-^{3}He is equivalent to $Q = 1$ in D-T from the impact on the plasma power balance and the study of burn physics.

In this section we present in detail the various effects included in the code. In the following sections, we then present a series of parametric calculations in order to determine how the various parameters influence the performance. From these one can determine the machine parameters which lead to an optimum ignition margin for a given set of constraints. Finally, we present possibilities for D-^{3}He breakeven ($Q = 1$) and ignition in NET.

Shown in Fig. 3.2-1 is a schematic of the plasma; the major radius is R, the horizontal half-width is a, the half-height is b, and the elongation $K = b/a$. The plasma cross-section is assumed to be elliptical; triangularity is required for maximum beta, but the effect of triangularity on the plasma volume is neglected in this analysis. The magnetic field strength is B_0 at the magnetic axis and B_c at the toroidal field coil; the separation point between the toroidal field winding pack on the inboard side and the plasma edge is Δ; this distance includes the cryostat, neutron shield, and plasma scrape-off layer. Because of the 1/r variation of the toroidal field, B_0 and B_c are related by

$$B_0 = B_c \left(\frac{R-a-\Delta}{R}\right) . \qquad (3.2\text{-}1)$$

It should be noted that B_c is the average field at the radius of the inboard side of the TF magnet and not the true peak field, which depends on the number of TF magnets and the details of the magnet design.

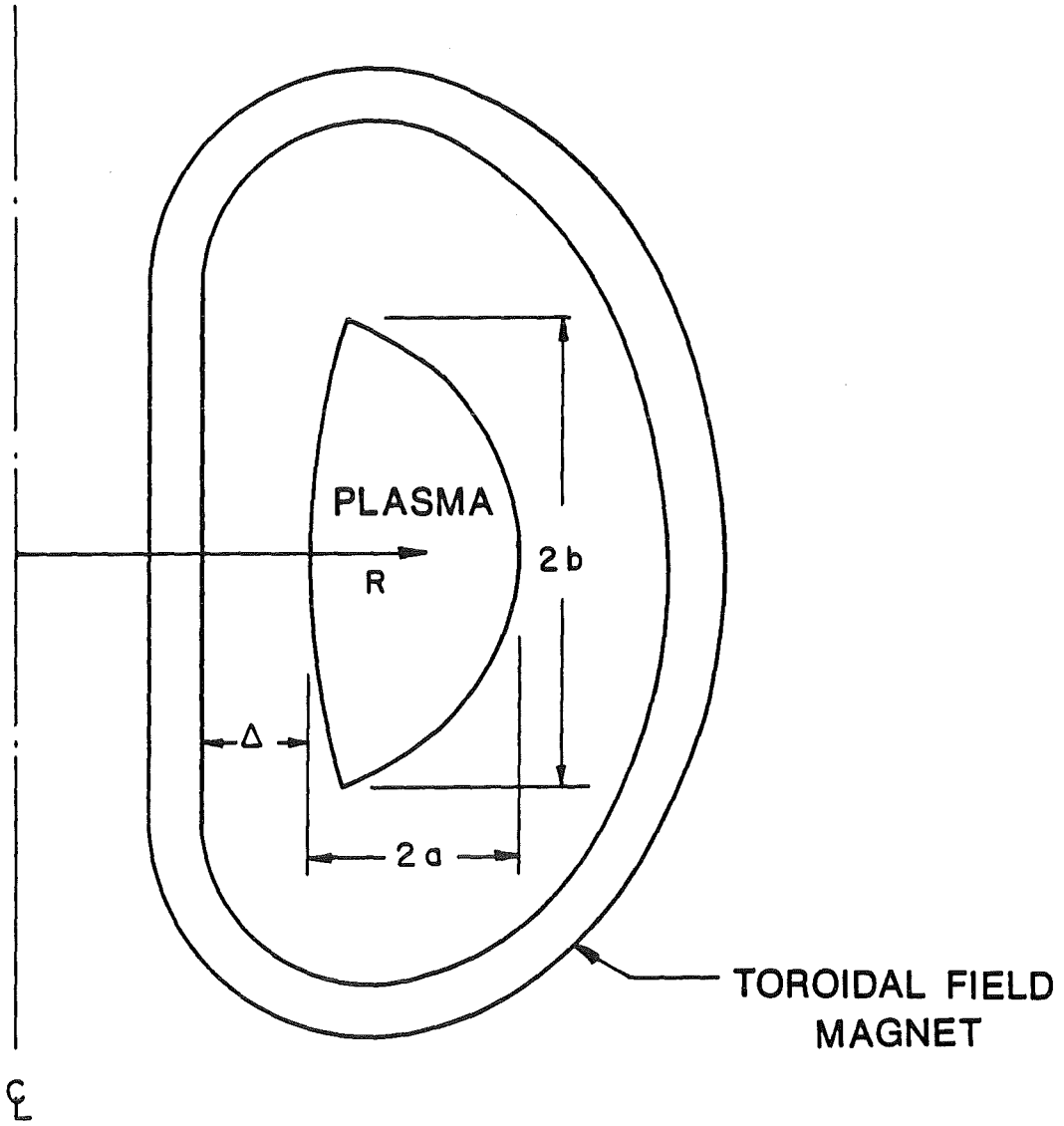

Fig. 3.2-1. Schematic of the plasma and toroidal field magnets defining the dimensions.

The plasma contains two fuel ion species (deuterium and ^{3}He) and three "ash" ion species (protons, alphas, and tritium). We also allow for a single impurity ion (e.g. oxygen), which is assumed to be fully stripped. Protons and alphas are produced primarily by the ^{3}He(d,p)^{4}He reaction. The D(d,p)T side reaction produces tritium which is important for evaluating the generation of 14 MeV neutrons. We denote these 6 ionic species by the subscripts 1, 2, 3, 4, 5, and 6, respectively. Thus, for example, $n_1(r)$ is the density profile for the deuterium. Here r is the distance of a flux surface from the magnetic axis in the midplane. The density profile of each charged particle species is taken to be of the form

$$n_j(r) = n_j(o)\ \left(1 - r^2/a^2\right)^{\alpha_N} \tag{3.2-2}$$

and the electron and ion temperature profile is

$$T(r) = T(o)\ \left(1 - r^2/a^2\right)^{\alpha_T} \tag{3.2-3}$$

where the exponents α_N and α_T are input data. For the calculations presented here, the values $\alpha_N = 1.$ and $\alpha_T = 1.5$ have been used. These functional forms have the advantage that the volume average of n^p is given by

$$\langle n^p \rangle = \frac{[n(o)]^p}{1 + p\ \alpha_N} \tag{3.2-4}$$

where p is an arbitrary exponent. An exception to this rule is that $\langle T \rangle$ is defined as a density weighted average,

$$\langle T \rangle = \frac{\int nT\ dV}{\int ndV} = \frac{\langle nT \rangle}{\langle n \rangle} = [T(o)]\ \frac{(1 + \alpha_N)}{1 + \alpha_N + \alpha_T}\ .$$

The fusion power, P_f, is given by integrating the local fusion power density over the plasma,

$$P_F = 2\pi\ R\ K \int_o^a n_1(r)\ n_2(r)\ \langle \sigma v \rangle_f\ 2\pi r dr\ Q_f\ . \tag{3.2-5}$$

Here, $\langle\sigma v\rangle_f$ is the Maxwellian-averaged fusion cross-section and depends on r through its dependence on the ion temperature. Note that $\langle\sigma v\rangle_f$ assumes the two ion species are Maxwellian at the same temperature. For subignited operation, higher Q can be obtained by using ICRF to generate an enhanced tail in one species; this increases the fusion power produced for a given injection power. This is not considered in the DHE3TOK code, but is discussed in Chapter 7. Equation (3.2-5) is written for a single nuclear reaction with yield Q_f; the code includes the contributions from all possible reactions, including D-D and D-T, but the power from the D-^{3}He reactions dominates.

We define f_d to be the fraction of the total fuel ion density which is deuterium; the helium fraction is then $1 - f_d$. We also consider the accumulation of fusion produced ash (protons, tritons, and alpha particles); the ash density is determined by the balance of the production rate and the loss rate. For example, the proton density is determined by

$$\int n_1 n_2 \langle\sigma v\rangle_f \, dV = \frac{1}{\tau_p} \int n_3 dV \ . \tag{3.2-6}$$

The particle confinement time, τ_p, is taken to be the same for all species. The electron density, n_e, is determined by quasineutrality. The total fuel ion density is n_f,

$$n_f = n_1 + n_2,$$

where $$n_1 = f_d n_f$$

and $$n_2 = (1 - f_d) n_f \ .$$

The volume averaged plasma beta is given by the Troyon formula,[1]

$$\langle\beta\rangle = \frac{C \ I_p \ (MA)}{a(m) \ B_0(T)} \tag{3.2-7}$$

where I_p is the plasma current. This equation requires that the quantities be entered in the units indicated. The NET team uses the value C = .035; we use the same value for this study. The volume-averaged plasma pressure is then given by

$$\langle p\rangle = \langle\beta\rangle \frac{B_0^2}{2 \ \mu_0} \ . \tag{3.2-8}$$

Included in the pressure are the effects of the various ion species, all of which are assumed to have the same ion temperature, the electrons, which have temperature $T_e(r)$, and also the pressure of the hot ions generated by fusion reactions. The distribution function of the hot ions is calculated using the slowing down approximation to the Fokker-Planck equation, and the pressure is evaluated as a moment of the distribution function. This analysis, which is given in Ref. 2, gives the local hot ion pressure. As an example, Fig. 3.2-2 shows the ratio of the fast ion pressure to the pressure of the background plasma for a 50:50 mixture of deuterium and ^{3}He. The resulting fast ion pressure is then averaged over the plasma volume to give the contribution to the volume-averaged plasma pressure. The total volume-averaged pressure is then

$$\langle p \rangle = \{[n_1(o) + n_2(o) + n_3(o) + n_4(o) + n_5(o) + n_6(o)]\, T_i(o) + n_e(o)\, T_e(o)\}/(1 + \alpha_N + \alpha_T) + \langle p_{fast} \rangle \ . \tag{3.2-9}$$

Using Eq. (3.2-8) and (3.2-9) coupled with the particle balance equations, Eq. (3.2-6), for each ash species to determine the densities, n_3, n_4, and n_5, we then get the allowed fuel ion densities, n_1 and n_2. The total ion density is then

$$n_i = \sum_i n_i \ .$$

To determine the injected power required to sustain the plasma at a specified operating temperature, it is necessary to account for the various mechanisms by which the plasma loses energy. Bremsstrahlung radiation from the electrons is given by[3]

$$P_B = \frac{5.31 \times 10^{-3}\, n_e^2(o)\, \sqrt{T_e}\, V}{1 + 2\,\alpha_N + .5\,\alpha_T} (Z_e(1 + .0155\, T_e + 7.15 \times 10^{-6}\, T_e^2) + .071\, Z_T/\sqrt{T_e} + .00414\, T_e) \quad (MW) \tag{3.2-10}$$

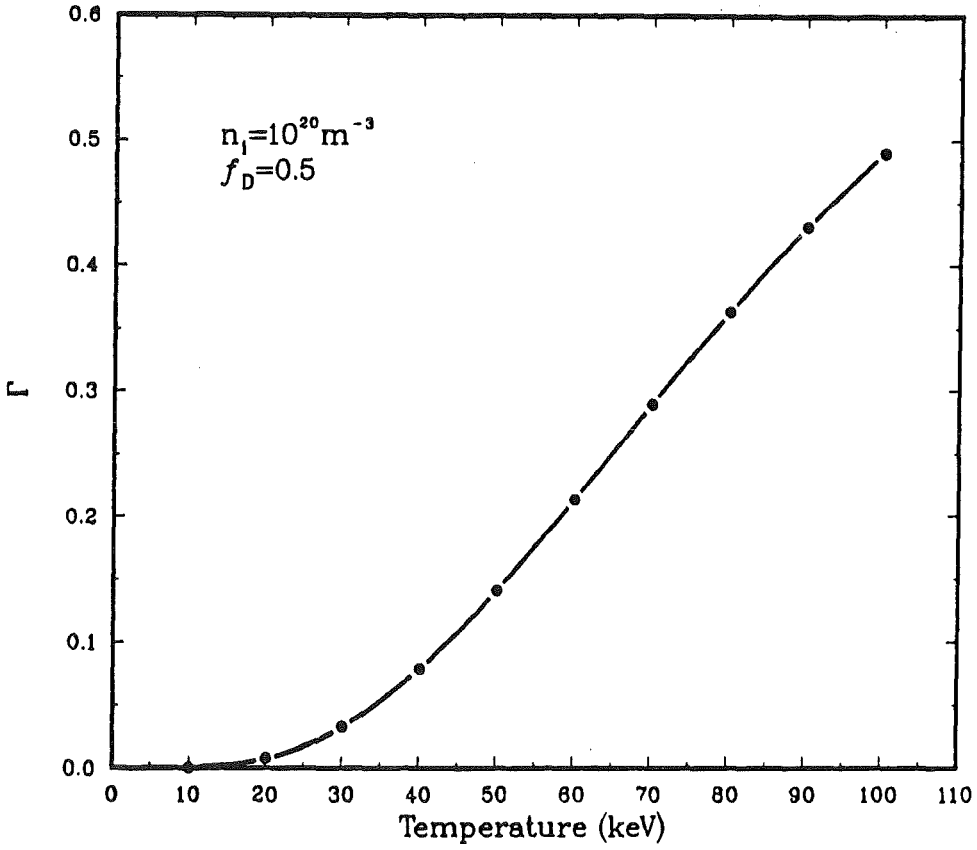

Fig. 3.2-2. Ratio of the fast ion pressure to the background plasma pressure in a D-He^3 plasma versus electron temperature.

where

$$Z_e = \sum_j n_j Z_j^2 / n_e$$

$$Z_T = \sum_j n_j Z_j^3 / n_e \qquad (3.2\text{-}11)$$

and V is the plasma volume. In Eq. (3.2-11) the sums are over the various ionic species in the plasma. Eq. (3.2-10) and the following equations are written in units where the temperature is in keV, the magnetic field is in tesla, the density is in units of 10^{20} m^{-3}s, the volume is in m^3, dimensions are in meters, the plasma current is in MA, and the power is in megawatts.

Synchrotron radiation from the electrons is another form of radiation loss. While this is a classical process and is in principle calculable, it is a difficult radiation transport problem because the plasma is both a strong emitter and absorber of synchrotron radiation. We use a "universal formula" developed by Trubnikov[4] to estimate the synchrotron power loss,

$$P_s = P_0 \Phi$$

$$P_0 = 6.24 \times 10^{-3} \, n_e \, B^2 \, T_e \quad \left(\frac{MW}{m^3}\right) .$$

P_0 is the radiation emitted not considering re-absorption and $1 - \Phi$ is the fraction re-absorbed. Trubnikov suggests a reasonable approximation for Φ is

$$\Phi = 60 \left(\frac{T_e}{m_e c^2}\right)^{1.5} \frac{1}{\sqrt{p_a}}$$

$$p_a = \frac{a}{1 - R_e} \left(\frac{1}{1 + x}\right) \frac{\omega_{pe}^2}{c \, \omega_{ce}}$$

where R_e is the reflectivity of the walls, ω_{pe} is the electron plasma frequency, ω_{ce} is the electron cyclotron frequency, and χ contains the effect of the torus,

$$\chi = \frac{2\,a}{R}\sqrt{\frac{2\pi\,T_e}{m_e\,c^2}}\,.$$

In the code we evaluate the electron cyclotron frequency at the magnetic axis, use the volume-averaged temperature in the computation of χ, and volume-average the remaining density and temperature dependences in P_0 and Φ to get the result

$$P_s = \frac{4.2 \times 10^{-7}\sqrt{n_e}\,B_0^{2.5}\sqrt{1 - R_e}\sqrt{1 + \chi}\,T_e^{2.5}\,V}{\sqrt{a_p}\,(1 - .5\,\alpha_N + 1.5\,\alpha_T)}\,(1 + \alpha_N + \alpha_T)\ (MW). \qquad (3.2\text{-}12)$$

This volume-averaging is not rigorous because photons emitted from the center of the plasma, where the emission is high, pass through a cooler and less dense plasma where they can be re-absorbed before escaping. It is not evident that this volume-averaging procedure includes this effect correctly, but there is no real alternative at the present state of development of this subject.

The reflectivity of the first wall is a concern. IPP Garching provided steel plates which had been exposed to plasma in the ASDEX divertor chamber. The JET team provided graphite tiles which were exposed to plasma in the JET tokamak. The reflectivity of the steel plates and graphite tiles was measured by G. Hochschild and H. Stickel of KfK. This yielded an average reflectivity of .95. It was assumed that 20% of the first wall surface is holes. Consequently, an effective reflectivity of .77 for synchrotron radiation was used in this study.

The remaining energy loss process is transport across the magnetic field by conduction and convection. This is treated using empirical energy confinement times. The NET team has used the ASDEX H-mode confinement time[5],

$$\tau_H = .1\ I_p\ (MA)\ R\ (m) \qquad (s) \qquad (3.2\text{-}13)$$

which is based on H-mode operation in the ASDEX tokamak. There are a variety of alternative "scaling laws" for energy confinement (probably as many as there are scientists analyzing energy confinement); the scaling law currently in favor in the U.S. is

the Kaye-Goldston[6] scaling law

$$\tau_{KG} \propto I_p^{1.24} P_{ext}^{-.58} R^{1.65} a^{-.49} K^{.28} n_e^{.26} A_i^{.5} B_0^{-.09} f_H \qquad (s)$$

where A_i is the atomic mass number of the ions. This scaling law is determined empirically from a larger set of data covering many tokamaks operating in the L-mode regime with sufficient auxiliary heating. To account for the improved confinement in the H-mode regime, the factor f_H is introduced. One normally takes f_H to be 2. The ASDEX H-mode scaling law is based on H-mode behavior in the ASDEX tokamak, which does not show degradation of the energy confinement time with increasing neutral beam power. Recent experiments with Doublet III-D[7] substantiate this result at an injection power up to 6 MW. The Doublet III-D results are quantitatively consistent with the ASDEX H-mode scaling law. The JET tokamak, however, shows degradation of the energy confinement time with neutral beam power and follows the Kaye-Goldston scaling law with a H-mode factor, f_H, of about 2.

The use of either of these scaling laws represents a considerable extrapolation from the data on which they are based when applied to either D-T or D-^{3}He operation. A rather strong assumption in the Kaye-Goldston scaling law is that charged particle heating by fusion reactions is no different than any other form of auxiliary heating. Since the fusion power achieved to date is negligible in comparison with the external heating power, there is no experimental evidence for, or against, this hypothesis. This assumption is made in the U.S. in order to introduce some conservatism in the analysis. It is possible, however, that drift-type instabilities can become worse at fusion plasma conditions and lead to even worse confinement. The lack of a good energy confinement scaling law is the biggest source of uncertainty in our analysis.

In the parametric studies we consider both the ASDEX H-mode and Kaye-Goldston scaling laws. In the Kaye-Goldston law the heating power, P_{ext}, can be eliminated by the self-consistency relation,

$$P_{ext} = P_t = \frac{3}{2} \frac{1}{\tau_E} \int (n_i T_i + n_e T_e)\, dV \,. \qquad (3.2\text{-}14)$$

With this relation, the Kaye-Goldston law can be rewritten in the form,

$$\tau_{KG} = \frac{.003\ R^{2.55} I_p^{2.95} A_i^{1.19} n_e^{.62} f_H^{2.38}}{a^{3.93} B^{.21} K^{.71} (n_i T_i + n_e T_e)^{1.38}} \quad (s) \ . \tag{3.2-15}$$

If the auxiliary heating power is small compared with the ohmic heating power, the empirically determined energy confinement time is[8]

$$\tau_\Omega = .071\ n_e\ a\ R^2\ q \quad (s) \ . \tag{3.2-16}$$

Goldston suggests that the two scaling laws can be combined in the form

$$\frac{1}{\tau_E^2} = \frac{1}{\tau_\Omega^2} + \frac{1}{\tau_{KG}^2} \tag{3.2-17}$$

to get a single result covering both ohmic and external heating. In our analysis we use Eq. (3.2-15) in conjunction with (3.2-16) to get the overall energy confinement time.

The transport energy loss is then given by Eq. (3.2-14) and is primarily due to the electrons in present experiments. The ion energy transport appears to be within a factor of 2 or 3 of the neoclassical energy transport. At the conditions appropriate for D-^{3}He the neoclassical energy confinement time for the ions is very long in comparison with the empirical energy confinement times given above.

The energy flow for the system is as follows: The fast ions produced by fusion reactions slow down in the plasma and transfer their energy to the background ions and electrons; the electrons get the larger share in a D-^{3}He plasma (about 80%). The fuel ions are also heated by the external heating system, if present, and lose energy to the electrons by Coulomb collisions. Because the energy flow has to be from the ions to the electrons, the ions are hotter than the electrons. The electrons radiate some of the power to the walls and transport the rest by thermal conduction across the magnetic field. Some of the external heating power may also be coupled to the electrons depending on the heating mechanism chosen. In this report, we assume that with suitable design of an ICRF system the power can be coupled only to the ions and neglect any coupling to

the electrons. If the plasma is ignited (M > 1) then the external heating power is zero and the radiation power must be increased to maintain a power balance.

The overall injection power, P_{inj}, required to sustain the plasma is determined by a power balance on the entire plasma

$$P_B + P_s + P_t = P_F + P_{inj} \quad . \tag{3.2-18}$$

The temperature difference between the electrons and the ions is determined by a power balance on the electrons if the plasma is not ignited, or on the ions if the plasma is ignited. For electron-ion energy transfer due to Coulomb collisions we use the Spitzer[9] formula. The equation for power balance on the electrons, for example, is

$$P_B + P_s + P_t = P_F \ (1 - f_i) + P_{ie} \tag{3.2-19}$$

where P_{ie} is the power flow from the ions to the electrons due to Coulomb collisions and f_i is the fraction[2] of the fusion power transferred to the ions. When the plasma is subignited the code finds a self-consistent solution to the above equations for a given ion temperature and calculates the injected power required to sustain that set of plasma conditions. If the plasma is ignited, the "injected" power is negative; in this case the equation for the ion power balance is solved and the code calculates the increased radiation power loss required to maintain a power balance on the plasma.

In the next section we present a series of parametric calculations to determine the influence of various effects on the ignition margin, or energy multiplication. From these calculations we can determine the "optimum" conditions to achieve breakeven or ignition in a D-^{3}He tokamak.

References for Section 3.2

1. F. Troyon et al., Plasma Physics Cont. Fusion 5, 261 (1980).

2. B.Q. Deng and G.A. Emmert, "Fast Ion Pressure in Fusion Plasmas", University of Wisconsin Fusion Technology Institute UWFDM-718, Jan. 1987.

3. J. Rand McNally, Nuclear Fusion/Technology, 2, 9 (1982).

4. B.A. Trubnikov, "Universal Coefficients for Synchrotron Emission from Plasma Configurations", Reviews of Plasma Physics, vol. 7, Plenum Press (1979) 345.

5. The NET team, "NET Status Report 1985", NET Report 51, Commission of the European Communities (1985).

6. S.M. Kaye and R.J. Goldston, Nuclear Fusion 25, 65 (1985).

7. K.H. Burrell, S. Ejima, et al., Phys. Rev. Lett. 59, 1432 (1987).

8. R.J. Goldston, Plasma Physics Cont. Fusion 26, 87 (1984).

9. L. Spitzer, Jr., Physics of Fully Ionized Gases, Interscience Publishers (1962) p. 135.

3.3 Parametric Studies

The plasma physics model described in Section 3.2 forms the basis for estimating the performance of NET, and variations of it, using D-^{3}He as the fuel. In this section we present the results of parametric studies using this model. In these studies one or more input parameters are scanned across some given range. A summary of the various parameter scans investigated is given in Table 3.3-1.

We first consider the NET-DT and NET-EP tokamak (see Chapter 2) with no changes in the dimensions or magnetic field, but change only the fuel composition from D-T to D-^{3}He and change the operating temperature to that required for D-^{3}He, with a corresponding change in the injected power because of the higher operating temperature. The objective here is to investigate the physics of ions slowing down in a hot plasma and the approach to Q = 1 with little or no modification to the NET device. This is parameter scan A in Table 3.3-1.

In parameter scan B we investigated a possible variation on the NET parameters to take advantage of the fact that tritium breeding is not required and less space for neutron shielding is needed with D-^{3}He (the details are in Chapter 4.) This means that the plasma major radius can be reduced. The reduced major radius increases the plasma current if the MHD safety factor, q, is held constant; the magnetic field at the plasma is also increased by the inward displacement. However, the magnetic field at the TF coil remains unchanged. These adjustments improve both the fusion power density and the confinement of the plasma.

The third parameter scan (C), we considered was to increase the toroidal field at the TF magnet while retaining the original plasma and machine dimensions. This gives a more modest increase in the plasma current, at constant q, but increases the fusion power density, while also raising the Q-value.

Table 3.3-1. Regimes Studied for the Burning of

D-^{3}He Fuel in a NET Class Tokamak

Parameter Scan	Objective	B_{max} at Coil	Inboard Shield Thickness	Plasma Radius R_p	Plasma Current I_p	Plasma Elongation K
A-1	Physics of Fast Ions	Ref*	Ref	Ref	Ref	Ref
A-2	Breakeven	Ref	Ref	Ref	Ref	Ref
B	High Q Operation	Ref	Thinner	Smaller	Higher	Ref
C	High Q Operation	Higher	Ref	Ref	Higher	Ref
D	Ignition	Higher	Thinner	Smaller	Higher	Larger

*Ref means as designed by the NET team for either the NET-DT or NET-EP configurations and reported in Chapter 2. Parameter scan A-1 uses the NET-DT data; all other scans use the NET-EP data as the starting point. These data are given in Table 2-1.

Finally, in parameter scan D we considered the effect of both reducing the major radius and increasing the toroidal field and/or the plasma elongation in order to see what parameters are required to achieve ignition with D-^{3}He in a modified version of NET.

In the parameter scans above, we leave out impurities and assume the particle confinement time, τ_p, equals the energy confinement time, τ_E. This is done in order to see what the potential performance is under optimum conditions (clean plasma, little ash accumulation). Later we consider the reduction of the performance caused by ash and impurity accumulation.

3.3.1 D-^{3}He in the Reference NET-DT and NET-EP Designs (Parameter Scan A)

Shown in Fig. 3.3-1 is the Q-value that can be obtained in the reference NET-DT tokamak (NET-DT described in Chapter 2) for the two scaling laws, Kaye-Goldston and ASDEX H-mode, versus the average ion temperature. We see that the optimum ion temperature (all temperatures quoted in this section are density weighted and averaged over the plasma volume) is about 45 keV. The higher temperature required for D-^{3}He arises from the fact that $\langle\sigma v\rangle_f/T^2$ peaks at 55 keV for D-^{3}He versus 13 keV for D-T, as shown in Fig. 3.1-2; an average temperature of 45 keV corresponds to a central temperature of about 80 keV for the profiles used in this analysis. It is obvious from Fig. 3.3-1 that the plasma performance is much more favorable for ASDEX scaling than for Kaye Goldston scaling. It is gratifying to note that $Q \tilde{=} 1$ could be achieved in the NET device as it is presently designed with essentially no modifications (or added cost)!

Shown in Fig. 3.3-2 is the injected power required to maintain the plasma at the operating temperature and the resulting fusion power; the injected power decreases with increasing ion temperature for ASDEX H-mode scaling since the beta is kept constant at the Troyon limit. Hence density is decreasing as the temperature is raised in Fig. 3.3-1 and 3.3-2. The power levels required are excessive if the confinement is Kaye-Goldston, but within the present NET limits if the confinement is ASDEX H-mode. Note that this power is the power coupled to the plasma since the details of the heating mechanism, and hence the coupling efficiency are beyond the scope of this study. (The NET design calls for 50 MW of coupled power for plasma startup and heating to ignition.)

Shown also in Fig. 3.3-2 is the fusion power released versus ion temperature. Here the fusion power is defined as the total power released in charged particles due to fusion reactions. The power in the neutrons produced is not included. Almost all the fusion power is due to D-^{3}He reactions, although there is a small amount of D-D power also.

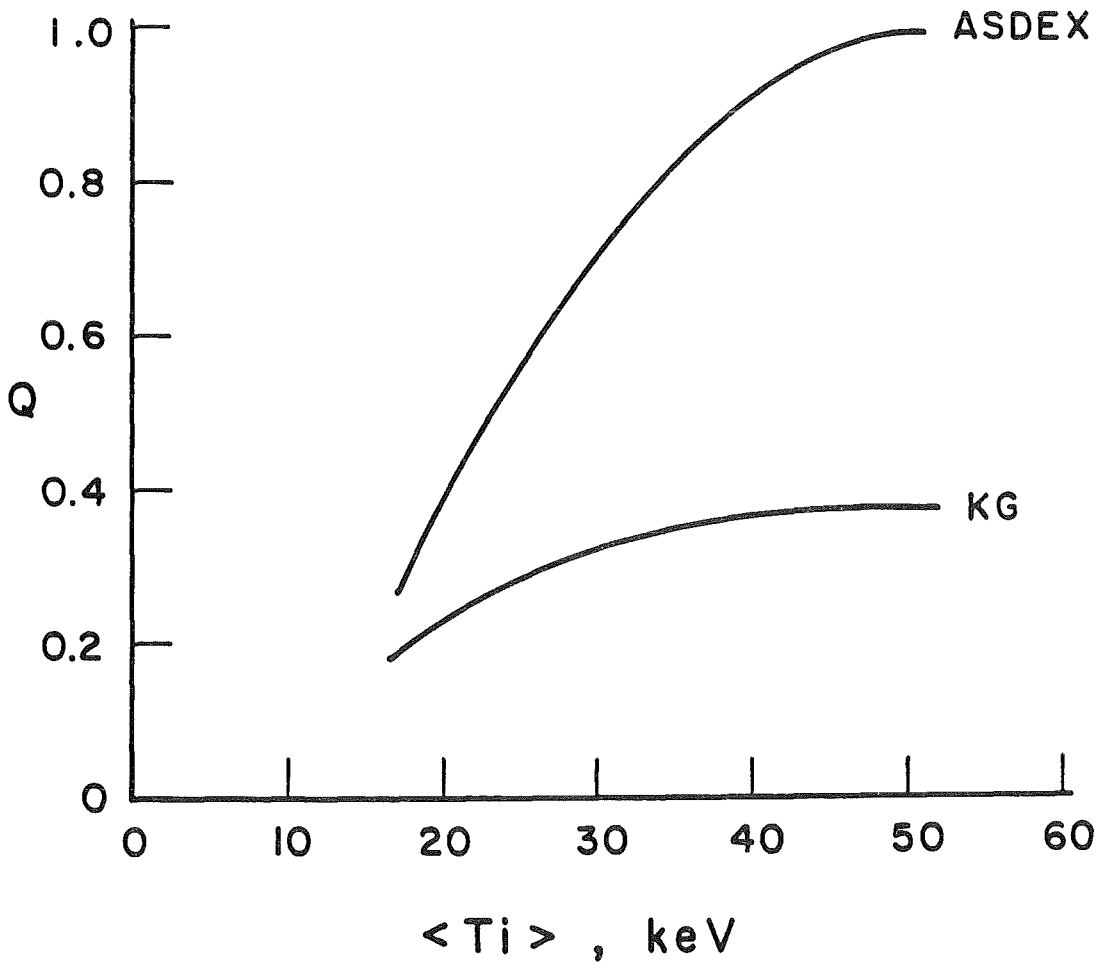

Fig. 3.3-1. Energy multiplication, Q, versus average ion temperature for D-^{3}He operation in NET-DT for both ASDEX H-mode and Kaye-Goldston energy confinement scaling.

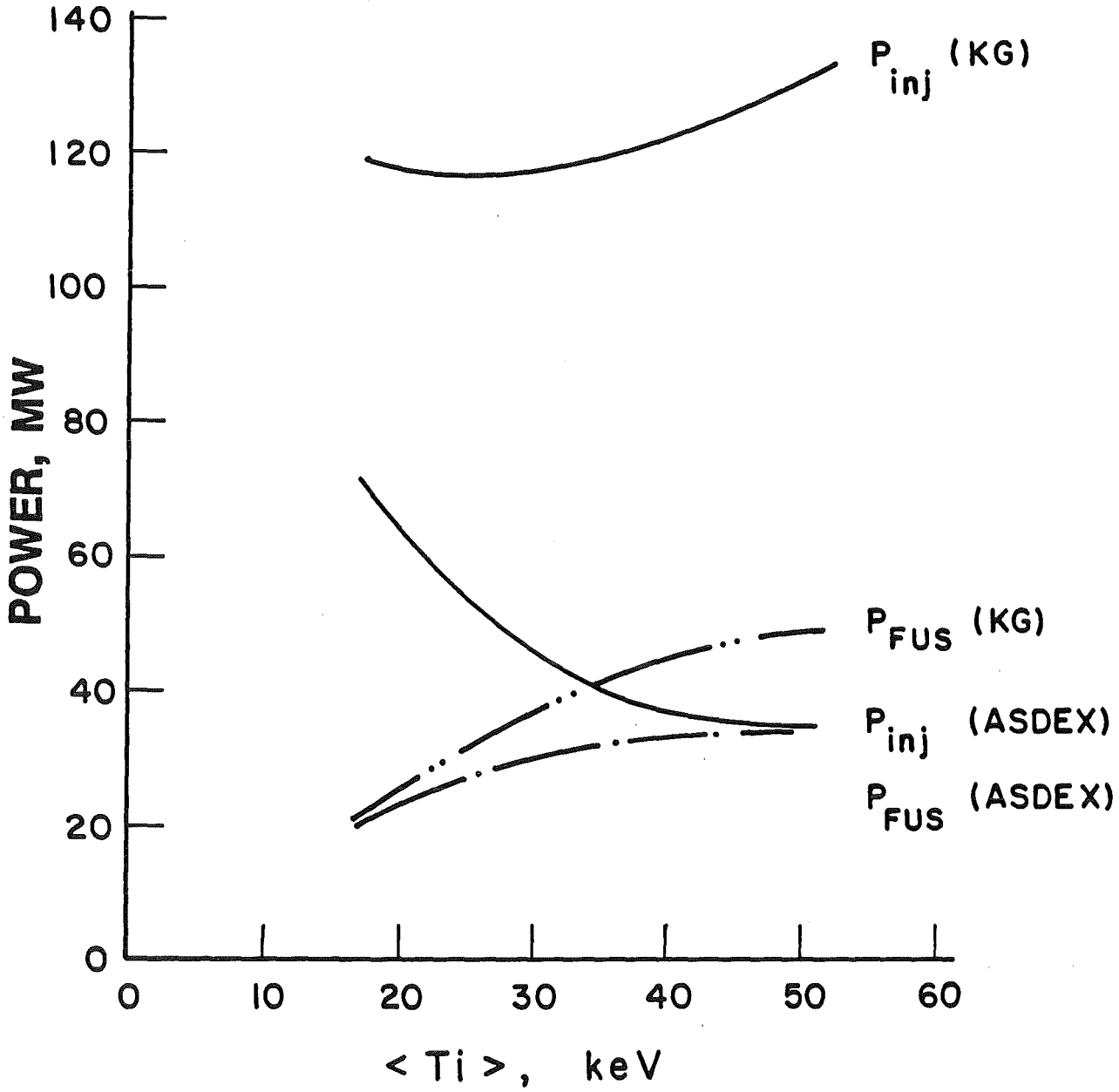

Fig. 3.3-2. Injection power and fusion power versus average ion temperature for NET-DT for both ASDEX H-mode and Kaye-Goldston energy confinement scaling.

The fusion power is slightly higher in the Kaye-Goldston scaling; this is because the electrons run colder because of the poorer confinement. This reduces the electron pressure and allows a slightly higher ion density for a given beta. The relatively low fusion power obtained in regime A is of concern since the fusion power density is low in the plasma. Consequently, the plasma will be sensitive to impurity accumulation which, in turn, affects the fusion power and the Q-values. The effect of impurity accumulation is considered later in this section.

Shown in Fig. 3.3-3 is the Q-value obtained with the NET-EP (see Chapter 2) configuration. The injected power and the fusion power versus ion temperature are shown in Fig. 3.3-4. We see that with ASDEX H-mode scaling a Q value of 1.45 is obtainable with an injection power of slightly less than 40 MW. With Kaye-Goldston scaling the maximum Q-value is less than .5 and the required injection power is almost 170 MW. Consequently, if the ASDEX H-mode scaling law holds, one can achieve breakeven in NET-EP with no change in the basic machine parameters except for the fuel composition and the operating temperature. There will need to be some modifications to the auxiliary heating system because of the change in fuel and operation temperature.

3.3.2 Reduced Major Radius Variations of NET-EP (Parameter Scan B)

The NET-DT and NET-EP reference designs have a large region for a thick tritium breeding blanket and shield between the plasma and the TF magnet. This is not needed for D-^{3}He operation. The blanket can be removed and the shield replaced by a thinner shield optimized for the D-^{3}He neutron spectrum (see Chapter 4). Consequently, the plasma major radius can be reduced; this leads to a lower plasma aspect ratio, higher beta, and higher plasma current if the MHD safety factor is held constant. The higher plasma current increases the energy confinement time. In addition, the reduced major radius of the plasma increases the magnetic field at the plasma and increases the fusion power output. All this is accomplished with the original TF coil design and operating conditions.

Shown in Fig. 3.3-5 is the effect of reducing the major plasma radius on the Q-value and the plasma current. In this figure, f_d is 0.65, and the average ion temperature is kept constant at 37 keV. The Q-value reaches a value of about 2.9 for ASDEX H-mode scaling and the plasma current increases from 14.8 to 20 MA when the plasma radius is reduced from 5.41 m to 4.61 m. The required injection power decreases slightly from

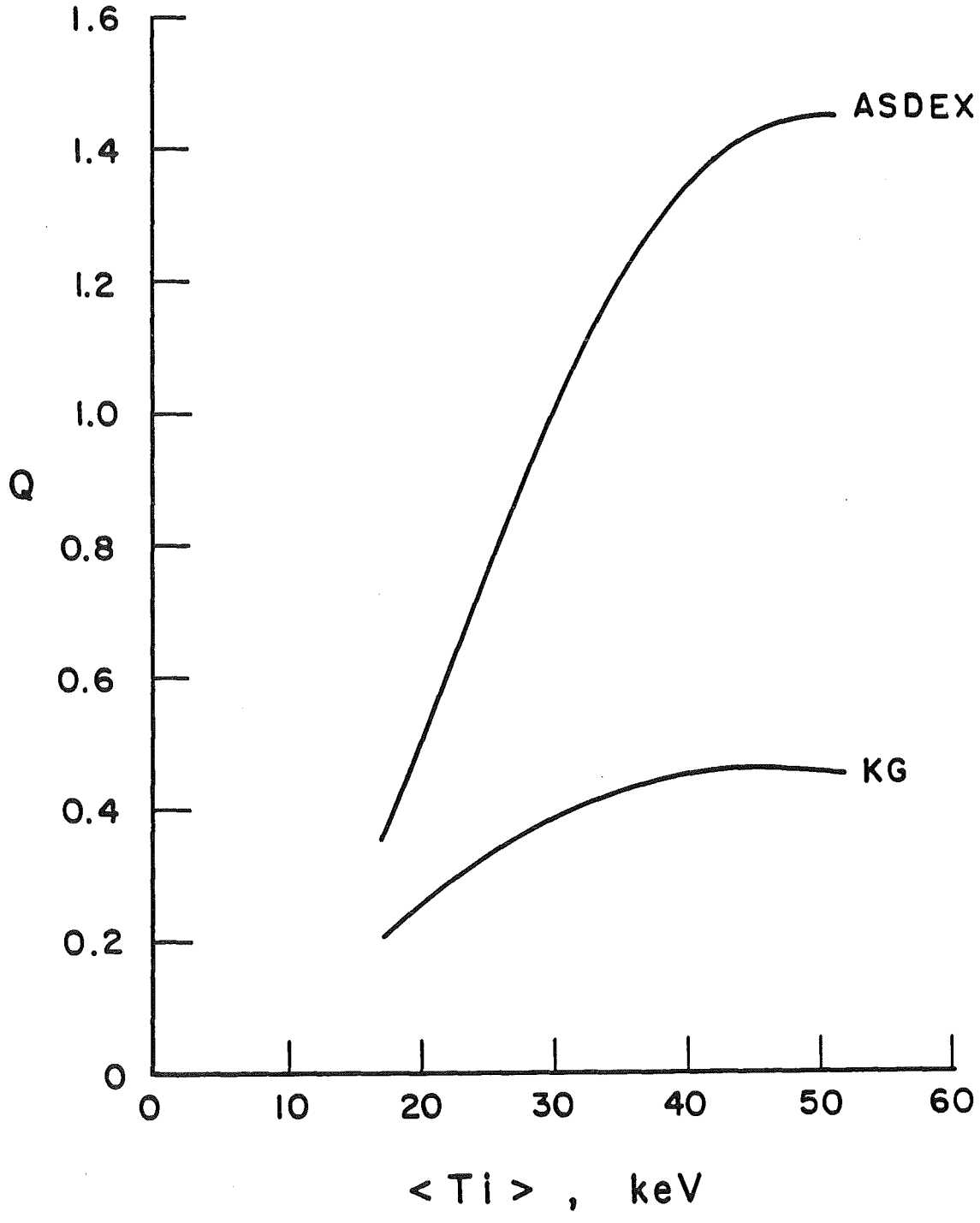

Fig. 3.3-3. Energy multiplication, Q, versus average ion temperature for NET-EP for both ASDEX H-mode and Kaye-Goldston energy confinement scaling.

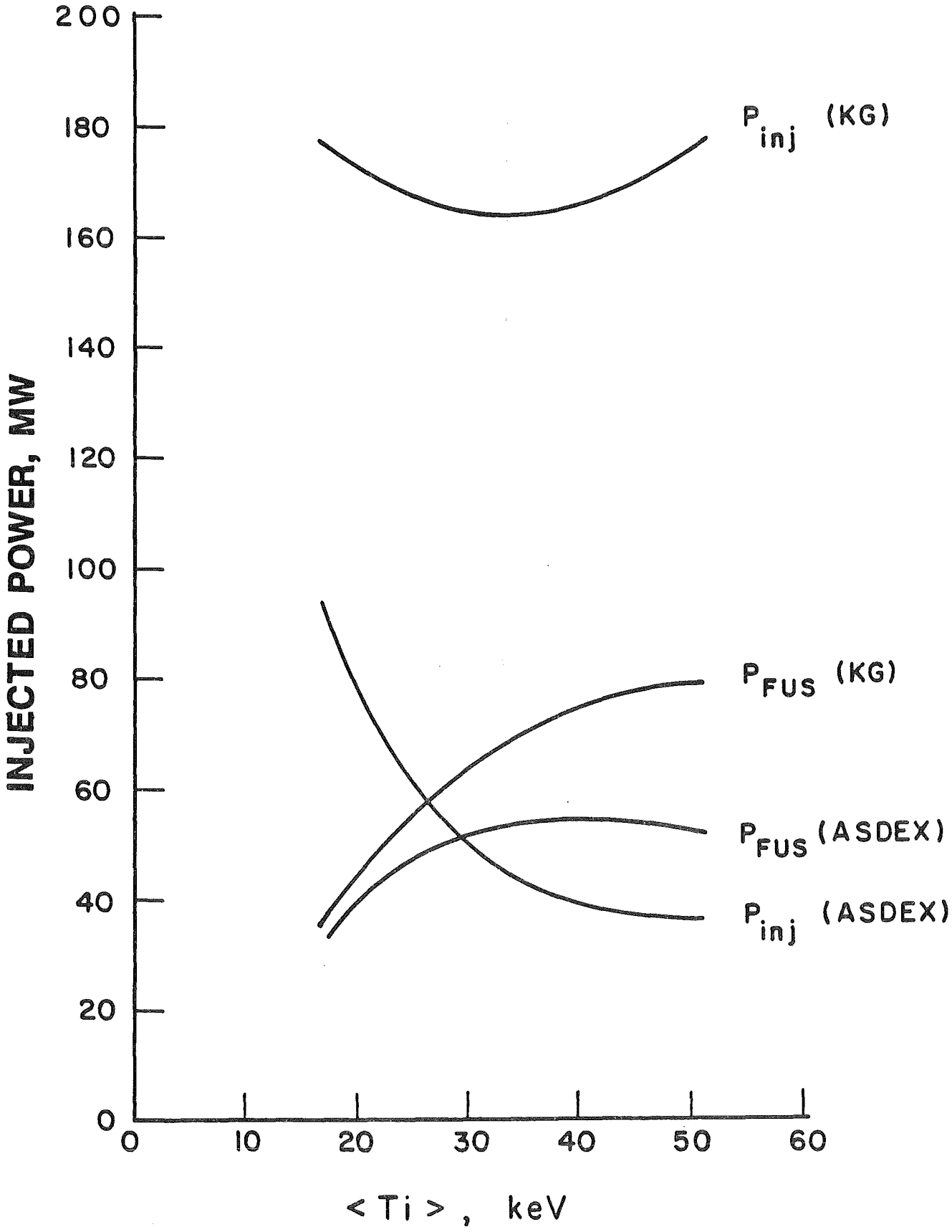

Fig. 3.3-4. Injection power and fusion power versus average ion temperature for NET-EP for both ASDEX H-mode and Kaye-Goldston energy confinement scaling.

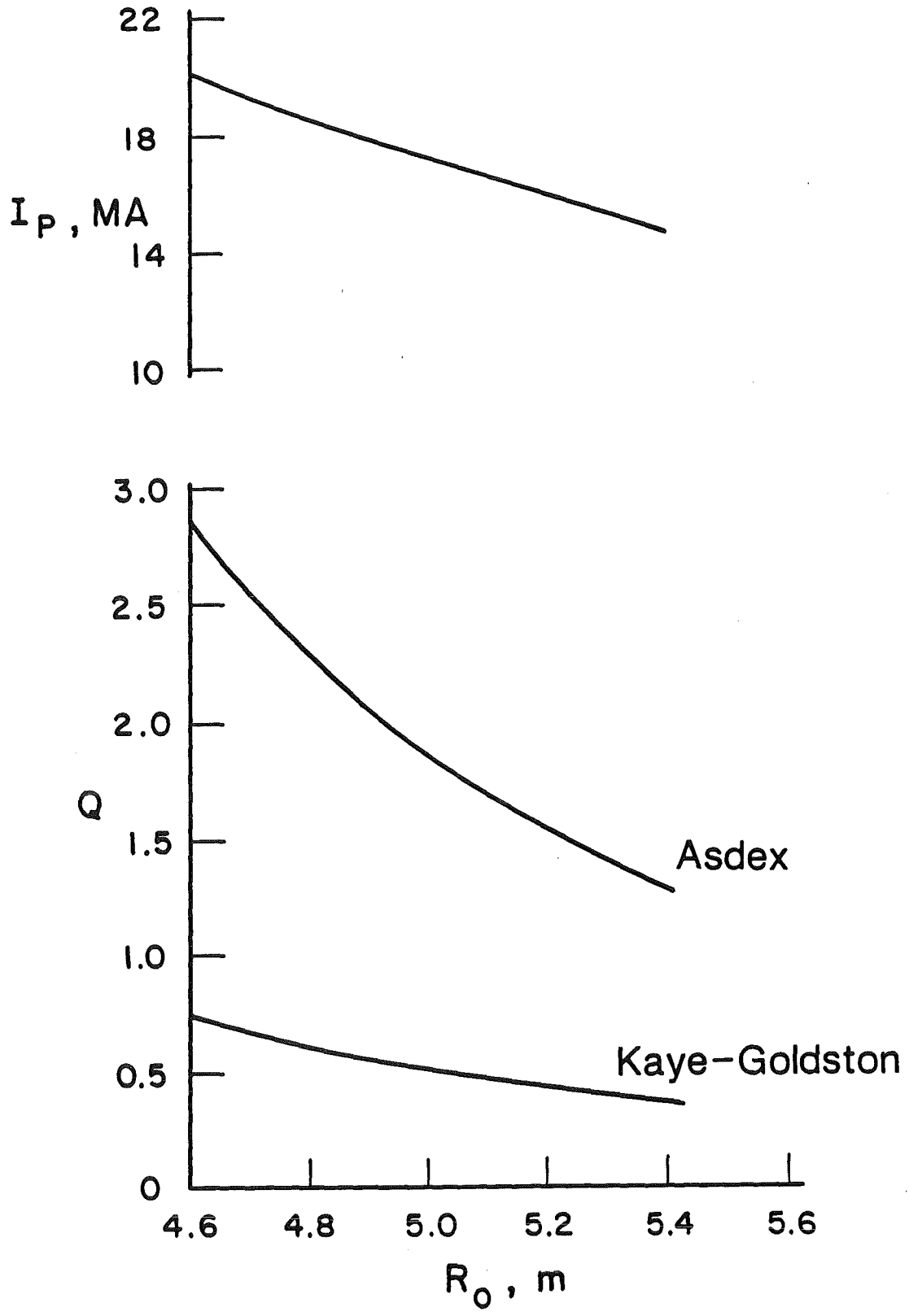

Fig. 3.3-5. Q and plasma current versus major radius; a = 1.69 m, B_c = 10.4 T, K = 2.17, $\langle T_1 \rangle$ = 37 keV.

40 MW to 35 MW. For Kaye-Goldston scaling, the ignition margin increases to .74 and the injection power to 180 MW when the major radius is reduced to 4.61 m.

At a major radius of 4.61 m, the space available for the shield, cryostat, and inboard scrape-off layer has been reduced to a total of 45 cm. Because of the greatly reduced neutron wall loading (0.019 MW/m^2), the magnet can still be protected adequately against nuclear heating and radiation damage effects. This is discussed further in Chapter 4. The production rate of neutrons can be reduced even further by changing the fuel mixture. The value f_d = .65 used so far has been chosen to optimize the Q-value. Reducing the percentage of deuterium in the fuel will reduce the D-D reactions and the production of tritium. Shown in Fig. 3.3-6 is the effect of f_d on the Q-value and the amount of power in D-T and D-D neutrons. This graph corresponds to the R = 4.61 m point in Fig. 3.3-5. We see that f_d = .65 is about the optimum fuel mixture and Q drops sharply as the deuterium fraction is increased or reduced. The reason for f_d = .65 being the optimum, and not f_d = .5 as in D-T, is that helium ions have Z = 2. Consequently, increasing the deuterium fraction (starting from .5, for example) decreases the electron density and the electron pressure. Consequently, the total ion density can be increased to maintain constant beta. This more than compensates for the reduced helium fraction in the fuel. Of course, if the helium fraction is too low, then the increased ion density is not sufficient and the fusion power drops as f_d is increased further. In addition, reducing the electron density reduces the bremsstrahlung and synchrotron radiation losses and improves Q.

It is worthwhile to consider the relative magnitude of the various loss terms to see the sensitivity of a possible operating point to uncertainty in the various loss terms. Shown in Fig. 3.3-7 is the power in the various loss mechanisms normalized to the fusion power versus ion temperature. This curve is for the R = 4.61 m, f_d = .65 case. We see that in the temperature range where Q is largest ($\langle T_i \rangle$ = 35 to 50 keV) transport is the largest single loss; synchrotron is next and bremsstrahlung is close behind. We see that bremsstrahlung dominates at low T_i, but drops rapidly as T_i increases; this is because the density is high when the temperature is low. Consequently, the Q-values given in this report are rather sensitive to uncertainties in the energy confinement time scaling laws.

The above calculations are based on the ASDEX H-mode scaling law for energy confinement. We now consider what H-mode factor is necessary to achieve breakeven (Q = 1) in a reduced major radius version of NET-EP. We fix the major plasma radius at

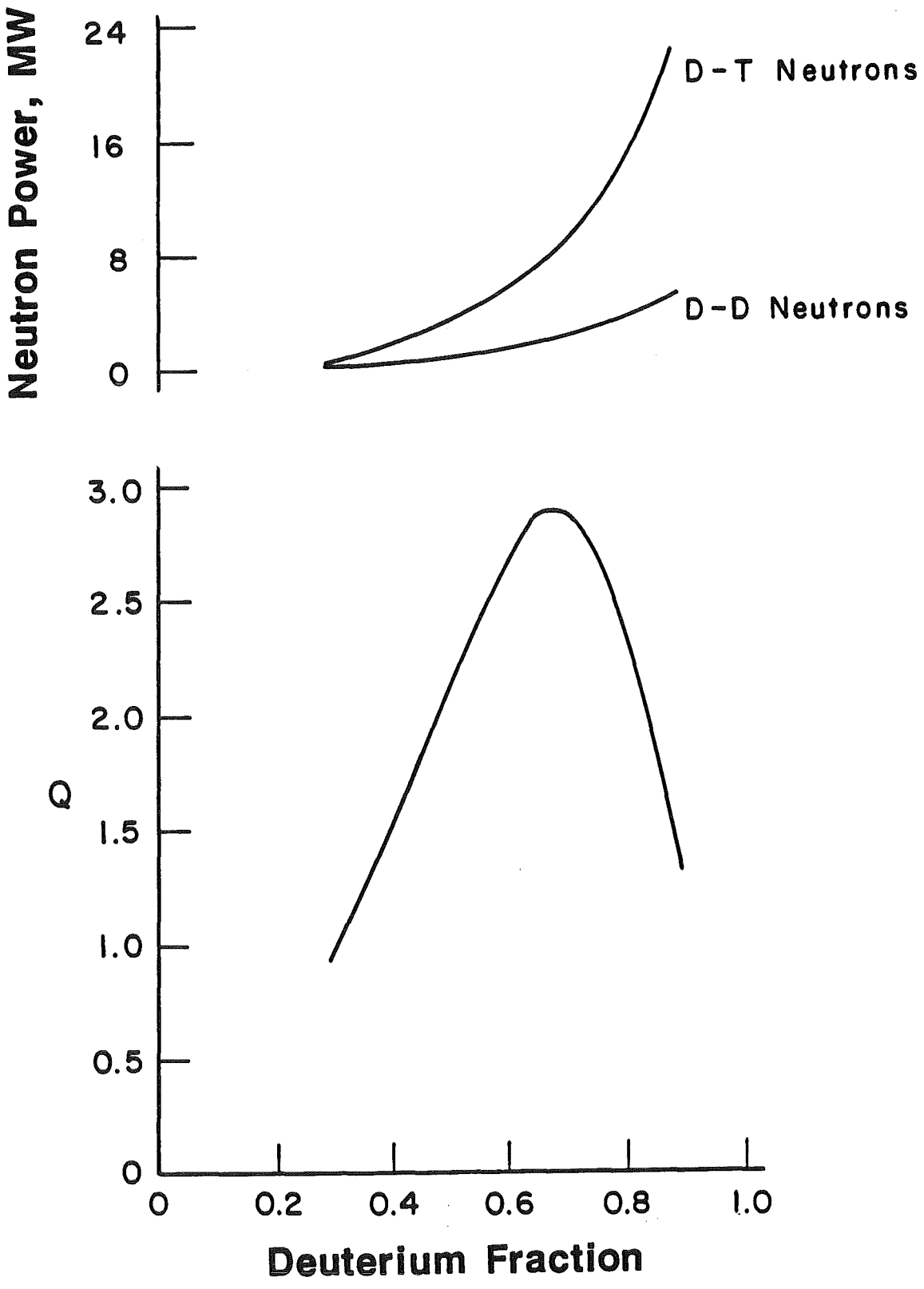

Fig. 3.3-6. Effect of changing fuel mixture on the energy multiplication, Q, and neutron power. R = 4.61 m, B_c = 10.4 T, $\langle T_i \rangle$ = 37 keV, ASDEX H-mode scaling.

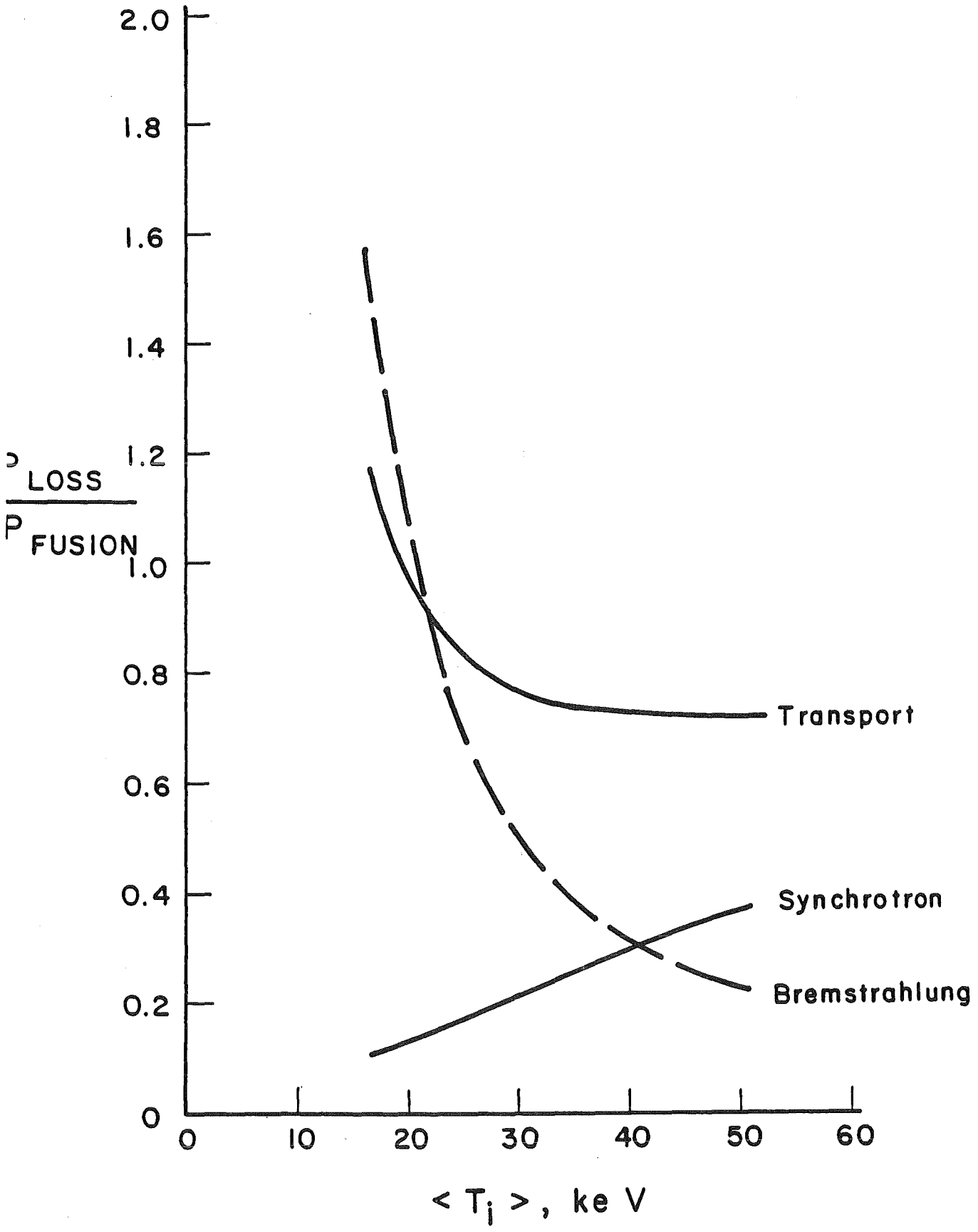

Fig. 3.3-7. Distribution of power loss versus average ion temperature. R = 4.61 m, B_c = 10.4 T, f_d = .65, ASDEX H-mode scaling.

4.61 m and the average ion temperature at 37 keV. Shown in Fig. 3.3-8 is the Q-value obtained versus the H-mode factor. Recall that the H-mode factor is defined as the improvement in energy confinement over the L-mode scaling law due to the H-mode. Consequently, an H-mode factor of 1 means no H-mode at all. Typical values achieved experimentally are about 2 to 3. We see that an H-mode factor of about 2.5 is necessary to obtain breakeven in this device. Further increases in the H-mode factor do not lead to significant increses in Q because of the saturation effect of the ohmic confinement term in Eq. (3.2-17). The required injection power at an H-mode factor of 2.5 is about 130 MW; this is a rather large amount of power in comparison with the 50 MW planned for NET and would require 100-200 million dollars in heating equipment.

3.3.3 Increased Magnetic Field Variations of NET-EP (Parameter Scan C)

A second option for improving the performance of NET-EP with D-^{3}He is to increase the magnetic field strength without changing the plasma dimensions. This regime does not benefit from the reduced aspect ratio obtained with the reduction of major plasma radius, but it has a lesser impact on the poloidal field magnet system since the plasma position is not changed. Shown in Fig. 3.3-9 is the Q-value and the plasma current versus maximum magnetic field strength at the TF magnet. This figure uses ASDEX H-mode scaling with the mean ion temperature held at 50 keV. As expected, we see that increases in the magnetic field strength also increase Q and the current. Comparing Figs. 3.3-5 and 3.3-9, we see that increasing B_c gives more increase in Q for the same increase in plasma current than reducing the plasma radius. Consequently, if the increased plasma current is a major concern, it may be better to get to high Q by increasing B_c at constant R, rather than reducing R at constant B_c. Of course, raising B_c does increase costs and we have not considered the exact amount within the context of this study. However, it appears that it should be less than 10% of the total cost of NET.

3.3.4 Ignition in NET with D-^{3}He (Parameter Scan D)

Finally, we consider the possibility of achieving ignition in a D-^{3}He plasma. To achieve ignition with ASDEX H-mode scaling, it appears necessary to both reduce the major radius and aspect ratio, and to increase the magnetic field at the TF coil. In addition, one can consider raising the plasma elongation; this affects both the beta and

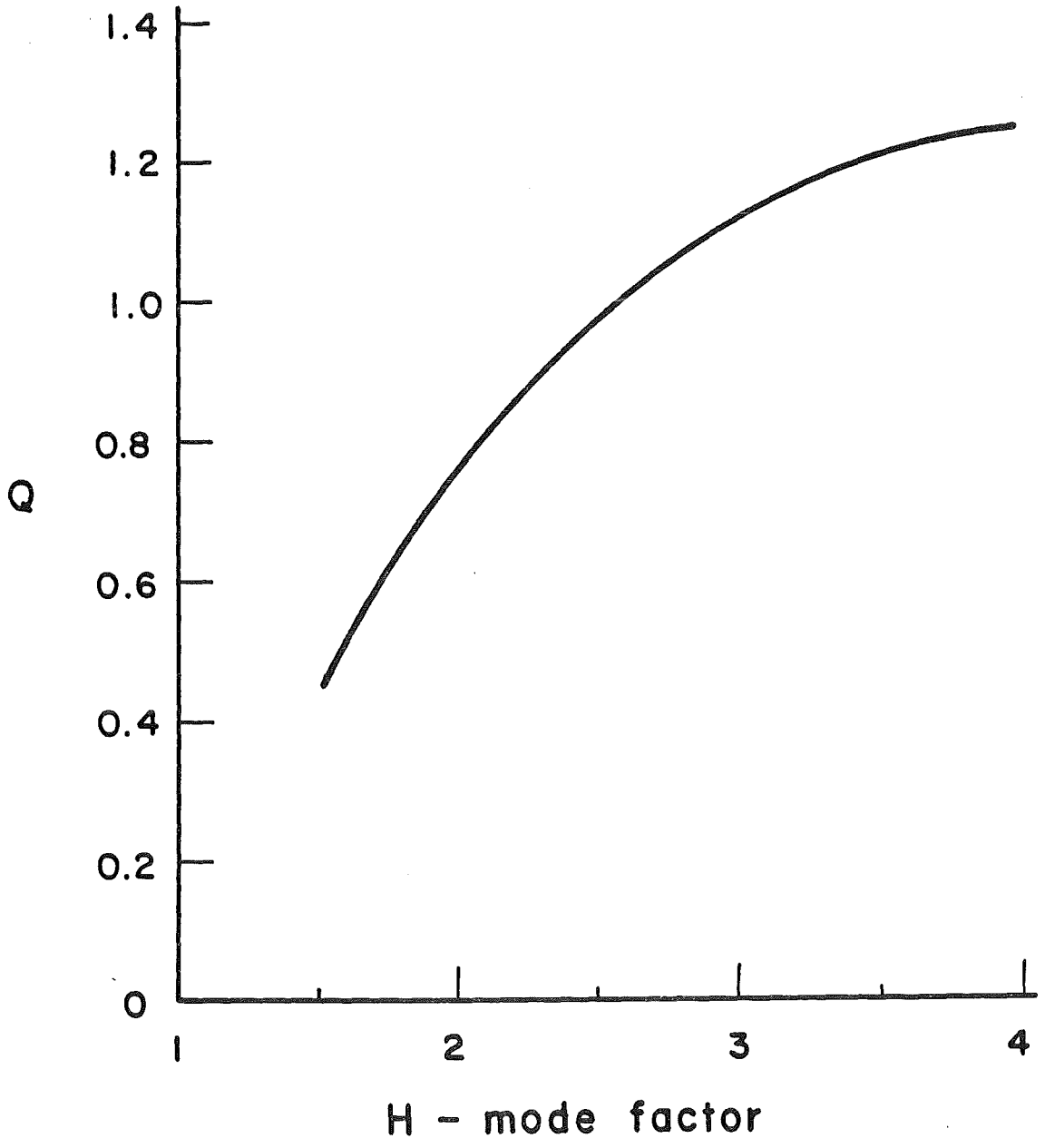

Fig. 3.3-8. Effect of the Kaye-Goldston H-mode factor on the energy multiplication, Q. R = 4.61 m, B_c = 10.4 T, f_d - .65, $\langle T_i \rangle$ = 37 keV.

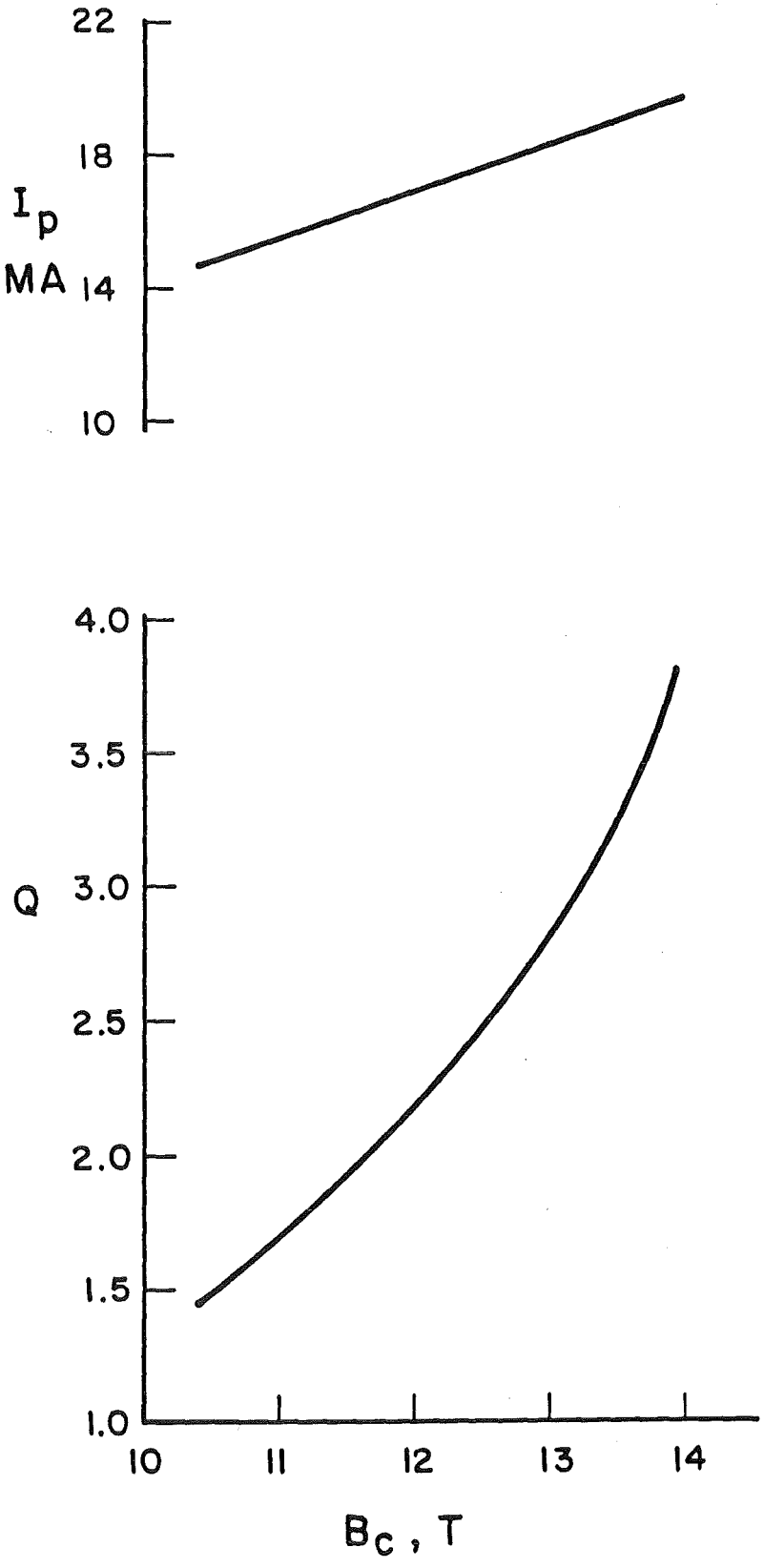

Fig. 3.3-9. The effect of raising the toroidal field at the magnet on the energy multiplication, Q, and the plasma current, I_p. R = 5.41 m, f_d = .65, $\langle T_i \rangle$ = 50 keV.

the confinement since it raises the plasma current. Shown in Fig. 3.3-10 is the elongation required for ignition versus magnetic field strength at the TF magnet. The major plasma radius is held constant at 4.61 m and the plasma half-width is 1.69 m. We see that one can trade elongation for magnetic field and still achieve ignition. It is somewhat surprising that the plasma current is essentially constant at about 29 MA along the curve in Fig. 3.3-10. This is probably due to strong coupling between plasma current, energy confinement, and beta. The range of plasma elongations shown in Fig. 3.3-11 is above the value (κ = 2.2) considered to be the limit from a MHD point of view. The higher magnetic field strength (13 T) is not considered to be feasible within the context of the guidelines used for the NET toroidal field magnet design. Because of these limitations, ignition in NET is not likely.

The above analysis assumes the fuel is not spin polarized. It seems to be well accepted that using spin polarized d and ^{3}He increases the reaction rate of the process d(^{3}He,p)^{4}He by a factor of 1.5.[1] The same authors claim a reduction of the cross section for the reaction channel d(d,n)^{3}He of about 0.6 at 75 keV if polarized deuterons are used; this is based on calculations of the corresponding matrix elements.

Another group predicts an even stronger reduction of the spin polarized d(d,n)^{3}He reaction by more than a factor of ten.[2] Thus, although the results are still controversial, taking the more pessimistic result into account it should be possible to decrease the ratio of the neutron power to total ion power in a D-^{3}He mixture by at least a factor of 2/3 for the 14.1 MeV neutrons and by a factor of about 3 for the 2.5 MeV neutrons. Questions concerning the production of polarized fuel as well as the expected lifetime of the particles in the polarized state are discussed in Reference 3.

The effect of polarizing the fuel on the ignition condition is easily assessed by increasing the effective $\langle\sigma v\rangle_f$ by 50%. With this change ignition is achieved at a plasma current of 21 MA using the same parameters as in Fig. 3.3-10. The required magnetic field at the TF magnet is 11 T at an elongation of 2.17 or 10.5 T at an elongation of 2.25.

3.3.5 Modest Changes to NET-EP

In Sections 3.3.2, 3.3.3, and 3.3.4 we considered parameters where substantial changes to the inboard shield and/or TF magnets are required. While the impact of these changes on the total cost of NET is small, nevertheless these changes can have an adverse effect of the operation schedule of NET since the shield for D-^{3}He operation will have to be replaced with that required for D-T operation. It is worthwhile to consider in

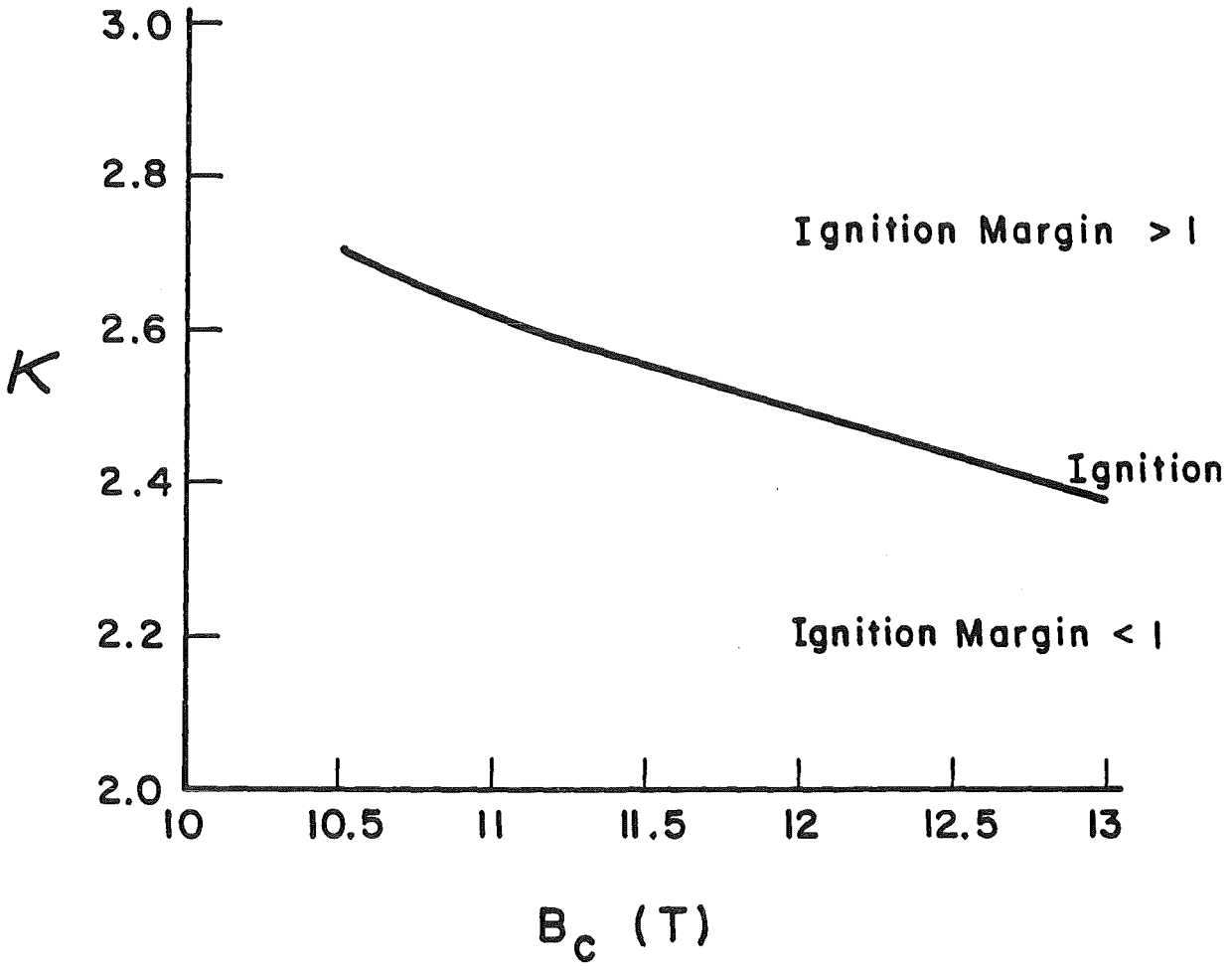

Fig. 3.3-10. The elongation required to achieve ignition versus toroidal magnetic field at the magnet. Points above the curve have ignition margin above 1; points below are subignited. R = 4.61m, a = 1.69 m, $\langle T_i \rangle$ = 37 keV, ASDEX H-mode scaling.

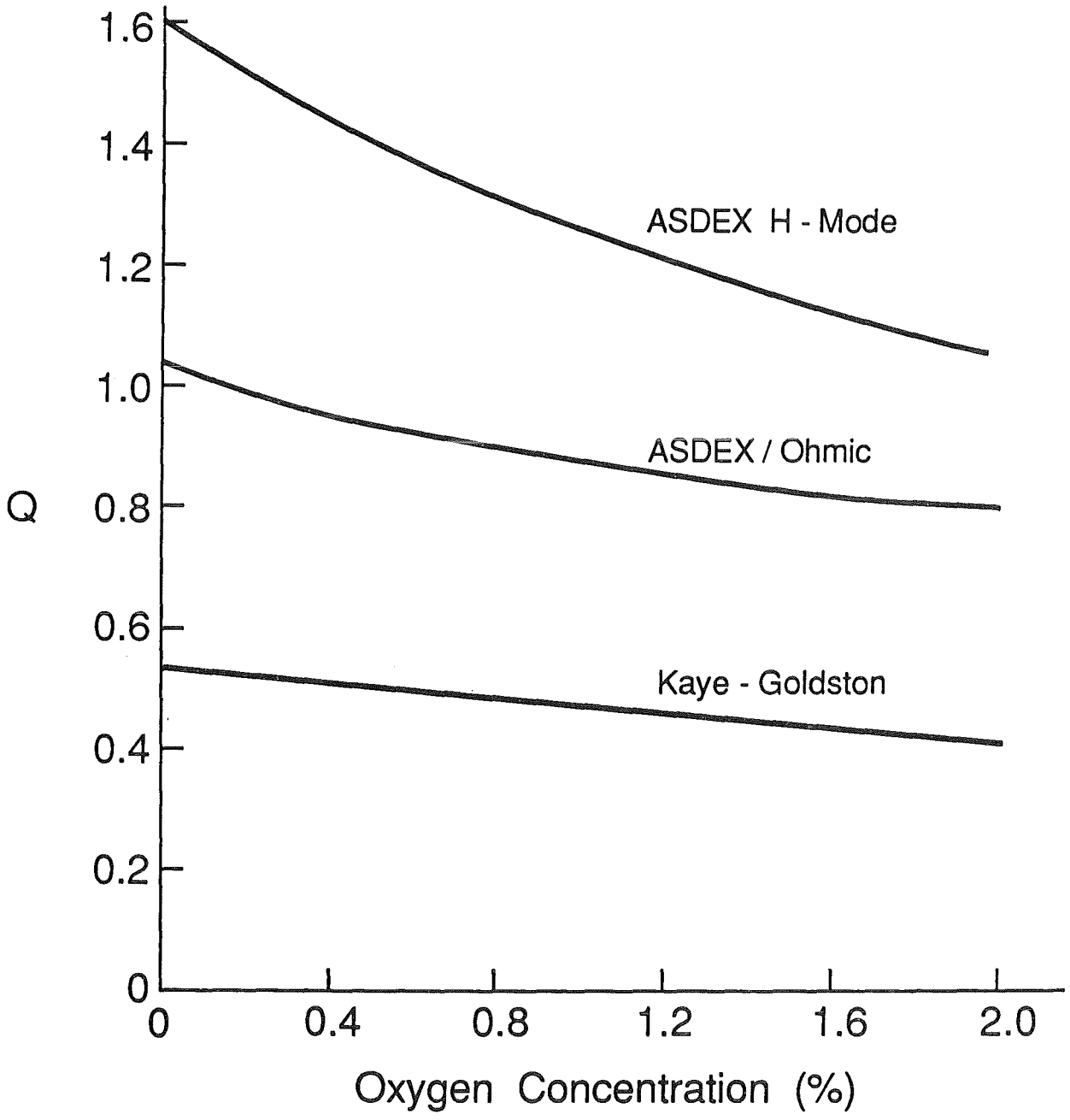

Fig. 3.3-11. Effect of impurity concentration on the Q-value for case A-3, using ASDEX H-mode, ASDEX/Ohmic, and Kaye-Goldston scaling.

more detail D-^{3}He operation using the D-T shield. The inboard blanket is assumed to be left out during the D-^{3}He phase and protective tiles are installed on the face of the steel D-T shield. Postponing the installation of the inboard blanket to after the end of the D-^{3}He phase of operation allows the plasma major radius to be reduced by 27 cm. In this section we consider the Q-value that can be achieved with this configuration, referred to as case A-3 in later discussion. We also consider the effect of impurity and ash accumulation on the Q-value achieved.

Shown in Fig. 3.3-11 is the effect of impurity concentration on the Q-value, assuming ASDEX H-mode confinement scaling. The impurity is assumed to be oxygen and is given as a percentage of the total fuel ion density. We see that raising the concentration from zero to 2% decreases Q from 1.6 to 1.0. In this calculation, the impurity affects the plasma through the increase of the electron concentration (required for quasi-neutrality) and the corresponding reduction of the fuel density for a given β. The synchrotron and bremsstrahlung radiation losses are also increased but the impurity ions are assumed to be fully stripped so that there is no line radiation from the impurity ions to consider.

The subject of particle confinement is at least as poorly understood as energy confinement in tokamaks. Particle confinement affects the power balance through the accumulation of ash in the plasma. Shown in Fig. 3.3-12 is the effect of varying the ratio of the particle confinement time to the transport energy confinement time, which is taken to be ASDEX H-mode confinement. This figure assumes the plasma has a 1% oxygen impurity concentration. We see that Q reduces from 1.26 at τ_p/τ_E = 1 to .96 at τ_p/τ_E = 10. The current understanding is that τ_p/τ_E is about 3 in the steady state for present discharges, but the effective τ_p is much less than τ_E in transients; this difference is because of the pinch effect playing a role in the steady state transport.

We see that we can tolerate a combined effect of 1% oxygen content and τ_p/τ_E = 3 and still achieve Q = 1.2 in this mildly revised NET configuration. With no impurities and τ_p/τ_E = 1, Q = 1.6, so the loss in Q is about 25%.

The operating space for case A-3 is shown in Fig. 3.3-13 for ASDEX H-mode scaling. This figure shows the injection power required to achieve a given average ion density and ion temperature; the electron temperature is calculated self-consistently. Also shown in the figure is the Q-value obtained at those plasma parameters. One can see the reduction in Q caused by having less power available. For example, at an injected power of 20 MW, the Q-value is .4. This figure also illustrates the path to take

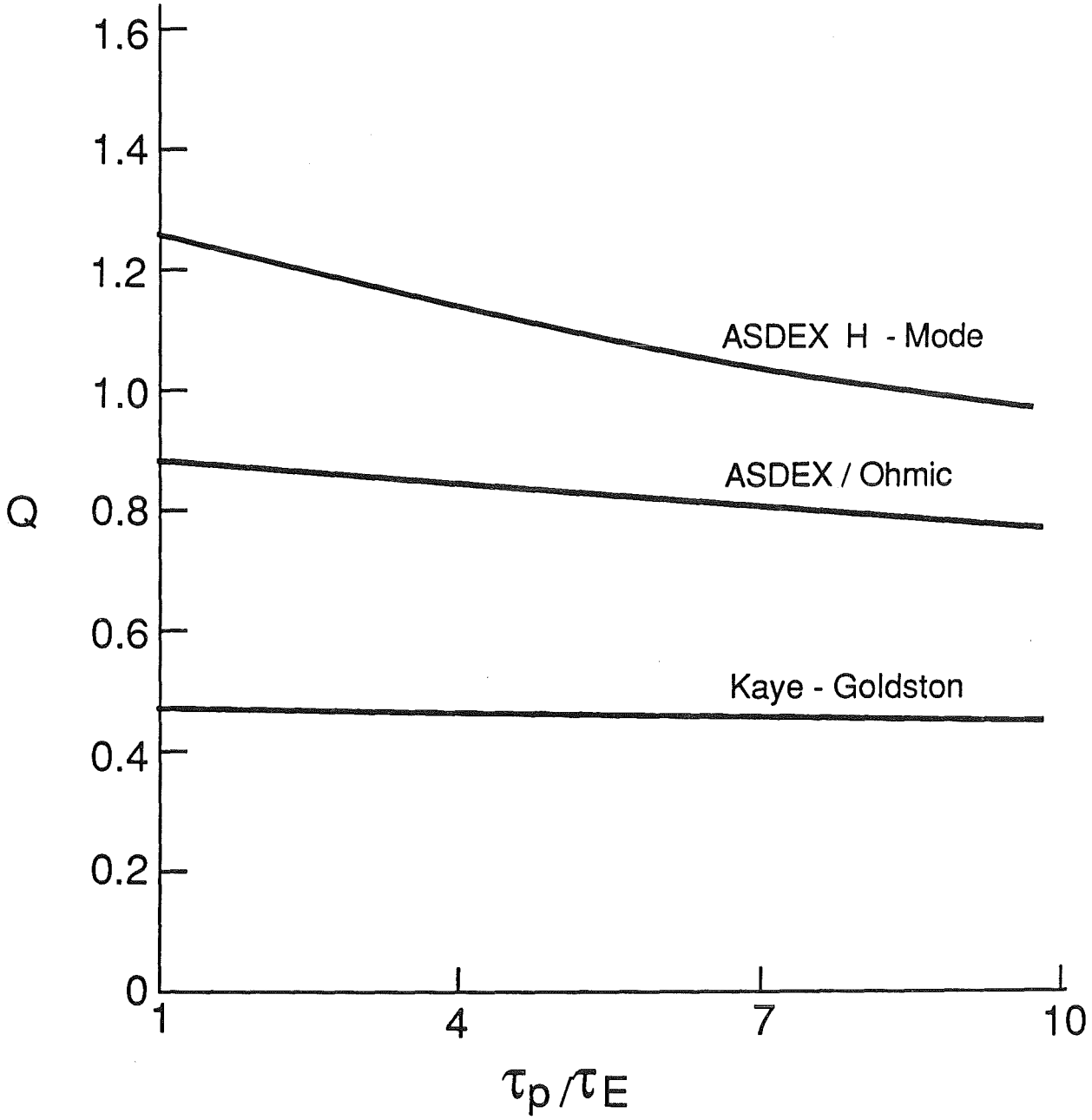

Fig. 3.3-12. Effect of varying central particle confinement time on the Q-value for case A-3, using ASDEX H-mode, ASDEX/Ohmic, and Kaye-Goldston scaling.

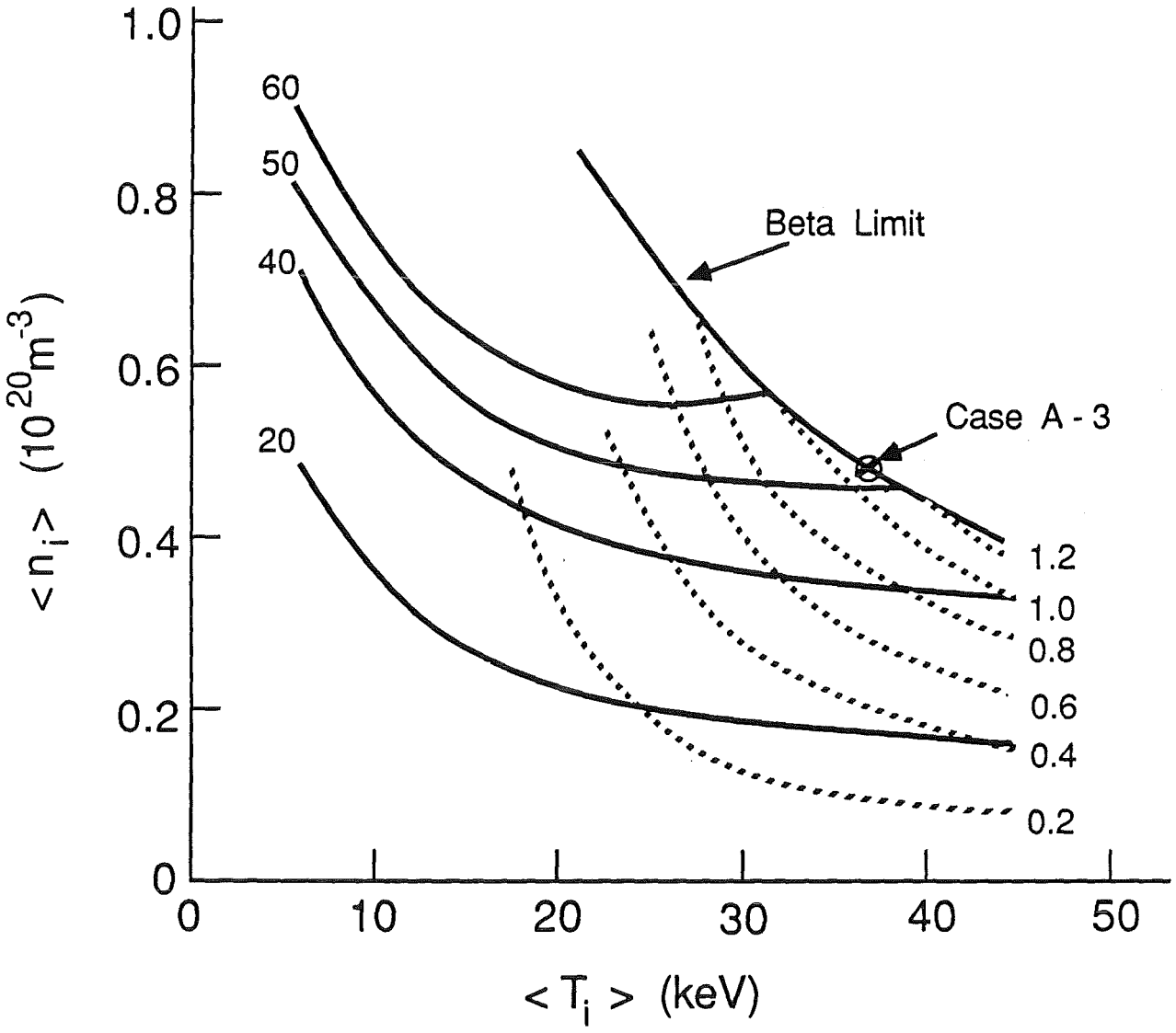

Fig. 3.3-13. Density-temperature operating space for case A-3 using ASDEX H-mode scaling. The solid lines are constant injected power (MW) and the dotted lines are constant Q.

in this density - temperature space during startup to minimize the required injection power to achieve a desired operating point. We see that startup of the plasma does not require more power than that required to sustain the plasma at the final operating point. This is a feature of driven systems with Q less than or near unity. Figure 3.3-14 shows the operating space for case A-3, but with Kaye-Goldston energy confinement scaling and an H-mode factor of 2. In this case, the power required to sustain the plasma at the beta-limit is rather large, about 175 MW. At this point Q = .47. Reduction of the injected power to 80 MW yields a maximum Q-value of .2.

At the high plasma temperatures associated with D-^{3}He it can happen that the ASDEX H-mode scaling law yields energy confinement times longer than the Ohmic scaling law, Eq. (3.2-16). This has not happened in current experiments; the improved confinement of the H-mode has yielded confinement times with auxiliary heating closer to, or about equal to, the Ohmic value. Another possible scaling law assumption is to use the lesser of ASDEX H-mode and Ohmic confinement scaling. The consequences of this are illustrated in Fig. 3.3-15. With this scaling the injected power contours show a saddle-point in the density-temperature parameter space. A Q-value of .84 with an injected power of 79 MW can be achieved. The Q-value drops rapidly with a reduction in the injected power; at P_{inj} = 70 MW, the Q-value is about .3. Consequently, there is a big penalty for a reduction of the injected power.

These calculations assume the reacting ions have a Maxwellian ion distribution function. If the plasma is heated by ICRF it is likely that the RF power will generate an enhanced tail in the ion distribution function. This effect will increase the fusion reaction rate, especially at lower ion temperatures, and improve the Q of the system. This is discussed in Chapter 7 of this report.

References for Section 3.3

1. H.M. Hofmann and D. Fick, "Fusion of Polarized Deuterons," Phys. Rev. Letters 52, 2038 (1984).

2. J.S. Zhang, K.F. Liu and G.W. Shuy, "Fusion Reactions of Polarized Deuterons," Phys. Rev. Letters 57, 1410 (1986).

3. W. Heeringa, "Polarization of Solid Deuterium-Tritium Fuel for Nuclear Fusion," KfK 4168 (1986).

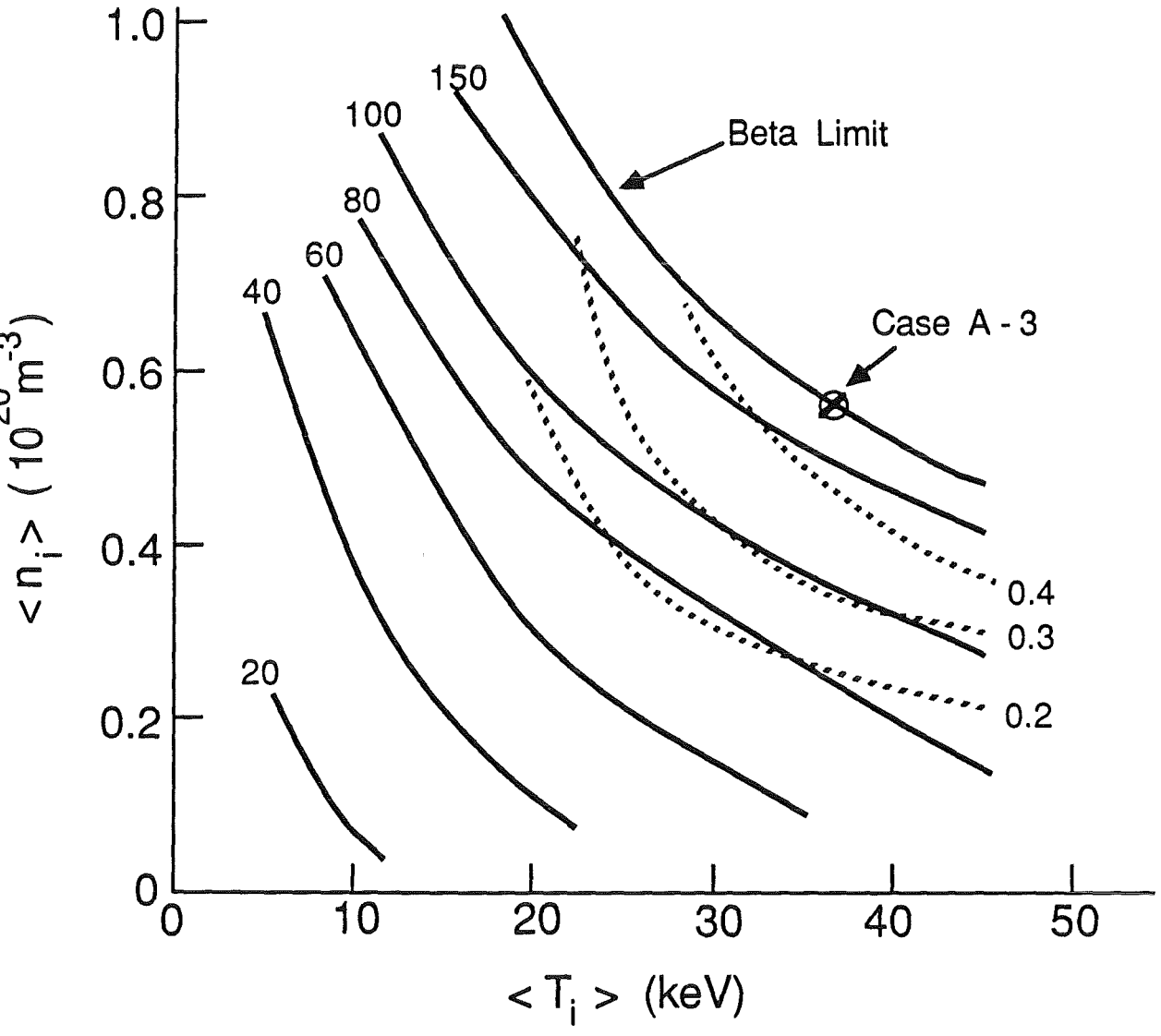

Fig. 3.3-14. Density-temperature operating space for case A-3 using Kaye-Goldston scaling with an H-mode factor of 2. The solid lines are constant injected power (MW) and the dotted lines are constant Q.

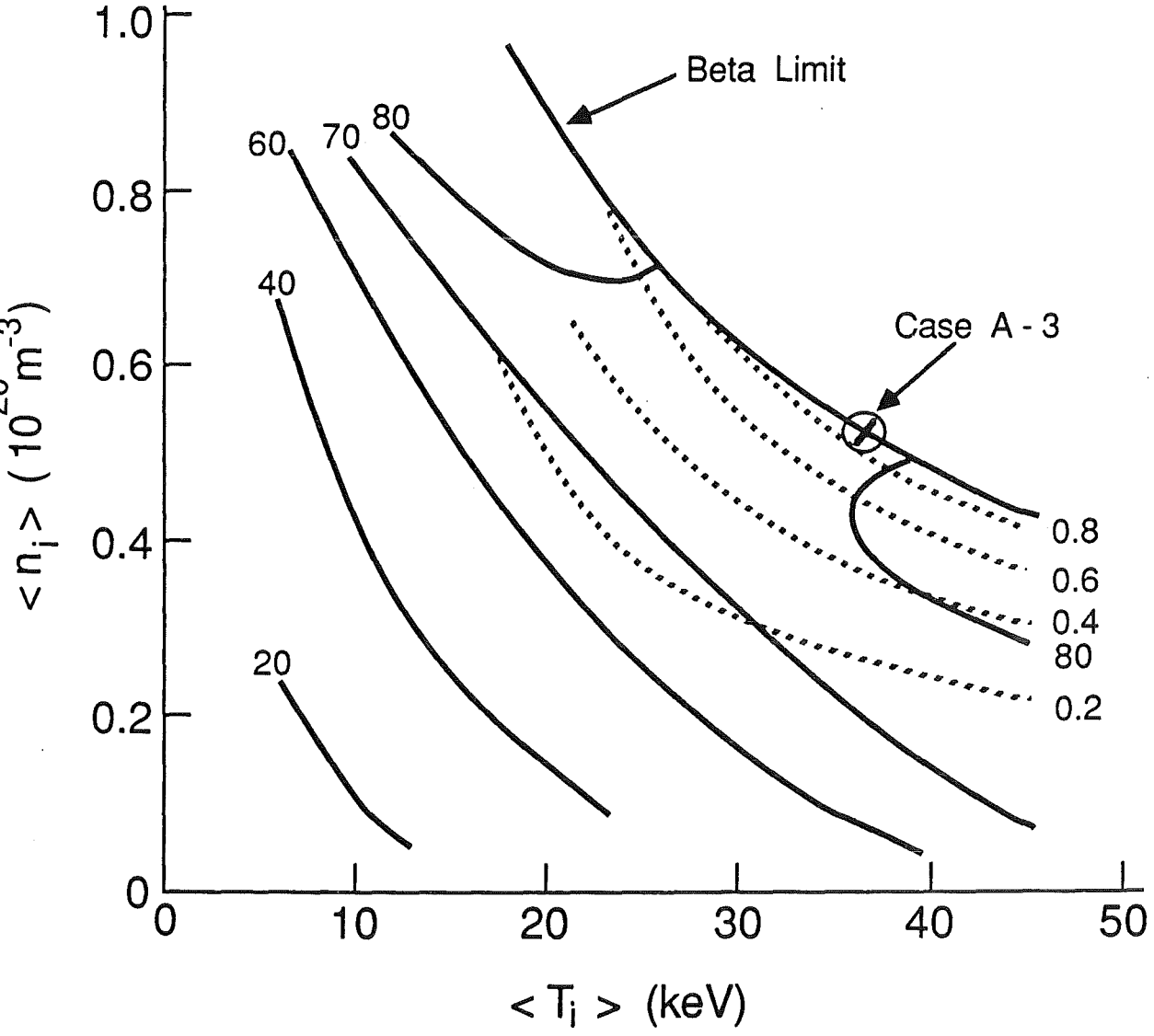

Fig. 3.3-15. Density-temperature operating space for case A-3 using ASDEX/Ohmic scaling. The solid lines are constant injected power and the dotted lines are constant Q.

3.4 Summary

We have developed a physics model which allows one to calculate the plasma performance for given dimensions, fuel composition, magnetic field, etc. The model is zero-dimensional, but uses specified profiles for the electron and ion temperatures and densities. The beta is assumed to be limited by the Troyon formula. The energy confinement is assumed to be given by an empirical scaling law; we have focussed on the ASDEX H-mode and Kaye-Goldston scaling laws in this report. With this model one can calculate the ignition margin and energy multiplication, injection power, and plasma parameters for specified plasma dimensions, toroidal magnetic field, and MHD safety factor.

This plasma model has been used in a parametric survey of D-^{3}He operation in NET, and variations of it. From this parametric survey, the following general conclusions may be drawn.

Breakeven (Q = 1) may be obtained in the present NET-DT design if ASDEX H-mode scaling is applicable. In addition, the required injection power is less than that planned for startup in NET-DT. If Kaye-Goldston scaling continues to plague tokamaks, then the Q-values obtained are much lower (Q = .4) and the injection power is much higher (P_{inj} = 120 MW). The enhanced plasma size NET case (NET-EP) can achieve a Q-value of about 1.4 using ASDEX H-mode scaling with no changes in the machine parameters except for the fuel and the operating temperature.

The Q-value can be increased in many ways in NET because of the low neutron production with D-^{3}He fuel and the reduced need for neutron shielding. Reduction of the major plasma radius to 4.61 m increases the Q-value to about 3. This improvement in Q is due to the increase in magnetic field at the plasma and to the reduced aspect ratio which leads to higher plasma current, energy confinement times, and beta. The reduction in major radius can be achieved by removing the inboard blanket designed for DT operation and using much thinner shield designed for the low DD and DT neutron exposure.

An alternative approach is to increase the magnetic field at the toroidal field magnets without changing the plasma dimensions from the NET-EP case. Q values of about 2.5 - 3 can be obtained by a 20% increase in the magnetic field strength at the TF coil.

Ignition with D-^{3}He in NET may be obtained if the plasma major radius is reduced in conjunction with an increase in the toroidal field and in the plasma elongation. The required elongation for ignition is about 2.4 at B_c = 13 T and 2.7 at B_c = 10.5 T. (B_c is the toroidal field at the TF magnet.) Present understanding of MHD limits on elongation restrict the elongation to about 2.2. In addition, a 13 T toroidal field magnet is infeasible for NET within the context of the present design guidelines.

A more modest modification to NET-EP is to utilize the inboard shield planned for D-T operation, but remove the inboard blanket. This allows the major radius to be reduced by 27 cm. The Q-value using ASDEX H-mode scaling is increased to 1.6 if impurities are neglected and $\tau_p = \tau_E$ is assumed. For 1% oxygen impurity concentration and $\tau_p = 3\ \tau_E$, the Q-value is reduced to 1.2. With Kaye-Goldston scaling and an H-mode factor of 2, the Q would be .47 and the required injection power is 175 MW. For Ohmic scaling, the Q is .85 and the required injection power is 79 MW.

The major parameters for possible operating points in these variation regimes are given in Table 3.4-1. Case A-1 is the reference NET-DT design and case A-2 is NET-EP. Case A-3 is NET-EP with the major radius reduced by 27 cm and 1% oxygen impurity content. In this case $\tau_p = 4\ \tau_E$, whereas $\tau_p = \tau_E$ in all other cases. Cases B-1 and B-2 are reduced major radius cases with different fuel composition. Case C-1 is the same size as A-2, but with increased toroidal field. Cases D-1 and D-2 represent possible ignition cases.

The above predictions are obtained using the ASDEX H-mode scaling law. Break-even in NET is possible with the Kaye-Goldston scaling law for an H-mode factor of about 2.5, but the required injection power is about 120 MW. This assumes the major radius of the plasma has been reduced to 4.61 m and the toroidal field at the magnet remains at the NET value of 10.4 T.

From these results we see that significant energy multiplication in a mildly revised form of NET can be obtained if nature is not too perverse. Significant energy multiplication means that the fusion reactions are as important as the external heating power in determining the power balance of the plasma. Consequently, important questions regarding burn physics and the effects of a significant number of fast fusion produced ions in the plasma can be studied with such a machine. In addition, the much reduced neutron production makes the environment more hospitable to performing physics experiments on burning plasmas than is the case with DT fuel.

Table 3.4-1. Summary of D-^{3}He NET Optimum Operating Parameters for Regimes A-D Using ASDEX H-Mode Scaling

	Case							
	A-1	A-2	A-3	B-1	B-2	C-1	D-1	D-2
Major Plasma Radius, m	5.18	5.41	5.14	4.61	4.61	5.41	4.61	4.61
B at Magnet, T	10.4	10.4	10.4	10.4	10.4	13	10.5	13
B at Plasma, T	4.96	4.75	5.0	5.57	5.57	5.93	5.63	6.97
Q	.96	1.4	1.15	3.06	.95	2.8	∞	∞
P_{inj}, MW	35	37	53	32	84	38	0	0
Plasma Current, MA	10.8	14.8	16.2	20.2	20.2	18.3	29.6	29.5
Elongation	2.17	2.17	2.17	2.17	2.17	2.17	2.7	2.38
Deuterium Fraction	.65	.65	.65	.65	.34	.65	.65	.65
$\langle n_i \rangle$, 10^{13} cm^{-3}	3.6	3.5	4.6	4.7	6.0	4.6	8.8	10.7
$\langle T_i \rangle$, keV	45	45	37	51	37	51	37	37
$\langle T_e \rangle$, keV	28	31	28	37	30	37	34	34
$\langle \beta \rangle$	.056	.064	.067	.075	.075	.064	.11	.088
Energy Confinement Time, s	5.6	7.9	8.3	9.3	9.3	9.9	13.6	13.6
Inboard Shield, cm	116	100	70	29	29	100	29	29
<Neutron Wall Load>, MW/m^2	.004	.006	.016	.016	.002	.016	.055	.08
Photon Heat Flux to Wall, W/cm^2	4.5	5.9	9.9	14.5	20.9	15	31	50
Fusion Power, MW	34	53	61	98	79	108	240	286
Neutron Power, MW	0.9	1.9	7.8	4.9	0.67	5.7	21.9	28.6
Power to Divertor, MW	53	62	69	71	79	76	94	103
τ_p/τ_E	1	1	4	1	1	1	1	1
Oxygen Impurity Concent. (%)	0	0	1	0	0	0	0	0

4. NEUTRONICS

The goal of the neutronics analyses is to determine the radiation level at the TF magnets for a D^3He fueled NET reactor. The analyses were carried out for two cases of the NET-D^3He reactor. The first part of the analysis is applicable to case B or D of the parametric studies (see Chapter 3). The aim of this analysis is to estimate the thickness of the thinnest possible inboard (i/b) shield that protects the inner legs of the TF coils and satisfies the limits and constraints for this particular case. A complete coverage of this analysis is given in Section 4.2. The second part of the analysis pertains to case A-3 where the breeding blanket is removed and the permanent shield is left in place. The neutronics analysis for this case is presented in Section 4.3.

The NET-D^3He device is a low fluence machine. It is expected to be designed for 1000 shots with a shot duration of 200 seconds. A machine lifetime of 2×10^5 s is anticipated and that is equivalent to 2.32 full power days (FPD).

4.1 Magnet Radiation Limits

The thickness, composition, and geometric configuration of the shield strongly depend on the allowable radiation limits for the TF magnets. The magnet components most sensitive to radiation damage are the electrical insulator (GFF epoxy), Cu stabilizer, Nb_3Sn superconductor filaments, and thermal insulator (mylar). The nuclear heating in the magnet affects the winding pack temperature and the economic performance of the reactor through the refrigeration cost.

The total nuclear heating in the 16 TF coils is currently limited to 20 kW. This heating can be accommodated by the present He refrigeration plant without much impact on the refrigeration cost.[1] The limits on the dose to the GFF epoxy and fast neutron fluence ($E_n > 0.1$ MeV) are taken from the NET report[2] to be 5×10^8 rads and 5×10^{17} n/cm^2, respectively.

4.2 Shielding Analysis for Cases B and D

The objective of this analysis is to design the thinnest possible i/b shield that satisfies the TF magnet radiation limits, engineering constraints, and physics requirements for regimes B or D. The primary shield design requirement is to limit the TF coil nuclear heating to that allowed by the NET coil designers, presently estimated to be 20 kW. The engineering constraints are that the geometry of the TF coils and the dimensions of specific regions (such as the cryostat, gaps, and scrape-off) remain the same

as that of the NET-DT design. Additional requirements include physics items such as the desirability of a high D:^{3}He ratio and small Δ (inboard distance between plasma edge and winding pack) in order to achieve the highest Q value possible.

The relation between Q, Δ, and f_D (deuterium fraction in the D^{3}He mixture) is illustrated in Fig. 4.2-1. This figure uses the parameters of case B-1 except that f_D is changing and the ions are at a lower temperature of 37 keV. As f_D increases, the required shield thickness to protect the magnet increases since more neutrons are produced in the plasma. Note that high f_D could be used when $Q >> 1$. For the same f_D, designing an efficient i/b shield will reduce the Δ and thus increase the Q. Furthermore, for the same Δ, the efficient shield will help the Q by allowing the use of a higher f_D value.

Figures 4.2-2a and 4.2-2b show cross sections through the upper halves of the NET-DT and NET-D^{3}He reactors. In the NET-D^{3}He design, the breeding blanket was removed, the outboard (o/b) permanent shield was left in place, and the i/b shield was thinned to accommodate the larger plasma size. In Section 4.2.1, the poloidal variation of the neutron wall loading for both NET-DT and NET-D^{3}He designs is presented. An optimized shield design for the i/b region is described in Section 4.2.2. Section 4.2.3 presents the magnet radiation effects for different f_D values and shows the sensitivity of the Q value to both the scrape-off zone thickness and the allowable nuclear heating in the magnet.

4.2.1 Neutron Wall Loading Distribution

In tokamak reactors, the neutron wall loading (Γ_n) exhibits a poloidal variation that can deviate considerably from the average value of the neutron wall loading, defined as the neutron power divided by the first wall area. The poloidal distribution of Γ_n is important in identifying the locations of the peaks so that enough shield is placed therein to protect the magnets and avoid hot spots. The distribution depends on the plasma shape, the neutron source distribution in the plasma, and the first wall shape. The NEWLIT code[3] was used to determine the poloidal variation of the neutron wall loading for both the NET-DT and NET-D^{3}He designs. The source distribution within the plasma is taken into account by properly representing the different magnetic flux surfaces. The D-shaped plasma outer boundary was represented by the parametric equations

$$r_p = R_p + a_p \cos (t + C_p \sin t) , \qquad (4.2\text{-}1)$$

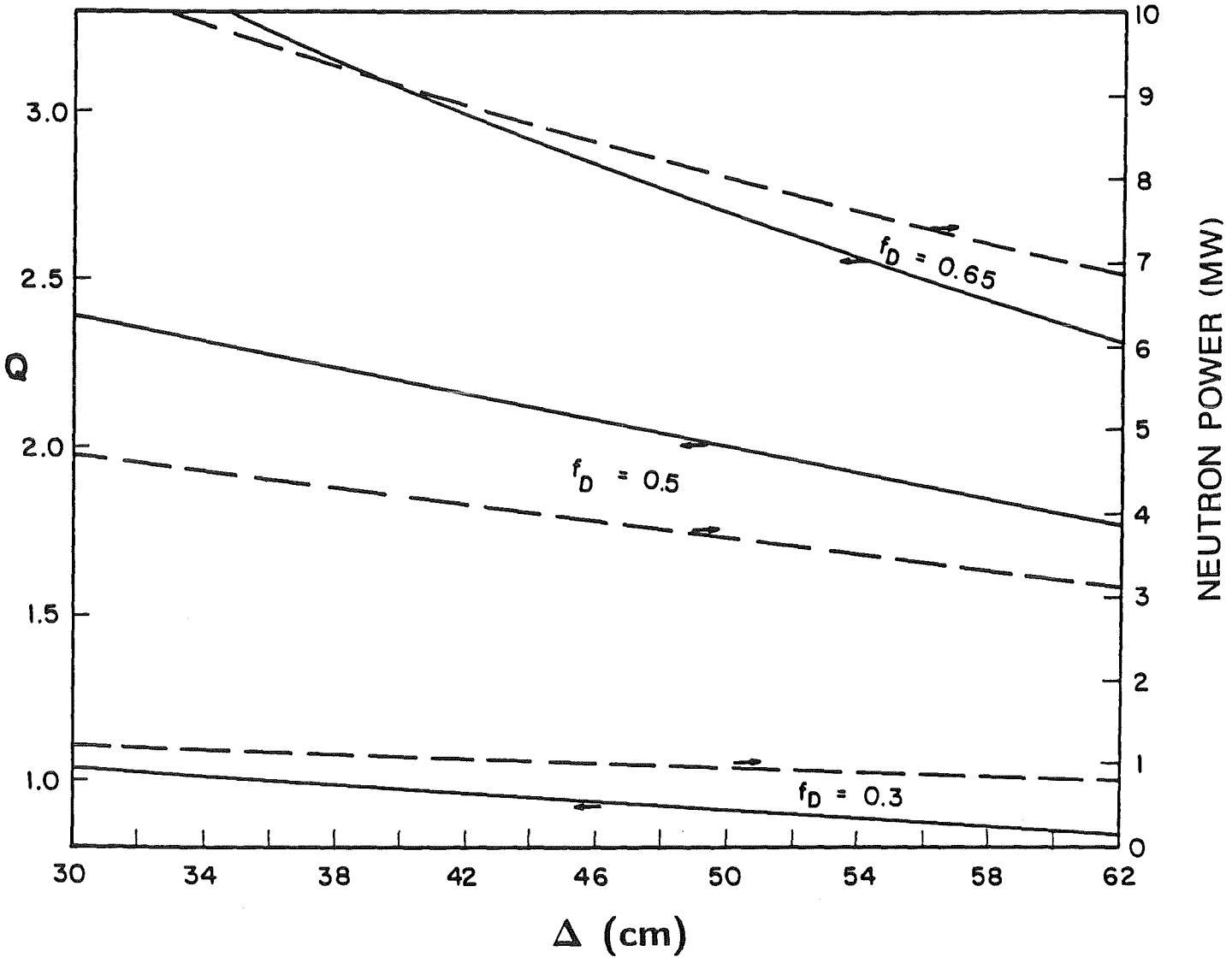

Fig. 4.2-1. Q and P_n vs. Δ in NET-D^3He reactor.

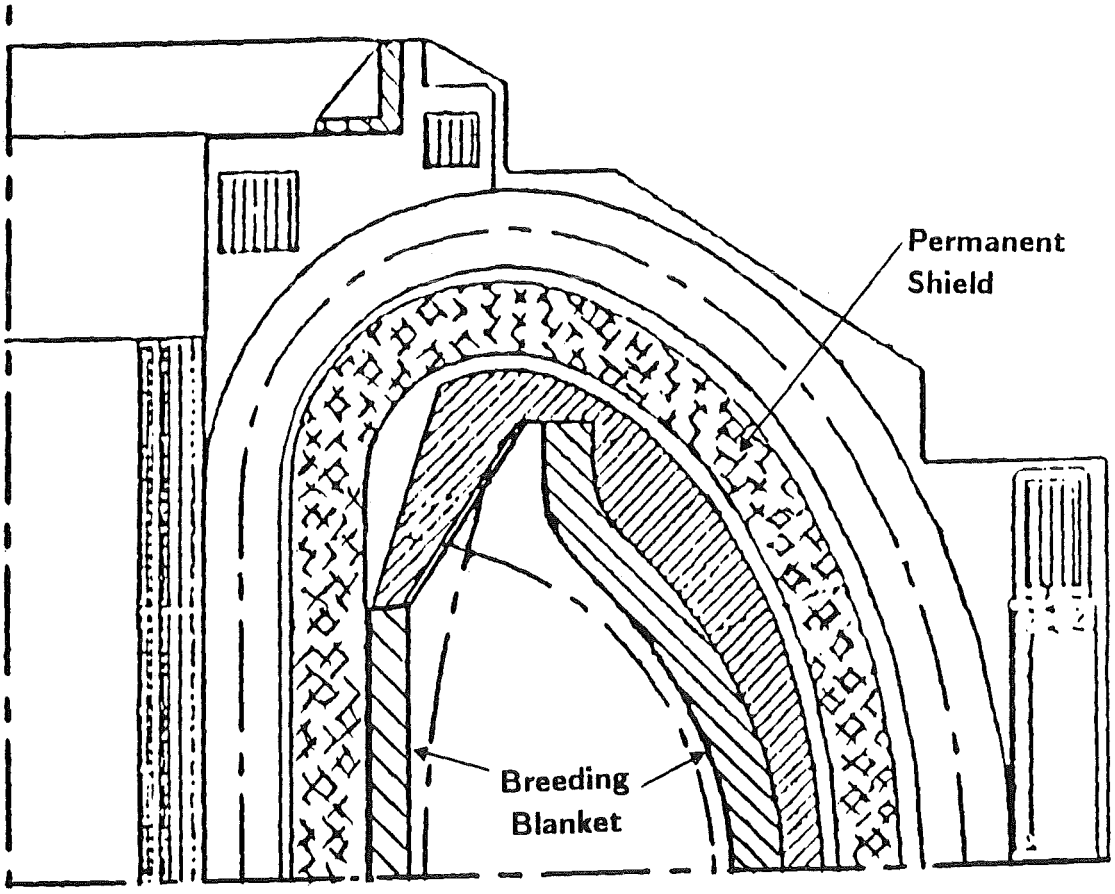

Fig. 4.2-2a. Cross section through the TF coil of NET-DT reactor.

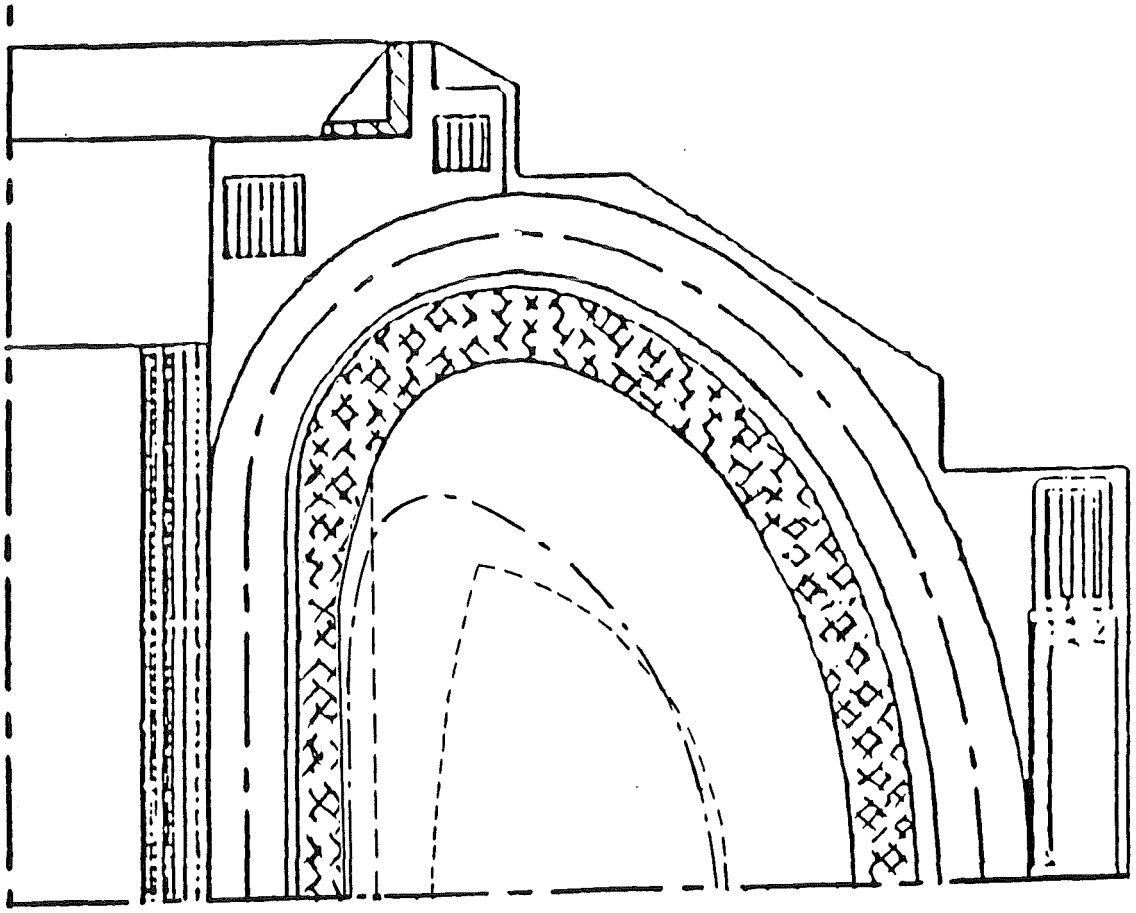

Fig. 4.2-2b. Cross section through the TF coil of NET-D^{3}He reactor - case B or D (dashed lines indicate the NET-DT permanent shield and plasma boundaries).

and $z_p = \kappa_p a_p \sin t$, (4.2-2)

with the NET plasma parameters listed in Table 4.2-1. The parameter t varies from 0 to π. The neutron source profile within the plasma was considered to vary from the magnetic axis to the outer boundary as $\{1 - (a/a_p)^2\}^4$, where a is the minor radius of any magnetic flux surface in the plasma. The results were normalized to the neutron power given in Table 4.2-1.

The results of the calculations are given in Figs. 4.2-3 and 4.2-4 for NET-DT and NET-D^3He (case B-1), respectively. The first wall and plasma shapes are shown, as are the magnetic flux surfaces. The wall loading distribution in each segment is indicated and the dashed line represents the average neutron wall loading. Figure 4.2-4 is generated for an i/b scrape-off thickness of 6 cm and a deuterium fraction of 0.65. A comparison between the wall loading values for the different cases is given in Table 4.2-1. As noticed, 2-3 orders of magnitude reduction in the wall loading is achieved by using the D^3He as a fuel. This translates into a reduction of several tens of centimeters in the thickness of the i/b shield, as will be shown later. Other advantages related to the low neutron production of the D^3He fuel are the low activation level, afterheat, and radioactive waste rating of the shield.

4.2.2 Shield Composition

The highest damage in the inner legs of the TF coils occurs at the midplane of the reactor where the neutron wall loading has its peak value. A schematic of the i/b shield and the inner leg of the TF magnet at the midplane of the reactor is shown in Fig. 4.2-5 for Δ = 45 cm. The 3 cm thick cryostat wall is cooled with 5 v/o liquid nitrogen and the winding pack composition is taken as 34.5 v/o 304 SS, 33.4 v/o Cu, 3 v/o Ni, 6.6 v/o Nb_3Sn, 11.7 v/o GFF epoxy, and 10.8 v/o liquid helium. The details of the 5.5 cm thick cryostat are shown in the figure and there is a 1.5 cm gap between the cryostat and the back of the shield. If we leave 2 cm for the first wall graphite tiles, then the space available for the shield (Δ_s) is 29 cm thick. The scrape-off thickness (S) is considered to be 6 cm and the effect of having a thicker scrape-off is discussed in the next section.

An optimization study was performed to determine the optimum shield composition that minimizes the nuclear heating in the magnets. Tungsten alloy is used as the main i/b shielding material to provide adequate protection for the inner leg of the magnet. The coolant is borated water (5 g boric acid/100 cm^3 of H_2O) and the structure is PCA.

Table 4.2-1. Major NET Parameters Needed for the NEWLIT Code

	NET-DT	NET-D^3He
Plasma Major Radius (R_p)	5.18 m	4.61 m
Plasma Minor Radius (a_p)	1.35 m	1.69 m
Elongation (κ_p)	2.18	2.17
Triangularity (C_p)	0.65	(0.65)
Magnetic Shift	16.2 cm	(16.2) cm
Neutron Power (P_n)	480 MW	8.5 MW
Fusion Power (P_F)	600 MW	97 MW
Deuterium Fraction (f_D)	—	0.65

Items in ( ) are assumed to be same as in NET-DT.

Table 4.2-2. Comparison of Key Neutronic Parameters for Various NET Designs

	NET-DT	NET-D^3He		
f_D	—	0.65	0.5	0.3
Neutron Power (MW)	480	8.53	3.96	1.0
Γ_n (MW/m^2)				
Average	1.0	0.0114	0.0053	0.0013
i/b peak	1.13	0.0193	0.00896	0.0023
o/b peak	1.5	0.0144	0.0067	0.0017

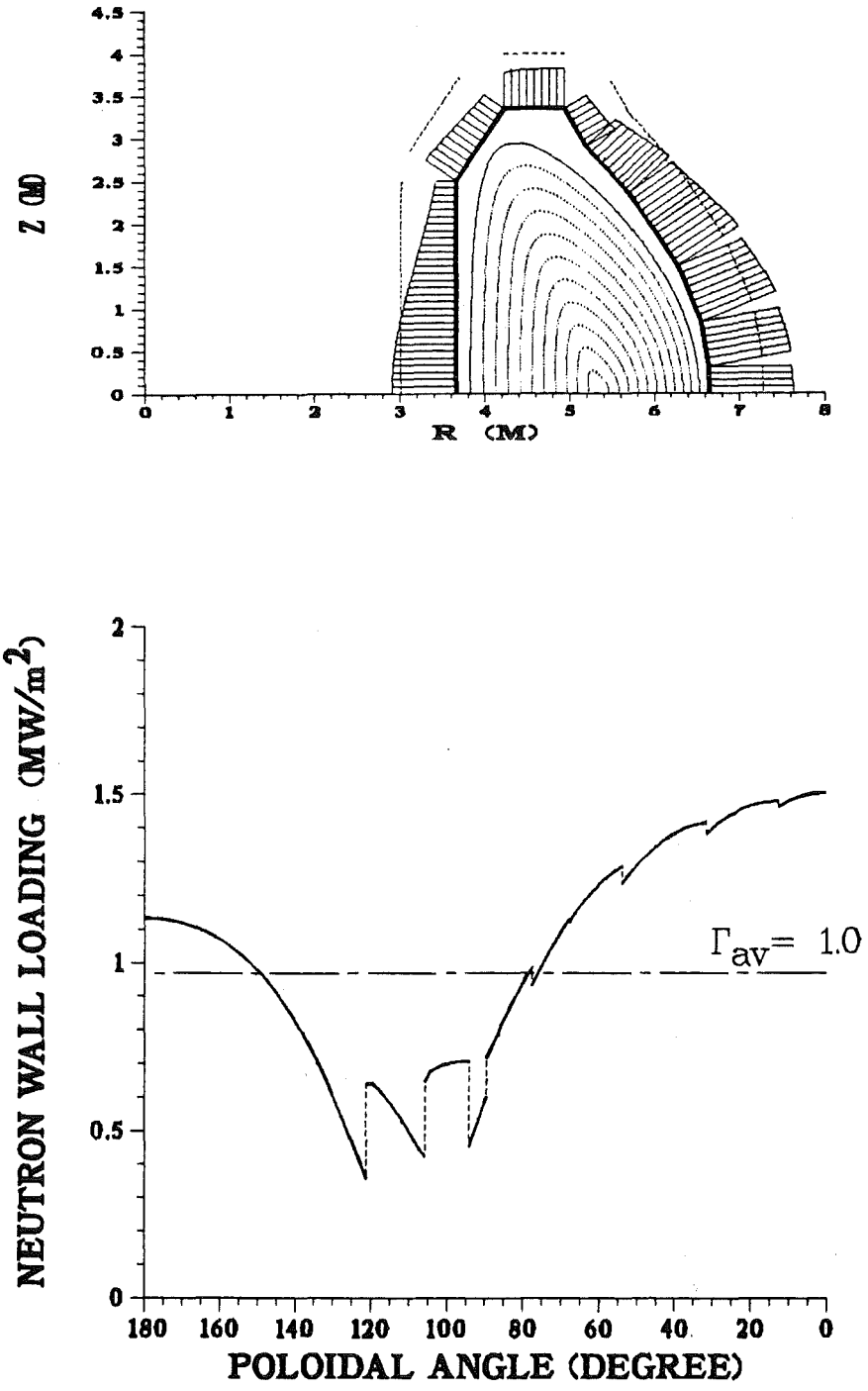

Fig. 4.2-3. Poloidal variation of the neutron wall loading in NET-DT reactor.

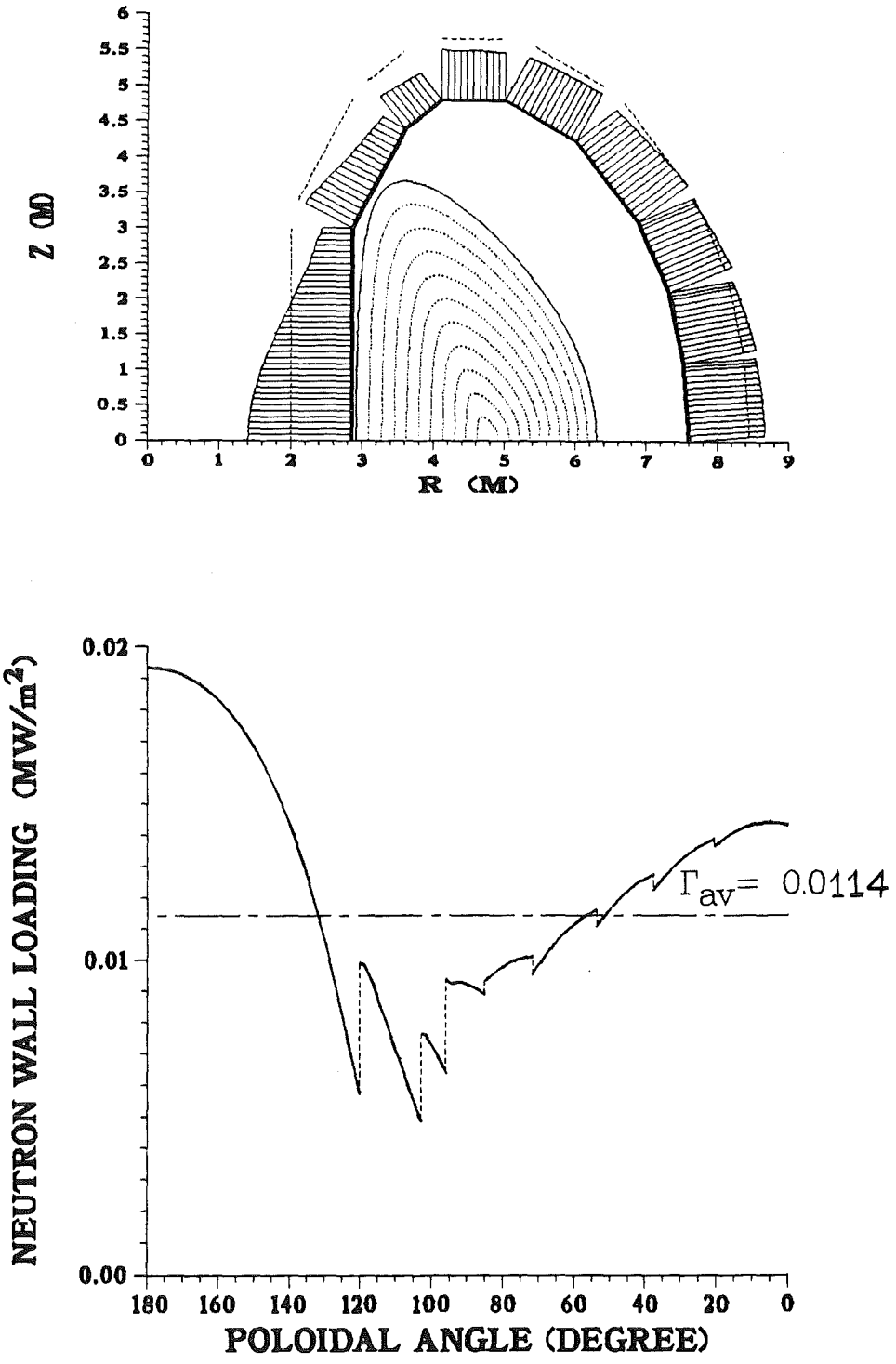

Fig. 4.2-4. Poloidal variation of the neutron wall loading in NET-D^{3}He reactor (case B-1 with lower ion temperature).

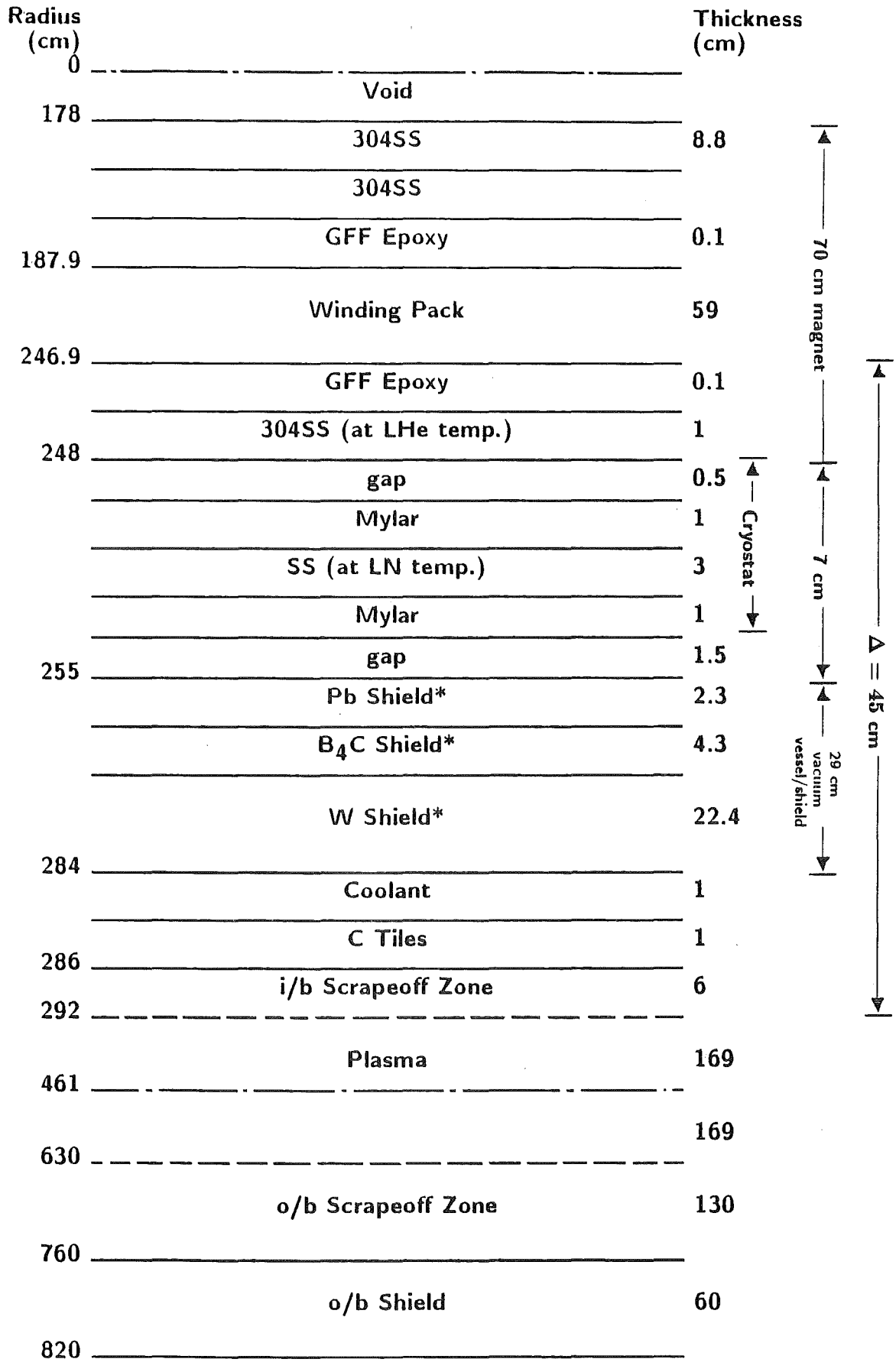

Fig. 4.2-5. Schematic of the i/b shield and inner leg of the TF coil in NET-D^{3}He reactor (case B or D).

*contains 10 v/o structure and 5 v/o coolant

Two additional shielding materials were considered as a backup to the W-shield. These are B_4C (at 90% density factor and 90% ^{10}B in B) and Pb. The o/b shield was taken as 90 v/o PCA and 10 v/o coolant. The problem was modeled as infinite toroidal cylinders around the machine axis and the calculations were performed using the one-dimensional code ONEDANT[4] with the MATXS5 data library based on ENDF/B-V in 30 neutron and 12 gamma groups, and the P_3-S_8 approximation.

The shield consists of alternate layers with a thick W-shield followed by a B_4C-shield and then, a Pb-shield. In all layers, we considered 10 v/o structure and 5 v/o coolant. In the optimization study, the three layers were varied in thickness to reduce the nuclear heating in the magnets. The optimum shield was found to consist of 77.3% W-shield, 14.7% B_4C-shield, and 8% Pb-shield by thickness.

4.2.3 Magnet Heating and Damage

The radiation effects at the TF coil are given in Table 4.2-3 for the three f_D values. The peak values occur at the midplane of the inner legs. The same Δ of 45 cm, Δ_S of 29 cm, and S of 6 cm were considered for the sake of comparison. As anticipated, the lower the f_D, the lower the radiation effects at the magnet. The dose to the GFF epoxy and the fast neutron fluence are much below the design limits. In addition, the end-of-life radiation-induced resistivity[5] in the stabilizer is less than ~ 1% of the unirradiated stabilizer resistivity at the operating field. In all cases, the nuclear heating in the TF coils is less than the 20 kW limit. This suggests that the shield can be made thinner in order to meet the heating limit.

A set of curves was generated to illustrate the variation of the heating in the magnets as a function of the shield thickness. Figure 4.2-6 shows this variation for the different f_D values. It should be mentioned that the drop in the neutron power, and thus the neutron wall loading, as Δ increases (see Fig. 4.2-1) was taken into account. In the calculations, the inner scrape-off thickness was varied (by moving the plasma out) to determine the sensitivity of the total nuclear heating in the magnets. The scrape-off thickness was increased to 10 cm and the NET-DT reference value of 15 cm. The figure indicates that the heating drops as the scrape-off thickness increases. This is due to the lower neutron wall loading as a result of the farther plasma location and the lower neutron power (see Fig. 4.2-1). The variation also shows that the total heating increases by a factor of 2 for each ~ 4 cm decrease in the shield thickness. Therefore, to meet the heating limit, the i/b shield can be as thin as 27, 23, and 16 cm for f_D values of 0.65, 0.5, and 0.3, respectively.

Table 4.2-3. Comparison Between the Radiation Effects at the TF Coils for Three Different Values of f_D

f_D	0.65	0.5	0.3
Q	2.87	2.1	0.95
$\Gamma_{i/b}$ (MW/m^2)	0.0193	0.00896	0.0023
Total Nuclear Heating in 16 TF Coils (kW)	13.3	6.2	1.65
Peak Dose in GFF epoxy (rad @ 2.32 FPD)	0.1×10^8	0.05×10^8	0.013×10^8
Peak Nuclear Heating in Winding Pack (mW/cm^3)	1.2	0.57	0.15
Peak dpa in Cu Stabilizer (dpa @ 2.32 FPD)	1.1×10^{-5}	5×10^{-6}	1.3×10^{-6}
End-of-Life Radiation Induced Resistivity (nΩm)	7.9×10^{-3}	3.6×10^{-3}	9.4×10^{-4}
Peak Fast Neutron Fluence (n/cm^2 @ 2.32 FPD)	1.7×10^{16}	7.8×10^{15}	2.1×10^{15}

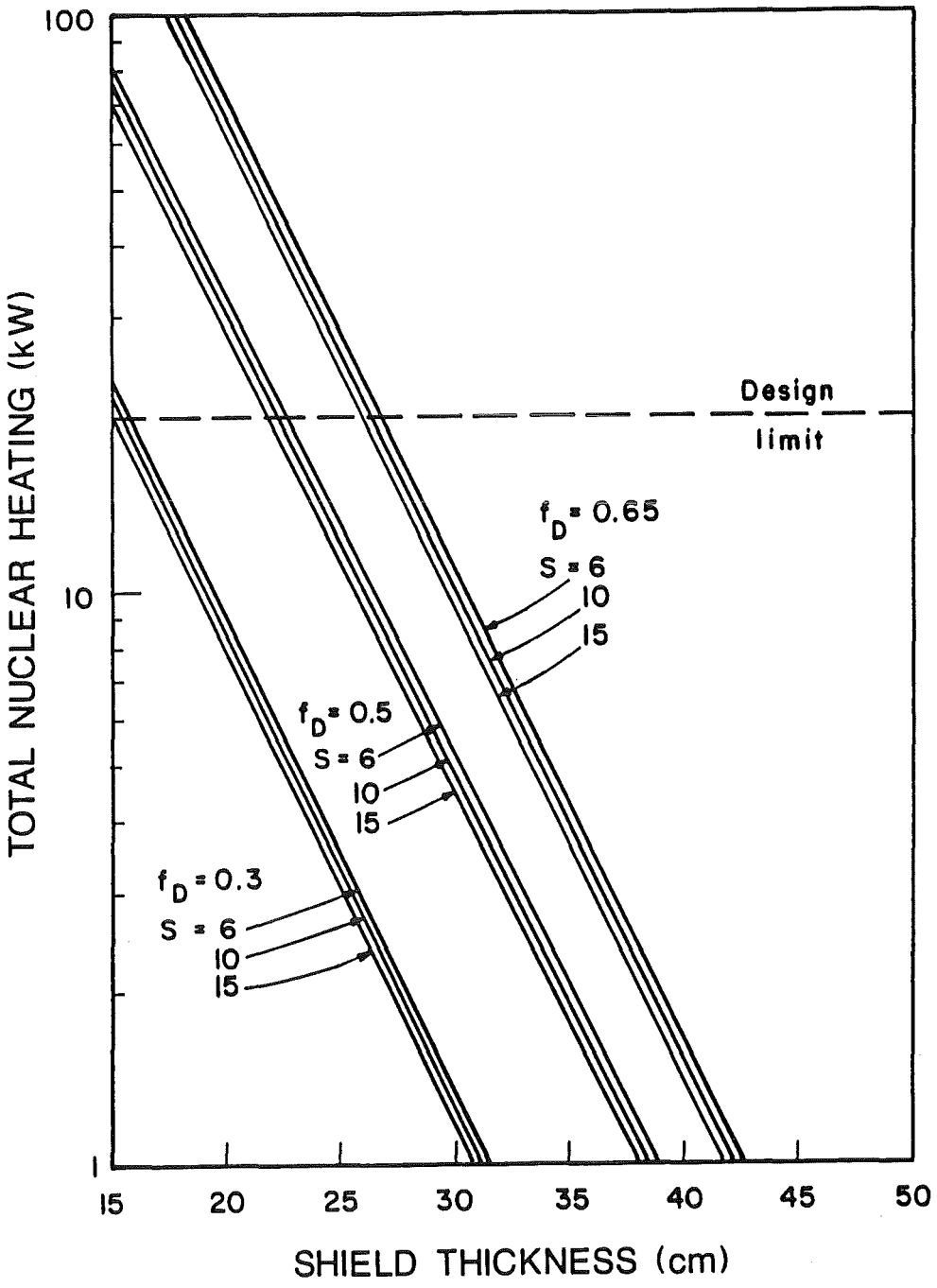

Fig. 4.2-6. Variation of the total nuclear heating in the 16 TF coils with the i/b shield thickness.

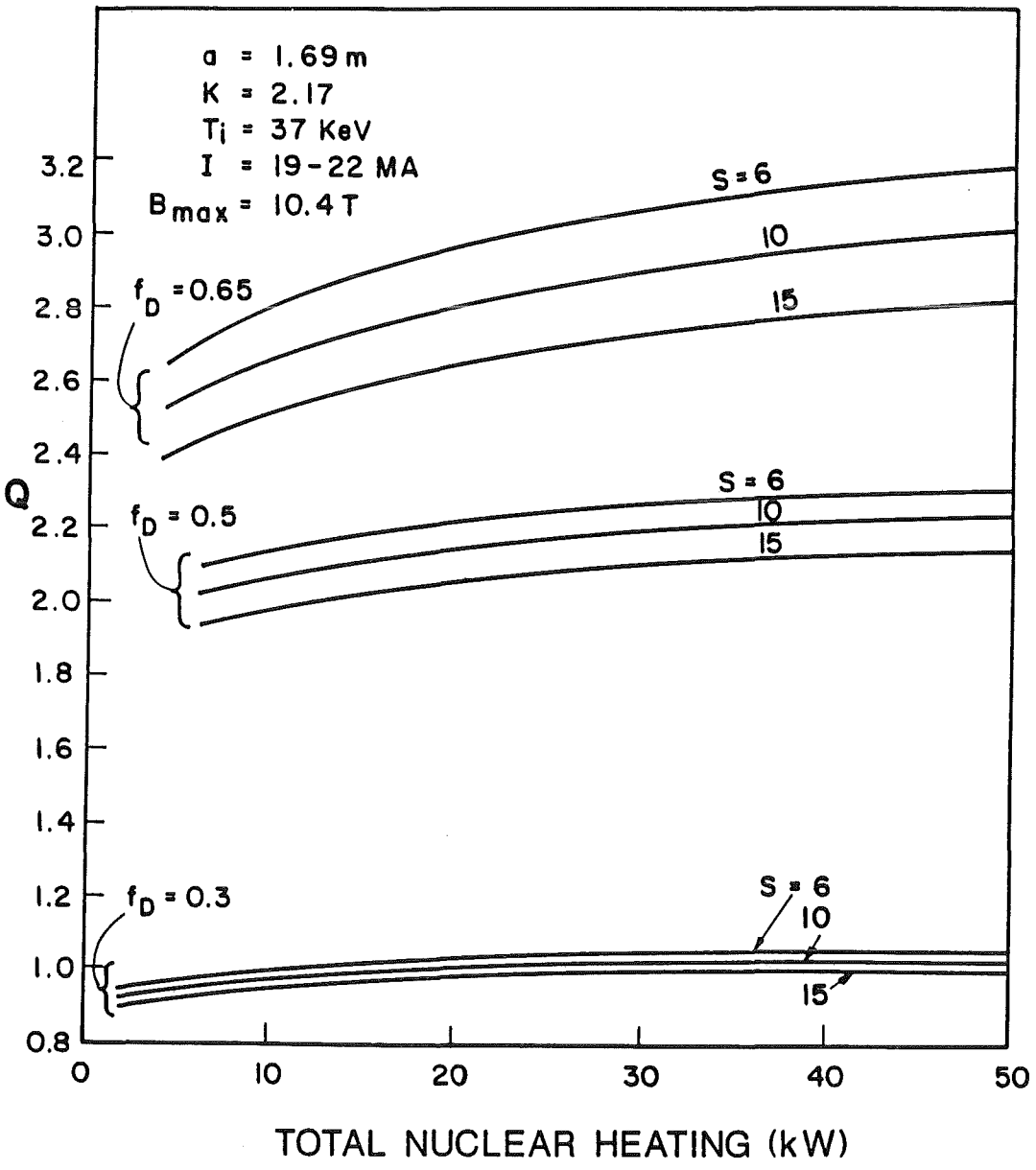

Fig. 4.2-7. Q vs. total nuclear heating in the 16 TF coils.

As mentioned earlier, one of the reasons for designing a thin i/b shield is to achieve a high plasma Q value. The items which have significant impact on the Q value are the i/b scrape-off, deuterium fraction, and the allowable heating limit of the magnet. Some questions thus arise as to how the Q, S, f_D, and magnet heating are related and what values are preferable to achieve a Q of at least 1. To answer these questions, Fig. 4.2-7 was generated to give the relation between the Q and the heating by combining Figs. 4.2-1 and 4.2-6 and parameterizing S and f_D. The figure reveals that the Q increases as the i/b scrape-off decreases and/or more heating is allowed in the magnet. Thicker scrape-off layers, e.g. 10 or 15 cm, can be obtained without a serious less of Q. In order to achieve breakeven (Q = 1), f_D should be at least 0.3 if S = 10 cm, for a total nuclear heating of 20 kW. If S is > 10 cm, the minimum f_D required for breakeven will be larger than 0.3.

4.3 Shielding Analysis for Case A-3

In case A-3, the tritium breeding blanket was removed and the only shield left in place is the permanent shield of the NET-DT design (see Fig. 4.2-2a). The permanent shield (acts also as a vacuum vessel) developed by the NET team is 70 cm thick on the inboard side and 59 cm thick on the outboard. It is cooled with borated water (4 g of boric acid/100 cm^3 of H_2O) and composed of two layers of steel shield. The front layers are 20 and 15 cm thick on the i/b and o/b, respectively, and contain 10 v/o coolant. The back layers have a higher coolant content of 25% by volume. The space between the back of the shield and the winding pack is 10 cm thick on the i/b and 20 cm thick on the o/b. The inner legs of the TF coils have no inner coil casing while that of the outer legs is 9.4 cm thick. This provides additional shielding for the outer legs of the coils. Leaving 2 cm for the C tiles and a 15 cm scrapeoff zone, the distance between the plasma edge and the winding pack is 98 cm on the i/b. For a plasma minor radius of 1.69 m, the major radius is 5.14 m and the i/b first wall is located at 3.3 m from the machine centerline.

The shielding analysis for case A-3 aims at estimating the radiation level at the TF magnets. Compared to regime B and D, case A-3 is not expected to have any shielding problem. For a deuterium fraction of 0.65, the neutron power is 7.8 MW. The neutron wall loading distribution for case A-3 was generated using the NEWLIT code and the results are presented in Fig. 4.3-1. The distribution peaks at the midplane of the i/b side at a value of 0.0155 MW/m^2. The average wall loading is 0.01 MW/m^2 and the o/b peak is 0.0145 MW/m^2.

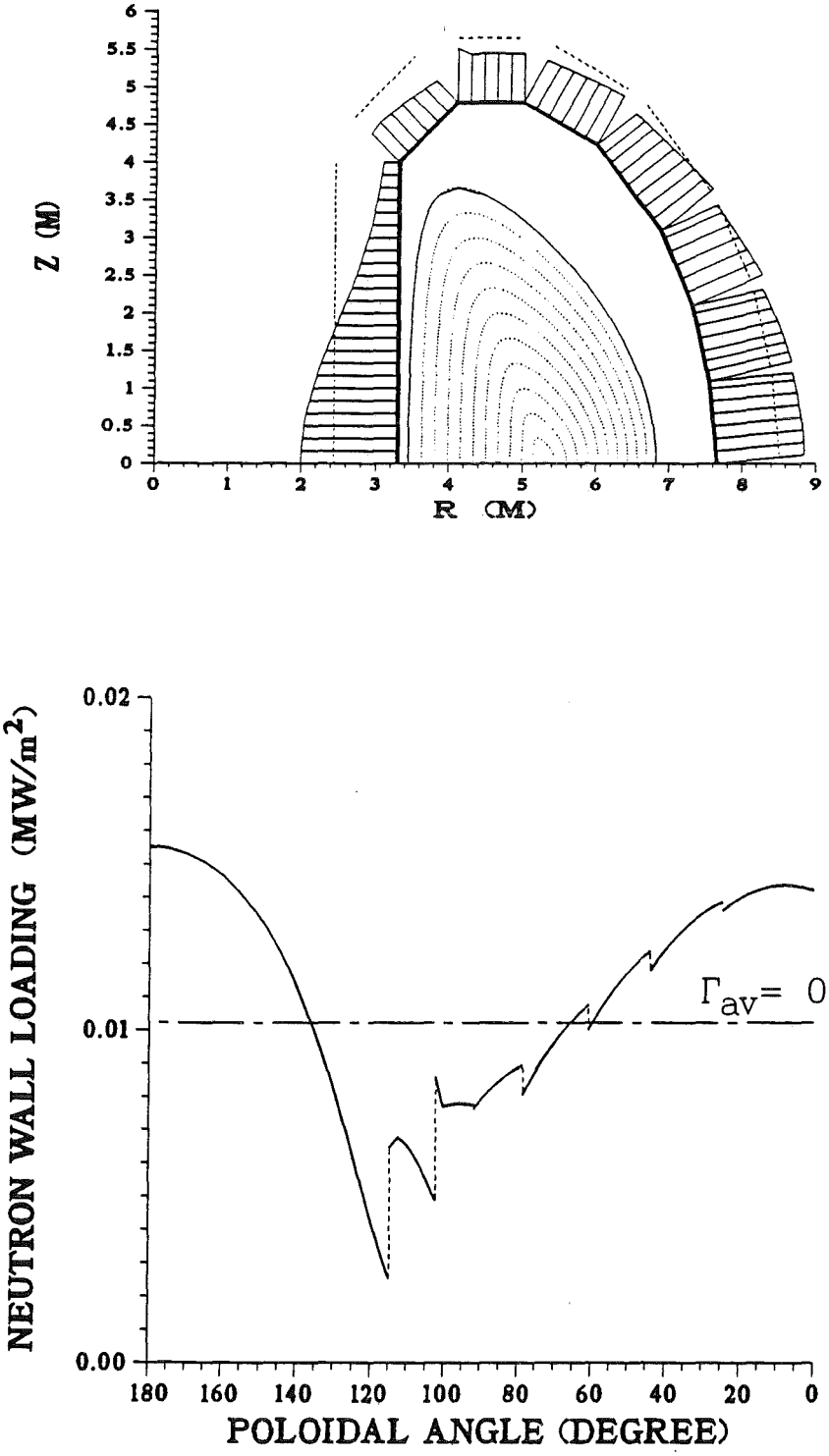

Fig. 4.3-1. Neutron wall load distribution for case A-3.

Table 4.3-1. Radiation Effects in the Inner and Outer Legs of the TF Magnets

	Inboard	Outboard
$\hat{r}_n$ (MW/m^2)	0.0155	0.0145
Shield Thickness (cm)	70	59
Coil Case Thickness (cm)	--	9.4
Nuclear Heating in		
Winding Pack (kW)	0.12	0.45
Coil Case (kW)	--	0.78
Peak Nuclear Heating in Winding Pack (mW/cm^3)	1.3×10^{-2}	1.25×10^{-2}
Peak Dose to GFF Epoxy (rad @ 2.32 FPD)	7.8×10^{4}	9.2×10^{4}
Peak Fast n Fluence (n/cm^2 @ 2.32 FPD)	5.3×10^{13}	1.2×10^{14}
Peak dpa in Cu Stabilizer (dpa @ 2.32 FPD)	4.0×10^{-8}	7.1×10^{-8}

The shield was modeled for the 1-D code ONEDANT as toroidal cylinders. Both i/b and o/b shields are modeled since the radiation effects in the inner and outer legs of the TF coils are predicted to be comparable. The results are listed in Table 4.3-1. The peak values occur at the midplane of the reactor where the wall loading maximizes. The outer legs have higher damage due to the difference in the material arrangement. The total nuclear heating in the 16 TF coils is estimated to be ~ 0.6 kW in the winding packs and ~ 0.8 kW in the cases of the outer legs. The other radiation effects are much below their design limits.

References for Chapter 4

1. E. Salpietro, KfK, Germany, Private Communication, June 1987.

2. The NET Team, "Next European Torus-Status Report #51," Max-Planck-Institut für Plasmaphysik, Garching, West Germany (December 1985).

3. H. Attaya and M. Sawan, "NEWLIT - A General Code for Neutron Wall Loading Distribution in Toroidal Reactors," Fusion Technology 8/1, 608 (1985).

4. R.D. O'Dell et al., "User's Manual for ONEDANT: A Code Package for One-Dimensional, Diffusion-Accelerated, Neutral Particle Transport," LA-9184-M, Los Alamos National Laboratory (February 1982).

5. M. Sawan, "Charts for Specifying Limits on Copper Stabilizer Damage Rate," J. Nucl. Mat. 122&123, 1376 (1984).

5. FAST ION EFFECTS

This section will address the status of alpha particle loss modelling for D-T tokamaks and the extrapolation to alpha particles and protons in D-^{3}He tokamaks. Two factors make D-^{3}He fusion reactors more susceptible to fusion-product losses than D-T reactors:

- Five times as much energy is produced in charged particles per reaction, and
- The gyroradius of the 14.7 MeV proton, which carries 80% of the D-^{3}He fusion energy, is twice that of the 3.67 MeV alpha particle.

The alpha particle part of the problem should be essentially the same for both D-^{3}He (3.67 MeV) and D-T (3.52 MeV) tokamaks, with appropriate modifications for plasma operating parameters. The larger total energy and gyroradius of the proton, however, will lead to larger prompt losses and, probably, larger losses as the protons thermalize.

A related workshop on alpha particle effects in an engineering test reactor was held recently. The March 1988 issue of Fusion Technology contains a number of papers stemming from that workshop.

Section 5.1 will give an overview of alpha particle loss modelling in D-T tokamaks. Prompt loss of fusion products for D-^{3}He operation of a device similar to NET will be treated in Section 5.2, and ripple loss will be examined in Section 5.3. Finally, Section 5.4 will provide a summary and conclusions.

5.1 Status of Alpha Particle Loss Modeling in D-T Tokamaks

There are five main fast-particle loss mechanisms in a tokamak:[1]

- Prompt loss, due to banana orbits intersecting the chamber walls;
- Direct ripple loss due to the birth of fast ions in the ripple loss cone;
- Collisional ripple diffusion, whereby collisions with fuel ions cause fast ions to become ripple-trapped;
- Collisionless ripple diffusion, in which finite orbit effects lead to ripple-trapping; and
- Banana-drift diffusion, where ripple modifies the banana orbits and causes a net radial drift.

Only the first of these, for which a method based on constants of the motion applies,[2,3,4] can be said to have a well-established theory. This is, perhaps, not surprising, because even the correctness of Maxwellian plasma tokamak transport theory[5] remains unverified, with discrepancies from experiment of over a factor of ten for electrons and of about a factor of three for ions. The present explanation of these discrepancies is that microscopic fluctuations lead to this anomalous transport, although there is considerable controversy about the detailed mechanisms.[6] This situation results primarily from the difficulty of analyzing plasmas in the complicated magnetic field geometry of the tokamak.

The fusion-product problem differs from the thermal-ion transport problem in some respects. In particular, collisional effects are much less dominant, because the fusion products lose most of their energy to electrons before they begin to scatter significantly off of ions--at which time their radial random walk due to pitch-angle scattering effectively begins. This is especially true for the 14.7 MeV D-^{3}He protons, which lose over 95% of their energy before pitch-angle scattering begins to compete with electron drag. Thus, the problem becomes one of following orbits perturbed by collisions, rather than analyzing transport driven by collisions. For 3-D, rippled tokamaks, either numerical codes must be used or extensive simplifications must be invoked. At present, unfortunately, the two main computer codes used for modelling fusion product loss in rippled tokamaks[7,8] differ in their predictions by a large amount[9] and there are supporting analyses on both sides of the question.[10,11] Another computer code, recently written by Bittoni and Haegi,[12] has not yet been benchmarked against these codes. All of these are large codes which consume considerable computer resources for each run. We have been closely monitoring the work on resolving this question, and had a two-day working meeting with Drs. Hively and Tani on August 18-19, 1987. Substantial effort appears to remain before these codes can be used with complete confidence,[13,14,15] as extensively documented in Ref. 9.

Although detailed orbit-following for D-^{3}He fusion products over their full lifetimes is thus not feasible at present, some of the more important effects lend themselves to analytic analysis. Prompt loss may be accurately assessed, because an elegant theory exists for axisymmetric tokamaks[2] and ripple should only slightly modify the first-orbit loss of fusion products. Collisionless ripple-loss may be estimated by the analytic map of Goldston et al.[16] or the two-step mapping formalism of White et al.,[17] which has been verified approximately by Hitchon and Hastie.[11] Most of the fusion-product loss

effort has concentrated on prompt loss and ripple loss, but there are other effects which may be important but which are more difficult to treat theoretically, such as finite gyroradii, electric fields, and instabilities (particularly sawteeth). These are summarized by Hively.[9]

5.2 Prompt Loss of Fast Ions

Prompt loss is defined here as loss of fusion products because their orbits intersect the first wall, limiter, or divertor within a single bounce time of their birth. A small fraction of the ripple-induced loss is prompt in this sense, but it will be termed ripple loss in this paper. The theory of Rome and Peng[2] for orbit analysis in an axisymmetric tokamak applies reasonably well to prompt loss in rippled tokamaks, because ripple will only slightly perturb most prompt-loss orbits. Hively and Miley[18] used a different formalism, and they appear to be the only reference also treating the D-^{3}He protons. The Rome and Peng theory allows treatment of noncircular, finite-beta tokamaks ($\beta \leq 10\%$), although up/down symmetry and a monotonic poloidal flux function are assumed. That theory is based on the constants of the motion v, $\zeta_m \equiv \frac{v_\parallel}{v}\Big|_{\psi_m}$ and ψ_m where v is the total velocity, $v_\parallel$ is the velocity parallel to the plasma current, and $\psi_m \equiv -RA_\phi$ is the maximum poloidal flux function along the ion's orbit (occurring in the equatorial plane due to the assumption that ψ is monotonic). Motivated by the Rome and Peng formalism, the variables $\zeta \equiv v_\parallel/v$, v, and ψ defined locally will be used here. The physical position of the wall and the local, fusion product source term are then calculated as functions of these variables and B, the local magnetic field magnitude.

The analysis begins with the conservation of energy, the conservation of magnetic moment $\mu = v_\perp^2/2B$, and the conservation of toroidal canonical angular momentum

$$p_\phi = \gamma m R v_\parallel \frac{B_\phi}{B} - ze\psi \qquad (5.2\text{-}1)$$

where R is the major radius, z is the ion's charge, m is the ion's mass, $\gamma = 1/(1-v^2/c^2)^{1/2}$ and c is the speed of light. From here on, relativistic effects will be assumed to be sufficiently small so that $\gamma = 1$. Using the conservation of μ,

$$\zeta_x = \pm \left[1 - (1-\zeta^2)\frac{B_x}{B}\right]^{1/2} \qquad (5.2\text{-}2)$$

where the subscript x indicates a point anywhere along an ion's orbit. Evaluating Eq. (5.2-1) at the first wall and at any point along the orbit, and also using Eq. (5.2-2), gives the general orbit equation

$$\frac{B_w}{B} = \frac{-(1-\zeta^2) + \{(1-\zeta^2)^2 + 4[\zeta - \frac{\omega_{ci}}{R_o B_o v}(\Psi_w - \Psi)]^2\}^{1/2}}{2[\zeta - \frac{\omega_{ci}}{R_o B_o v}(\psi_w - \psi)]^2} \qquad (5.2\text{-}3)$$

where $RB_\phi = R_o B_o$ has been assumed and the subscript w indicates a value at the first wall. Note that Eq. (5.2-3) differs from the Rome and Peng formulation in that ζ, not ζ_m (which they call ζ), is used.

The importance of this equation is that it is very general, and the values for B(R,z) and Ψ(R,z) for a high-beta, noncircular equilibrium can be extracted from a sophisticated computer code and used to calculate whether a fusion product born at (R,z) with v and ζ will hit the first wall (at Ψ_w and B_w). At this point, in general, numerical methods will be needed to insert equilibrium values for B, Ψ, j, n, and T into these formulas and to calculate the first wall surface heat load. The simplest means of numerically solving the problem is to use a Monte Carlo method to generate source particles and to count the resulting impacts on the first wall. Because some solutions to these equations are topologically disconnected, it may be necessary to follow the orbits rather than simply to solve Eq. (5.2-3) and an equation for the wall position simultaneously.[14] This Monte Carlo approach was essentially the method of Bauer et al.[19] although they used (R,z) coordinates and only treated the zero-beta, circular tokamak case. The present method will apply also to finite-beta, non-circular tokamaks.

The surface heat load can be estimated by examining the case of a circular plasma generating the same fusion power as a D-shaped plasma. For this estimate, a computer code provided by Lee M. Hively was used.[18] The Hively code follows trajectories in (r,θ) space for a given fusion power source density.

The density and temperature radial profiles are assumed to be those of Sec. 3.2, that is

$$n(r) = n_o[1 - (\frac{r}{a})^2] \qquad (5.2\text{-}4)$$

and

$$T_i(r) = T_{io}\,[1 - (\frac{r}{a})^2]^{3/2} \qquad (5.2\text{-}5)$$

where the subscript "o" indicates an on-axis value and a is the plasma minor radius. The plasma current radial profile is assumed to be

$$j(r) = j_o[1 - (\frac{r}{a})^2] \ . \qquad (5.2\text{-}6)$$

With the assumption that the plasma density and temperature are constant on a flux surface, the local fusion-product production density, $S_{fus}(R,z)$, is equal to

$$S_{fus}(R,z) = n_D(R,z)\, n_{He}(R,z)\, \langle\sigma v\rangle_{DHe} \qquad (5.2\text{-}7)$$

where $n_D(R,z)$ is the deuterium density, $n_{He}(R,z)$ is the ^{3}He density, and $\langle\sigma v\rangle_{DHe}$ is the D-^{3}He fusion reaction rate.

Three cases were run, all modelling Case A-3 of Section 3.4 with a fusion power of 62 MW:

1. A circular plasma with R = 5.14 m, a = 1.69 m shifted 0.33 m toward the inboard side, first wall radius = 2.17 m, and I_p = 16.2 MA;
2. A circular plasma with R = 5.14 m, a = 1.69 m shifted 0.33 m toward the inboard side, first wall radius = 2.17 m, and q(a) = 2.44; and
3. A circular plasma with R = 5.47 m, a = 2.02 m concentric with a circular first wall of radius 2.17 m, and q(a) = 2.44.

These cases are listed in order from most optimistic to most pessimistic. Case 2 has a plasma current of only 6.3 MA, while Case 3 only allows 0.15 m between the plasma and first wall on all sides of the plasma.

However, in all cases, the first wall surface heat load due to fusion-product, prompt-loss ions was found to be less than 0.1 W/cm^2 and, therefore, negligible. These low values are due to the high plasma current, and are consistent with the behavior resulting from increasing the plasma current in the TFTR-I case of Hively and Miley.[18] That is, a factor of two increase in plasma current for their TFTR-I case gives a decrease in average first wall surface heat load of more than a factor of five. In the present case, the toroidal magnetic field remains nearly the same, but the major radius

has increased by about a factor of two and the plasma current has increased by factors of 6 to 16, depending on the model used.

Thus, prompt loss is not expected to be a problem for the high current cases examined in this report, even if the model implementing Eq. (5.2-3) for finite-beta, non-circular tokamaks were used.

5.3 Ripple Loss of Fast Ions

Although substantial discrepancies remain between the results from the large computer codes used to address the rippled tokamak particle loss problem,[9,13,14,15] a large fraction of the ion loss does appear to occur during the first few hundred ion orbits as shown in Figures 5.3-1a[7] and 5.3-1b[8]. Since the mechanism for this loss depends only very weakly on collisions,[1] some analytical progress can be made.

The chief mechanism causing fast ion loss seems to be ripple-induced stochasticity of banana orbits due to radial drift at the turning points. Using an analytic mapping, Goldston et al.[16] found a limit on the ripple at the banana-orbit turning point of

$$\delta \lesssim \left[\left(\frac{\pi N q}{\epsilon}\right)^{3/2} \rho \frac{dq}{dr}\right]^{-1} \qquad (5.3\text{-}1)$$

where δ is the local ripple, N is the number of magnetic field coils, q is the safety factor, $\epsilon \equiv r/R$, and ρ is the gyroradius in the toroidal field. This limit applies to particles with large banana orbits, that is

$$\rho_p \gtrsim \frac{r}{\pi^{3/2}\, \epsilon^{1/2}\, (Nq)^{1/2}} \qquad (5.3\text{-}2)$$

where ρ_p is the gyroradius in the poloidal field. Almost all banana-orbit fusion products in both the D-T and D-^{3}He cases will satisfy Eq. (5.3-2). These formulas impose a constraint on the ripple magnitude at $\theta \simeq \pi/2$ on the order of 0.3% for INTOR alpha particles. The more sophisticated two-step mapping of White et al.[17] and the guiding-center, orbit-following code of Hitchon and Hastie[11] lead to somewhat more pessimistic values. However, as shown in Figure 5.3-2, taken from Hitchon and Hastie,[11] the analytic criterion of Goldston et al.[16] is fairly good at the low ripple values under consideration here. The analyses indicate that stochastic ripple diffusion of alpha particles will occur only at the outer edge of the INTOR plasma for a δ_0 (peak to average) of 1.2%, which is also the NET-DN ripple value. Since the allowed

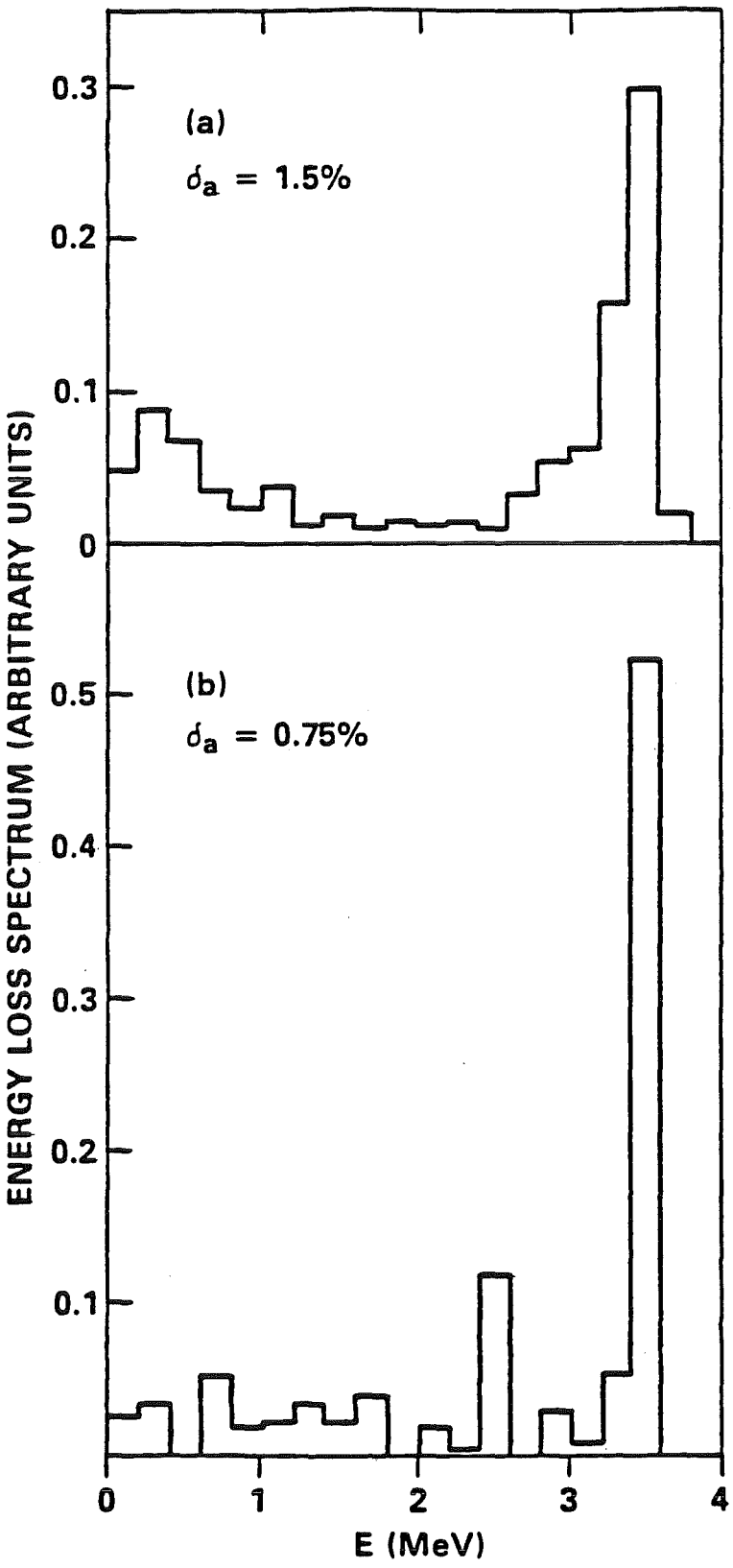

Fig. 5.3-1. Energy loss spectrum for alpha particles in a D-T tokamak from a) Tani et al.[7] and b) Hively[8].

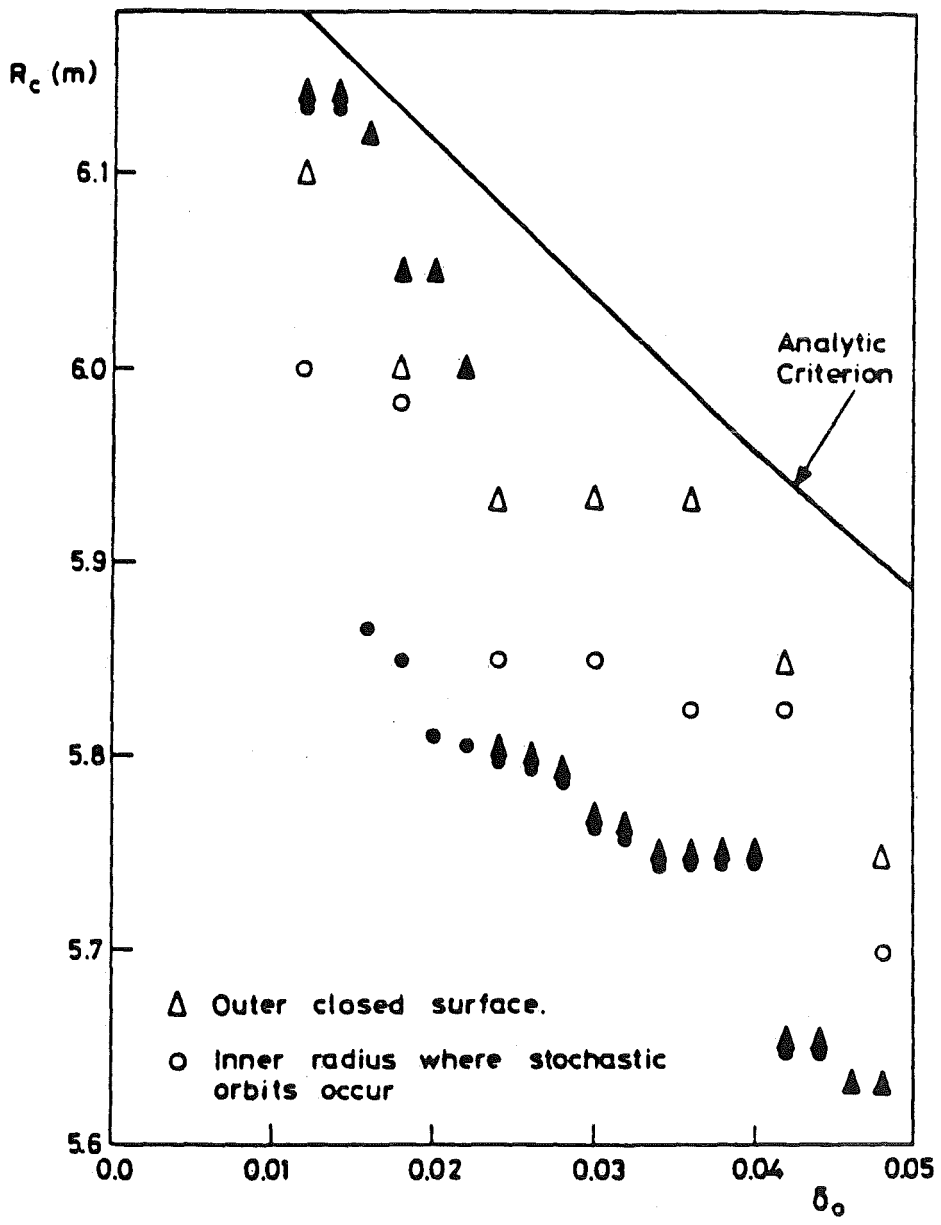

Fig. 5.3-2. Radius of onset of stochasticity versus ripple amplitude δ_o. Solid symbols refer to the analysis of White et al.,[17] hollow symbols to Hitchon and Hastie,[11] and the solid line to Goldston et al.[16] The figure is from Hitchon and Hastie.[11]

ripple in Eq. (5.3-1) is directly proportional to ρ^{-1}, the criterion for avoiding stochastic ripple diffusion of D-^{3}He protons will be approximately twice as stringent as that for INTOR alpha particles. A preliminary plot of the ripple in NET is shown in Figure 5.3-3.[12] This plot indicates that the present NET design will be operating very close to the proton stochastic ripple diffusion limit of 0.15% at $\theta \simeq \pi/2$, and a more sophisticated analysis will be required. Because the banana orbits extend a considerable distance in the toroidal direction, most of the energy from this loss channel should end up on the divertor plates rather than on the first wall. Nevertheless, since the fraction of trapped fusion products for NET will be approximately 62%, only a small portion of them may be allowed to be lost due to ripple without negatively affecting power balance.

Another mechanism which may lead to a localized surface heat load is fast ion loss due to the birth of fusion products in the ripple-trapped region. These ions quickly drift out of the device vertically along the ripple well. The direct ripple-loss region is proportional to $(2\delta)^{1/2} \simeq 0.15$ and this energy will be localized near the ripple minimum. The distribution of surface heat will depend on the detailed toroidal variation of the ripple, and will be weighted along the poloidal direction of the wall by the angle of the wall and by the fusion source term as given in Eq. (5.2-6). This loss region in velocity space is small compared to the prompt (first-orbit) loss discussed in Section 5.2, as shown in Figure 5.3-4,[7] but may lead to localization of the surface heat at different points on the first wall.

5.4 Summary

The loss of D-^{3}He fusion-product ions in a NET-like tokamak and the effect on first wall heat loads has been considered in comparison to the corresponding loss in a D-T plasma. Unfortunately, there is major disagreement in the field concerning ripple losses during slowing down, even in D-T plasmas. Prompt loss is expected to account for approximately one-half of the first wall heat load due to fusion products. It has been analyzed for an axisymmetric circular tokamak and found to produce only a small heat load if the wall is sufficiently far from the plasma. The extension to finite-beta, non-circular plasmas such as in NET or ITER has been formulated but not yet implemented. Clearly, further work in this area is required, but this is beyond the scope of the present study.

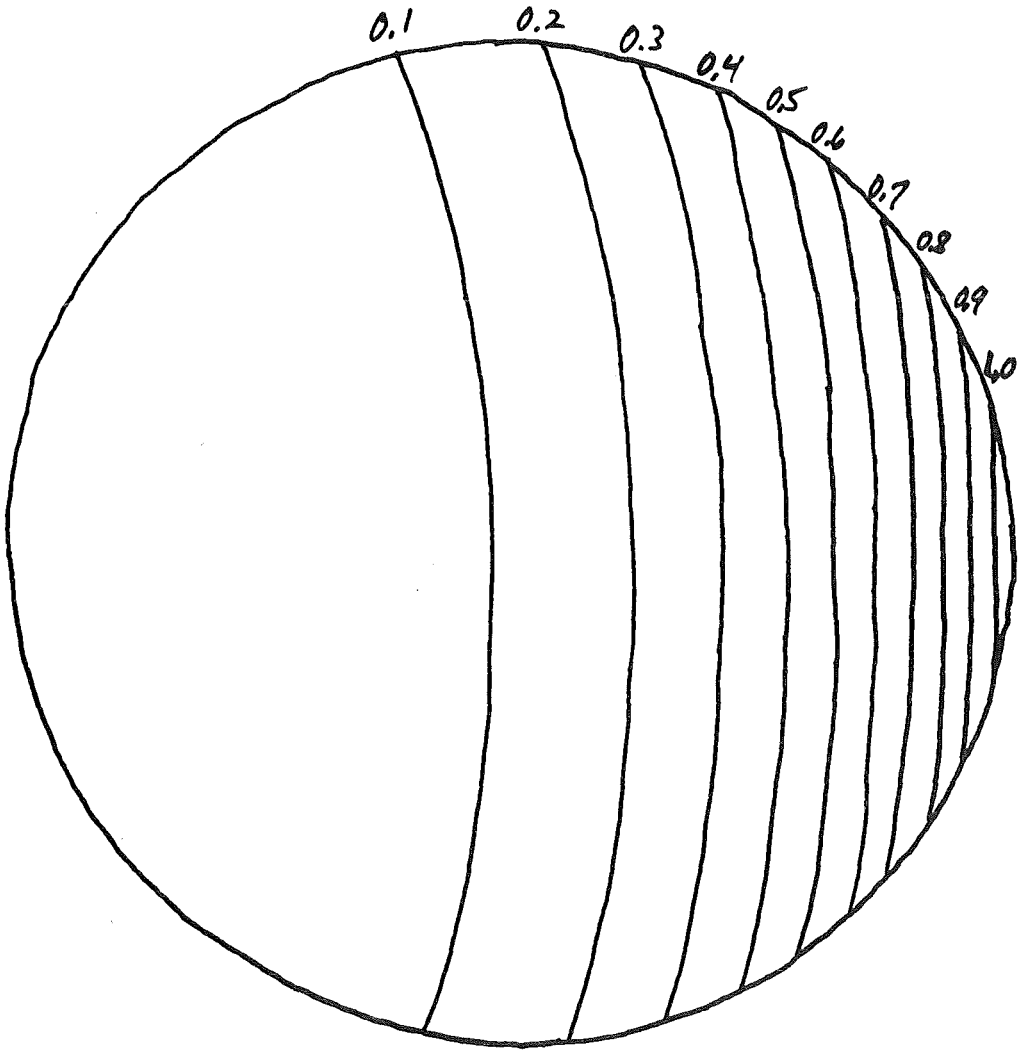

Fig. 5.3-3. Typical ripple contours (%) in NET from Bittoni and Haegi.[12]

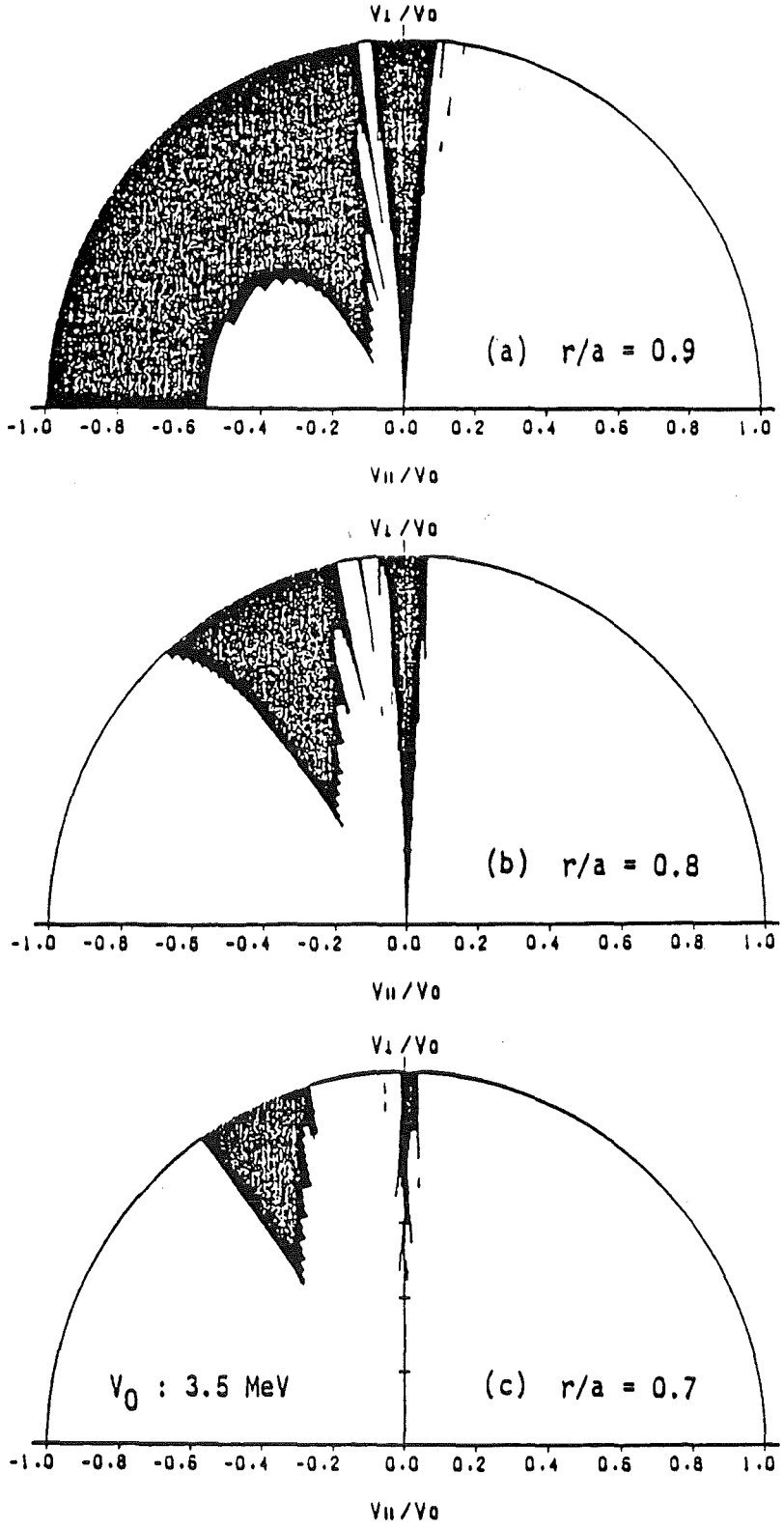

Fig. 5.3-4. Prompt (first-orbit) loss and ripple loss regions for INTOR with δ_0 = 0.75% from Tani et al.[7]

Acknowledgements

Thanks are gratefully extended to Dr. L.M. Hively, both for helpful discussions of the issues and for use of his prompt-loss computer code for axisymmetric tokamaks. Thanks are also due to Drs. K. Tani and J.A. Rome for useful discussions.

References for Chapter 5

1. R.J. Goldston and H.H. Towner, "Effects of Toroidal Field Ripple on Suprathermal Ions in Tokamak Plasmas," J. of Plasma Phys. 26, 283 (1981).

2. James A. Rome and Y-K.M. Peng, "The Topology of Tokamak Orbits," Nucl. Fusion 19, 1193 (1979).

3. James A. Rome, J.F. Lyon and R.H. Fowler, "Using a Constants-of-Motion Space to Clarify Measurements Involving Energetic Ion Orbits in Tokamaks," Oak Ridge National Laboratory Report ORNL/TM-7913 (1981).

4. L.M. Hively, G.H. Miley and J.A. Rome, "Fast-Ion Thermalization in Non-Circular Tokamaks with Large-Banana-Width Effects," Nucl. Fusion 21, 1431 (1981).

5. F.L. Hinton and R.D. Hazeltine, "Theory of Plasma Transport in Toroidal Confinement Systems," Rev. Mod. Phys. 48, 239 (1976).

6. D.W. Ross, P.H. Diamond, J.F. Drake, F.L. Hinton, F.W. Perkins et al., "Thermal Particle Transport - Theoretical Model for Ignition Studies," University of Texas Fusion Research Center Report FRCR-295 (1987).

7. K. Tani, T. Takizuka, M. Azumi and H. Kishimoto, "Ripple Loss of Suprathermal Alpha Particles During Slowing-Down in a Tokamak Reactor," Nucl. Fusion 23, 657 (1983).

8. L.M. Hively, "TF-Ripple Losses from a Non-Circular Tokamak," Nucl. Fusion 24, 779 (1984).

9. L.M. Hively, "Problems in Modeling TF Ripple Loss of Fast Alphas from a Tokamak Reactor, Fusion Technol. 13, 438 (1988).

10. F.S. Zajtsev, A.P. Smirnov and P.N. Yushmanov, "Integral Stochastic Alpha Particle Losses in a Tokamak Reactor," Nucl. Fusion 26, 1311 (1986).

11. W.N.G. Hitchon and R.J. Hastie, "The Confinement of Alpha Particles in a Slightly Asymmetric Tokamak Reactor," Nucl. Fusion 23, 533 (1983).

12. Z. Bittoni and M. Haegi, "Alpha Loss Calculation (NET)," Workshop on Alpha Particle Effects in ETR, June 15, 1987, U.S. Department of Energy Headquarters, Germantown, MD.

13. L.M. Hively - Private communication (1987).

14. L.M. Hively - Private communication (1988).

15. K. Tani - Private communication (1987).

16. R.J. Goldston, R.B. White and A.H. Boozer, "Confinement of High-Energy Trapped Particles in Tokamaks," Phys. Rev. Lett. 47, 647 (1981).

17. R.B. White, A.H. Boozer, R. Goldston, R. Hay, J. Albert and C.F.F. Karney, "Confinement in Toroidal Systems with Partially Destroyed Magnetic Surfaces," 9th IAEA, Baltimore, Vol III, IAEA-CN-41/T-3 (1982).

18. L.M. Hively and G.H. Miley, "Fusion Product Bombardment of a Tokamak First Wall," Nucl. Fusion 17, 1031 (1977).

19. W. Bauer, K.L. Wilson, C.L. Bisson, L.G. Haggmark, and R.J. Goldston, "Alpha Transport and Blistering in Tokamaks," Nucl. Fusion 19, 93 (1979)

6. PLASMA REFUELLING

6.1 Introduction

Refuelling of a reactor grade plasma is a difficult task. The techniques used in present day experiments (gas puffing, neutral beam injection, and pellet injection) become more difficult, if not impossible, under the higher densities and temperatures envisioned for reactors. Gas puffing is basically surface refuelling, even in the larger present day experiments, and depends on plasma transport processes, e.g. the pinch effect, to carry the fuel to the center of the discharge. There is no control over the density profile; Alcator-C experiments have shown a saturation of confinement with increasing density using gas puffing; with pellet injection, however, the fuel could be deposited near the center of the discharge and improved confinement was observed. The highest $n\tau$ values achieved in Alcator-C were with pellet injection. In addition gas puffing leads to an enhanced charge exchange loss bombarding the first wall and, in divertor discharges, leads to deposition of a sizeable fraction of the fuel in the scrape-off layer. Gas puffing is generally dismissed as a possibility for refuelling in the next generation of devices. Pellet injection offers the possibility of depositing the fuel near the center of the plasma and providing control over the density profile. The required injection velocity, which depends on the ablation mechanisms, is a concern, both in terms of developing a suitable injector and maintaining the integrity of the pellet during the acceleration process. Neutral beam injection also offers the possibility of deep refuelling, but the required beam energy is a concern for neutral beam development. In addition, the power deposited by the neutral beam may be excessive and upset the plasma power balance. Plasma injection is an old idea which is now receiving more experimental attention as an alternative to the above approaches. In the following sections we consider the possibilities of pellet injection, neutral beam injection, and plasma injection for refuelling a NET-like tokamak operating on D-^{3}He.

6.2 Pellet Fuelling

6.2.1 Introduction

The fuelling of a large, high temperature plasma, such as proposed for NET, represents a formidable task, as summarized by Lengyel.[1] This task is difficult because the plasma temperature in NET fuelled with DT is much higher than in any existing plasma experiment in which pellet fuelling has been attempted. Also, no experience is available on actual DT fuelling in which the effect of the energetic α-particles has been

observed. Operational models have been developed to simulate the mechanisms involved in plasma fuelling but these models have not been tested at high plasma temperatures or in the presence of fusion reaction products. Consequently, suggesting a fuelling scheme for a D-^{3}He plasma is difficult at this time because the plasma temperature in this case will be ~ 3 times higher than for a D-T device and the reaction products will include not only a 3.5 MeV α-particle but also a 15 MeV proton.

The experimental techniques presently demonstrated for plasma fuelling are gas puffing and pellet injection using frozen particles of H_2 or D_2. Several plasma experiments have demonstrated that pellet injection is a viable fuelling technique and superior to gas puffing because it delivers fuel into the center of the plasma much faster than the time required for a gaseous fuel to diffuse into the plasma. Such fuelling results in increased density limits and energy confinement in the plasma. Multiple pellet injection into TFTR[2] has demonstrated ($n\tau$) values of 1.4×10^{20} m^{-3} at central electron temperatures of 1.4 keV. Because of this success with pellet fuelling, the concept of D-^{3}He fuel pellets is considered in this study for fuelling the early experiments in NET.

6.2.2 Fabrication of D-^{3}He Fuel Pellets

The fabrication of a fuel pellet containing ^{3}He is extremely difficult because the critical temperature (3.2 K) is the lowest of any substance. As the temperature is decreased further it remains a liquid, requiring a pressure of ~ 3 MPa to cause solidification. Because a fuel pellet could not be delivered into the plasma at such a high pressure, the fuel pellet must contain liquid ^{3}He. An exposed liquid droplet could neither be accelerated nor remain intact during its penetration of the plasma; therefore, the liquid must be encapsulated. Any encapsulating material will contaminate the plasma. We are suggesting, therefore, that the liquid ^{3}He be encased in a thin-walled polymer sphere which is coated with D_2 ice.

The fabrication of the fuel pellet would begin with the production of hollow, thin-walled spheres. The mass-production of high-quality, hollow glass and polymer membrane spheres has been extensively studied for the ICF program[3] and this technology will be utilized for our study. The wall thickness of the spheres will need to be < 2.5 μm in order to minimize the carbon contamination of the plasma. These hollow spheres will be loaded into a pressure vessel at 300 K to which ^{3}He will be added. This gas, which diffuses into the spheres, will be slowly increased in pressure to ~ 45 MPa at which temperature and pressure the gas density will equal the density of ^{3}He liquid at 3 K.

The entire pressure vessel containing the spheres and the ^{3}He gas will be cooled to ~ 16 K. During the cooling process the helium permeability of the spherical membrane approaches zero, so that the ^{3}He is trapped in the sphere. At 16 K D_2 gas is mixed with the ^{3}He in the pressure vessel and a coating of D_2 ice is formed on the spheres using fluidized-bed technology. Following the coating process, the entire apparatus is cooled to 3 K and the excess ^{3}He removed from the vessel. The ^{3}He pressure in the spheres is now only 0.11 MPa (1 atm) and the strength of the spheres is calculated to retain this pressure. The spheres must be kept at 3 K until injection into the plasma.

6.2.3 Ablation of Fuel Pellet in the Plasma

The models[4] proposed for the ablation of the pellet in the plasma suggest that the pellet is rapidly bombarded by the plasma electrons which heat the surface of the pellet and vaporize fuel material. The fuel molecules released from the surface rapidly accelerate and form a vapor cloud surrounding the pellet. This vapor cloud begins to attenuate incoming electrons, forming a shield. At steady-state the electron energy deposited in the cloud is ~ 10^3 times greater than the energy deposited on the pellet. The ablation of the pellet due to the heating caused by energetic particles in the plasma has been modelled in a similar manner.[5] The results of such calculations indicate that 40 keV protons, supplied by neutral beam injectors, contribute approximately the same heating energy to the pellet as the electrons when the electron density is high; therefore, the combined effects of electrons and energetic particles have been simply added, in the absence of any experimental verification.

Based upon a simplified relationship by Milora and Foster[4] for electron heating, the velocity of a D-^{3}He pellet required to penetrate the plasma has been calculated for several different input parameters and is given in Table 6.2-1. For the ignition case, in which the central electron temperature is 60 keV, the velocity required of a pellet to approach the center of the plasma would be too high (> 100 km/s) for any pellet launching system; therefore, this case was set aside pending further experimental data, and the fuelling required to achieve energy breakeven (Q = 1) was considered with the results given in Table 6.2-1. For Case A, with T_e = 30 keV, the velocity is excessively large, 370 km/s. We can consider the technique of multiple pellet fuelling, as demonstrated in TFTR, in which the electron temperature decreased significantly for pellet penetration of only 50% of the plasma radius. This technique could be used with D-^{3}He plasma because ICRF heating would keep the central ^{3}He ions hot and their heating of the

Table 6.2-1. Velocity Requirements for Fuel Pellets Injected into the NET Reactor Operating on D-^{3}He Fuel at Low Q Values

Case	Pellets Injected	T_e (a) keV	f (b)	Velocity Required r/a (c)	km/s
A	single	30	0.1	0.5	370
B	multiple	7.5	0.1	0.5	36
C	multiple	7.5	0.4	0.5	16
D	Multiple	7.5	0.4	0.7	3.5

(a) $n_e = 9 \times 10^{19}$ m^{-3} for all cases

(b) fraction of the total fuel in the plasma contained in one fuel pellet.

(c) r = radius of the plasma at which the pellet disappears
a = distance from the plasma core to the outside edge of the plasma (1.7 m for all cases)

electrons at the periphery would be low. On the assumption that T_e could be reduced by 75% (Case B), the velocity required is reduced to 36 km/s, which is still excessive. Up to this point, we have considered pellets which contain only 10% of the mass of fuel in the plasma. Now, we consider fuel pellets which contain 40% (Case C), of the ions in the plasma. The density fluctuation associated with this large pellet is a concern, although larger pellets have been injected successfully in some experiments. For Case C, the velocity is reduced to 16 km/s. Finally, we consider pellet penetration to only 30% of the distance into the plasma, Case D. For Case D, the velocity required is only 3.5 km/s which is a reasonable extrapolation from presently available pneumatic pellet accelerators.[6]

The examples given in Table 6.2-1 illustrate some of the choices which may be possible for the design of fuel pellets and the requirements for the design and mode of operation for the pellet accelerators. The conclusion of the brief study is that fabrication of D-^{3}He pellets can be developed and that these pellets could probably be used to provide edge fuelling. Much more experimental work is needed, however, regarding the pellet fueling of high temperature plasmas before our conclusions can be evaluated.

References for Section 6.2

1. L.L. Lengyel, "Assessment of Pellet Injection for NET (Summary and Conclusions)," EUR-FU/XII-80/86/53, December 1985.

2. G.L. Schmidt, et al., "Pellet Injection Results During TFTR Ohmic and Neutral Beam Heating Experiments," Paper CN-47/A-III-4, Eleventh Intnl. Conf. on Plasma Phys. Controlled Nucl. Fusion Res., Kyoto, Japan, Nov. 13-20, 1986.

3. R. Crawley, "A Hollow Droplet Generator for Polymer Shell Production," J. Vac. Sci. Technol., A4, 1138 (1986).

4. S.L. Milora and C.A. Foster, "ORNL Neutral Gas Shielding Model for Pellet-Plasma Interactions," ORNL/TM-5776, May 1977.

5. Y. Nakamura, H. Nishihara and M. Wakatani, "An Analysis of the Ablation Rate for Solid Pellets Injected into Neutral Beam Heated Toroidal Plasmas," Nucl. Fusion, 28, 907, (1986).

6. S.K. Combs, S.L. Milora, C.R. Foust, G.L. Schmidt and T.P. McBride, "Operation of a Repeating Pneumatic Hydrogen Pellet Injector on TFTR," J. Vac. Sci. Technol., A4, 1113 (1986).

6.3 Neutral Beam Refuelling

Neutral beam refuelling has been a beneficial side effect in neutral beam heated tokamaks; the primary purpose of neutral beam injection (NBI) has been heating, not refuelling. Nevertheless, it is worthwhile to consider the possibility of refuelling the central core of a NET-like tokamak by NBI. Since helium does not charge exchange well with hydrogen isotopes, one might think the required injection energy may be considerably less for a helium beam than it is for a deuterium beam.

The relevant atomic reactions for a neutral ^{3}He beam penetrating the plasma are:

	Cross-section
Electron impact ionization:	
$He^0 + e^- \rightarrow He^+ + 2\,e^-$	σ_1
Ion impact ionization:	
$He^0 + D^+ \rightarrow He^+ + D^+ + e^-$	σ_2
$He^0 + He^{++} \rightarrow He^+ + He^{++} + e^-$	σ_3
Charge exchange with deuterium:	
$He^0 + D^+ \rightarrow He^+ + D^0$	σ_4
One-electron charge exchange with He^{++}:	
$He^0 + He^{++} \rightarrow He^+ + He^+$	σ_5
Two-electron charge exchange with He^{++}:	
$He^0 + He^{++} \rightarrow He^{++} + He^0$	σ_6

We denote the cross-sections for these reactions by σ_1 through σ_6, respectively. The only cross-sections we have found are for the ^{4}He isotope, not ^{3}He. We assume here that the different mass of the ^{3}He nucleus does not matter and that the cross-sections depend fundamentally on the relative speed of the two interacting particles. For electron impact ionization we use the Maxwellian-averaged cross-section, $\langle\sigma v\rangle_e$, data given in Ref. 1. For ionization by D^+ impact we use the cross-section for proton impact ionization, which is also given in Ref. 1. We have not found data for ionization by He^{++} impact; for this process we also use the data for proton impact ionization. For charge

exchange of He^0 with D^+ we use the cross-section data for He^0 with H^+. The cross-sections for the two He^{++}-He^0 reactions are given in Ref. 2. The cross-sections for these processes are shown in Table 6.3-1 as a function for the ^3He beam energy. The relative weights of these processes depends not only on the cross-sections, but also on the fuel composition. The important processes in the few hundred keV range are impact ionization by ions and He^0-He^{++} charge exchange.

All of the above reactions lead to stopping of the injected He^0 beam. The beam intensity along the beam line is given by

$$I(x) = I_o\, e^{-\mu(x)}$$

where μ can be written as

$$\mu(x) = \left[\frac{\langle\sigma v\rangle_e}{v_b}\frac{n_e}{n_1} + (\sigma_2 + \sigma_3)\, f_D + (\sigma_4 + \sigma_5 + \sigma_6)(1-f_D)\right] \int n_i dx \ .$$

Here v_b is the velocity of the He^0 atoms, n_e is the electron density, n_i is the total fuel ion density, and f_d is the deuterium fraction in the fuel. For penetration to the center of the plasma we want $\mu = 1$. This determines the required injection energy as a function of the line - integrated density. Using the cross-section data above, the relationship between the injection energy and the line - integrated density was calculated and is given in Table 6.3-2. For NET-DT (Case A-1 in Table 3.4-1) the line - integrated density is $.65 \times 10^{16}$ cm^{-2}, while it is $.78 \times 10^{16}$ cm^{-2} for NET-EP (Case A-2). This assumes perpendicular injection; injection at an angle to the magnetic field will yield a somewhat higher line integrated density. We see that penetration to the center requires about a 300 keV He^0 beam.

The next concern is the required injection power; this depends on the beam current which is determined by the particle confinement time in the center of the discharge. If we consider refuelling inside the a/2 flux surface by NBI and assume the confinement time is four times the energy confinement time (see Sec. 3.3) then the required absorbed current in the central zone is 20 A for Case A-2. Allowing for absorption of the beam in the outer regions, the required current at the plasma edge is 32 A equivalent (assuming Z=1). This is 9.6 MW of refuelling beam power, which is small compared with the 37 MW

Table 6.3-1

Cross-Sections Affecting Absorption of H_e^o Beam

E (keV)	$\frac{\langle\sigma v\rangle_e}{v_b}$ (10^{-16} cm^2)	σ_2 (10^{-16} cm^2)	σ_3 (10^{-16} cm^2)	σ_4 (10^{-16} cm^2)	σ_5 (10^{-16} cm^2)
10	.62	1.0	.9	.5	1.6
30	.35	.9	.5	1.4	1.4
60	.25	.8	.3	3.2	1.0
100	.20	.8	.15	3.2	.7
300	.11	.6	.06	1.0	.1
600	.08	.6	.02	.3	.01
1000	.06	.5	.01	.1	5×10^{-4}

Table 6.3-2

Penetration Depth Versus Energy for H_e^o Beam

E (keV)	$\int n_i dx$ (10^{16} cm^{-2})
10	.32
30	.37
60	.35
100	.40
300	.85
600	1.2
1000	1.6

required to drive the plasma at this operating point. (The technical feasibility of a 300 keV He neutral beam is not assessed as part of this study.)

Helium refuelling of the outer half of the plasma is not really required. A reduction of the helium content in the annular region $a/2 < r < a$ does not cause a significant loss of fusion power, because the power density is proportional to $n^2\langle\sigma v\rangle_f$, which is localized to the center through the spatial dependence of $n(r)$ and $T_i(r)$.

Applying the same analysis to the refuelling of deuterium by NBI, we get the line integrated density versus beam energy shown in Table 6.3-3. This calculation includes the beam absorption by charge exchange and impact ionization with D^+, but ignores the impact ionization with He^{++} for lack of data. The dominant absorption process above 100 keV is impact ionization - not charge exchange. Again we see that the required injection energy is about 300 keV assuming perpendicular injection. For central refuelling, the required beam current is 60 A equivalent and the beam power is 18 MW. The 300 keV D^0 beam, however, is beyond the range for reasonable neutralization efficiency for the positive ion sources used in present experiments. Refuelling the outer half of the plasma with deuterium requirs a 28 MW, 60 keV NBI system, if we assume the "edge" τ_p equals τ_E. The total NBI power for both helium and deuterium refuelling would be 56 MW, which is above the 40 MW required to sustain the plasma. The additional 16 MW could be considered as a safety factor for impurities and other losses.

Not included in this analysis is the very outer edge of the plasma where the recycling is high. This region refuels itself through recycling processes in the divertor and scrape-off layer.

Consequently, we see that the NBI power required to refuel the central zone of the discharge is not unreasonable. Since 300 keV is much less than E_{crit} in a plasma with a 50 keV electron temperature, most of the power will be coupled to the ions. Furthermore, the fast ions produced in the plasma will increase the net fusion reaction rate over that in a Maxwellian plasma and improve Q. We have not assessed this effect quantitatively, however. The entire ^3He fuelling can be provided by a 10 MW, 300 keV NBI system since edge fuelling of He is not required.

References for Section 6.3

1. R.L. Freeman and E.M. Jones, "Atomic Collision Processes in Plasma Physics Experiments", Culham Lab. Rept. CLM-R 137 (May 1974).

2. C.F. Barnett, J.A. Ray, et al., "Atomic Data for Fusion", Oak Ridge National Laboratory Rept. ORNL - 5206 Vol. 1, Feb. 1977.

Table 6.3-3

Penetration Depth versus Energy for D° Beam

E (keV)	$\int n_i dx$ (10^{16} cm^{-2})
10	.10
30	.14
60	.26
100	.43
300	.85
600	1.40
1000	2.07

6.4 Plasma Injection

Refuelling by plasma injection is an old idea[1,2] that has been revived recently for refuelling of tokamaks. There are two basic ideas for plasma injection. The first, and oldest, is injection of plasma from a Marshall gun or other suitable source which crosses the external magnetic field by polarization electric fields. The second is the formation and acceleration of compact toroid plasmas which have a very high energy density and cross the magnetic field by "punching" a hole in the field. In this section we consider both of these possibilities for refuelling of a NET-like tokamak operating on D-^{3}He. The interest in these refuelling techniques stems from the difficulty of making pellets containing ^{3}He and the required injection velocities for adequate pellet penetration, as discussed in the previous section.

6.4.1 Gun Plasma Injection

It is well-known[3] that a moving plasma can cross a vacuum magnetic field provided it meets the condition $\omega_{pi}^2/\omega_{ci}^2 >> 1$, where ω_{pi} and ω_{ci} are the ion plasma and ion cyclotron frequencies, respectively. As the moving plasma with velocity $\vec{V}$ encounters a magnetic field, ions are deflected one way and electrons the other way. This creates a polarization electric field, $\vec{E}$, which builds up until $\vec{E} = -\vec{V} \times \vec{B}$. At this point the interior of the plasma beam can move across the magnetic field with its original velocity $\vec{V} = \vec{E} \times \vec{B}/B^2$. In this situation there is no electric field in the frame of reference moving with the plasma beam and hence no current flow. The stopping of such a plasma beam has to be done by shorting out the polarization electric field with an external conductor.[4] The external conducting path allows a net current flow depending on the induced emf and the impedance of the circuit. The resulting current density, $\vec{J}$, provides a $\vec{J} \times \vec{B}$ force decelerating the plasma stream.

This depolarization induced deceleration has also been observed in toroidal devices with only a poloidal magnetic field, such as toroidal octupoles.[1] The plasma is injected perpendicular to the torus and the magnetic field. It initially crosses the magnetic field by virtue of the polarization electric field until it gets to the center of the confinement region where the direction of the magnetic field is reversed. This change in direction of the magnetic field reverses the polarization of the plasma at the leading edge of the stream and produces an electric field parallel to the motion. Depending on the cross-field resistivity of the plasma, one can now get a shorting of the polarization electric field and a $\vec{E} \times \vec{B}$ force stopping the plasma.

Tokamaks have both toroidal and poloidal magnetic fields with a spatially changing rotational transform. Consequently, the depolarization process in octupoles mentioned above can occur in tokamaks and produce stopping of the plasma stream. In addition, in refuelling, the plasma stream is injected into a torus already containing a well-formed tokamak plasma with very low resistivity because of its high electron temperature. An additional depolarization possibility is the flow of current along the magnetic field in the external plasma which can short out the polarization electric field. These processes require evaluation to assess the suitability of refuelling by this means.

Refuelling of a tokamak by gun injection has been accomplished successfully in the Tokapole II experiment.[6,7] In this experiment involving a small tokamak (major radius = 50 cm, minor radius = 10 cm, B = 5 kG) the density on axis was increased by about 50% in a single shot from a Marshall gun. The theoretical model developed for this experiment was based on current flowing radially across the magnetic field by the electric field produced by the changing pitch angle of the magnetic field. This is shown schematically in Fig. 6.4-1. An important ingredient in the model is the effect of the magnetic field reducing the effective cross-field conductivity of the plasma through the Hall effect;

$$\sigma_{eff} = \left(\frac{1}{2}\right) \frac{\sigma_s}{1 + (\omega_{ce}/\nu_{ei})^2}$$

where σ_s is the usual Spitzer conductivity parallel to the magnetic field, ν_{ei} is the electron-ion collision frequency and ω_{ce} is the electron cyclotron frequency. A detailed quantitative comparison with the experiment was not possible, but the model gave estimates for the stopping length in reasonable agreement with the data and also predicted qualitatively the observed scaling of the trapping with plasma current and toroidal magnetic field.

Plasma contamination due to gun injection is always a concern since gun plasmas have the reputation of being "dirty". In this regard it is important to note that the gun plasma did not noticeably increase the impurity content of the Tokapole discharge. If this were a problem, then alternative plasma sources which don't involve drawing a current between electrodes could be developed.

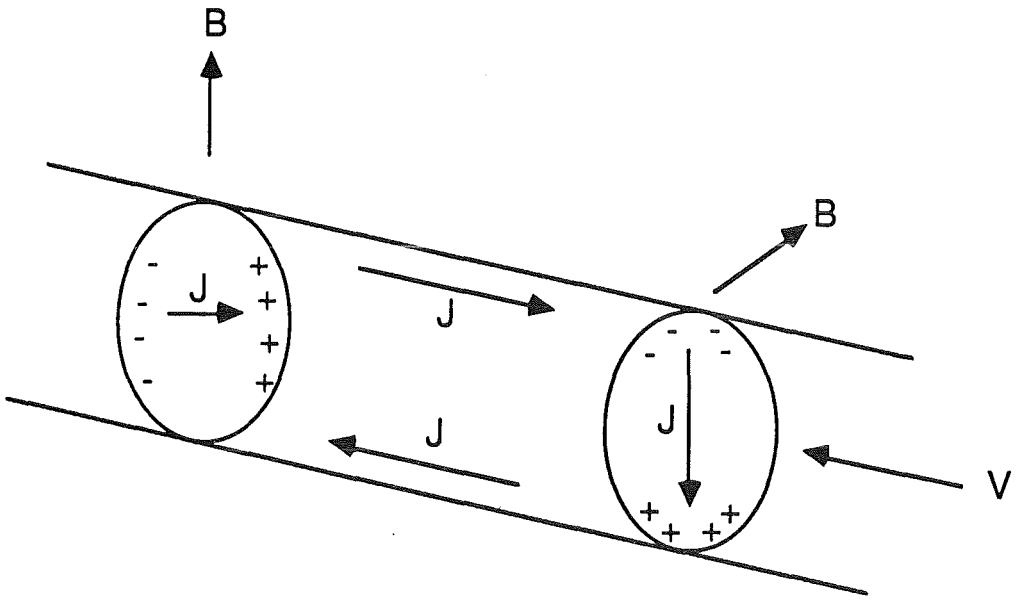

Fig. 6.4-1. Electric field and depolarization current path considered in Tokapole II.

Finally, we note that the gyroradius of the injected ions evaluated using their injection velocity is only 1% of the minor radius of the discharge. Consequently, the gun plasma penetrated at least 100 gyroradii beyond the divertor separatrix and 200 gyroradii beyond the edge of the toroidal magnetic field. This is in strong contrast to the early experiments at Culham involving gun injection where the injected plasma penetrated only 10 - 15 gyroradii.[2]

Applying the model developed for the Tokapole experiments to refuelling of NET with D-^{3}He gives one assessment of the possibility of refuelling of NET using gun injection. If we assume the gun produces a plasma with a density of 10^{16} cm^{-3} with $T_e \sim 10$ eV, a velocity of 10^7 cm/s, a beam radius of 25 cm and a beam length of 1 m, then the stopping distance predicted by the Tokapole model is 5 m. This is more than adequate to insure penetration to the center and longer than desired since the plasma half-width in the horizontal midplane is 1.7 m. Each refuelling shot introduces a fuel charge which is about 6% of the fuel present in the discharge; hence the density fluctuation with each shot is only about 6%. To maintain the fuel density, a repetition rate of 1 shot every 1.5 s is required. This can be provided by a number of refuelling guns firing less frequently.

A possible competing process for shorting out the polarization electric field is current flow through the external plasma along the magnetic field. Because the MHD safety factor is about 2, a field line connects the top of the plasma stream, where the polarization charge density has one sign, to the bottom, where the charge density has the opposite sign, after one transit around the torus, as shown in Fig. 6.4-2. It is important to note, however, that this current path has a high inductance and, consequently, the pulse time of the plasma beam entering the discharge is important in determining the impedance of this current path. For the Tokapole discharge this impedance was estimated to be too large for this effect to be significant. Assuming this is the only depolarization process, a simple model for the stopping of the beam is to consider the circuit equation,

$$L \frac{dI}{dt} = \varepsilon$$

where I is the depolarization current, ε is the induced emf caused by the plasma stream crossing the magnetic field, and L is the inductance of this current path. We neglect the

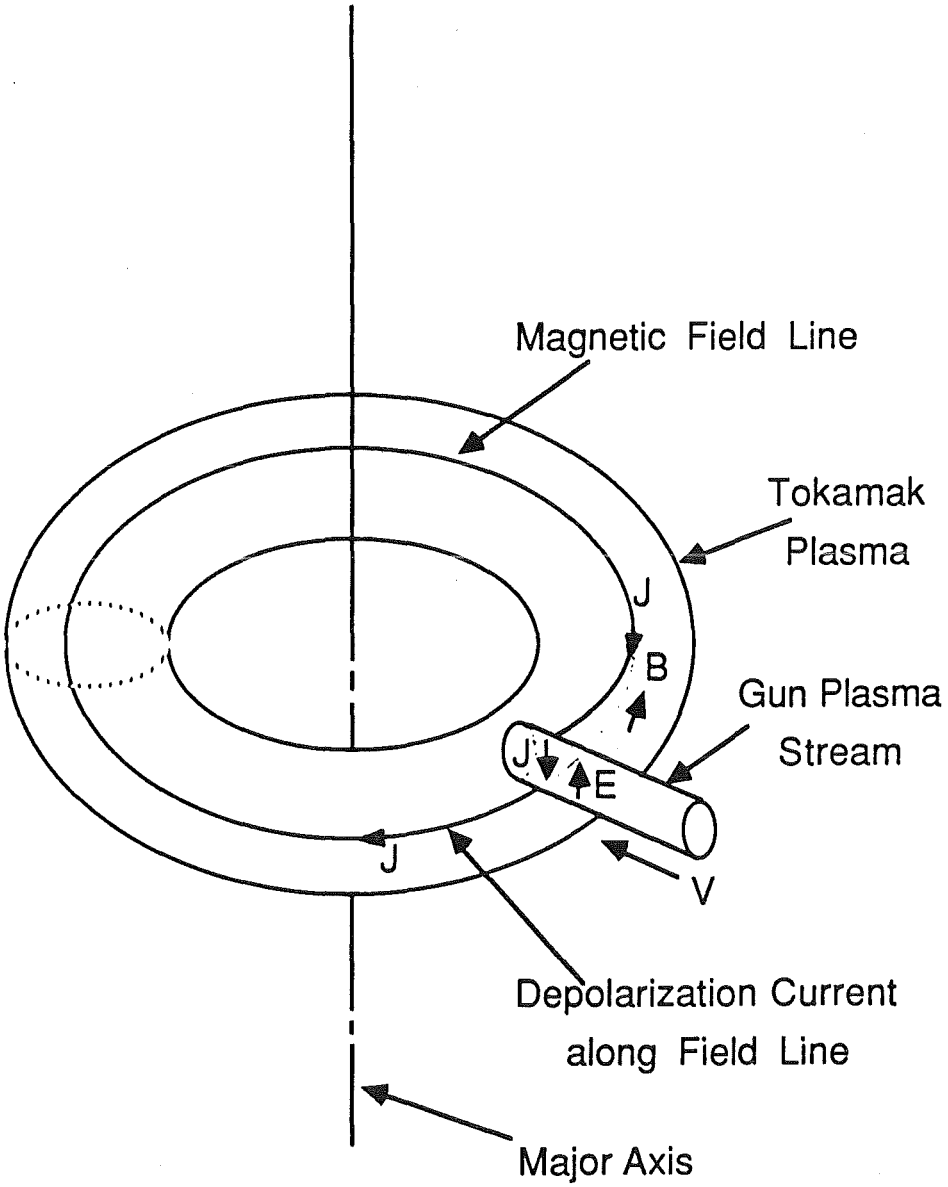

Fig. 6.4-2. An alternative depolarization current path for stopping the injected plasma.

resistance of this current path since the electron temperature of the external plasma is so high. Using

$$\varepsilon = VB\, r_b$$

and

$$M \frac{dV}{dt} = - IB\, r_b$$

for the equation of motion of the plasma stream, where M is the injected mass per shot and r_b is the radius of the plasma stream, we get the result that the current I satisfies

$$\frac{d^2I}{dt^2} = - I/\tau_s^2 , \qquad \tau_s = \sqrt{LM}/Br_b .$$

Consequently, the stopping distance is

$$d = V_o\, \tau_s$$

where V_0 is the initial velocity. Applying this model to refuelling of NET, using the parameters mentioned earlier, gives a stopping distance of 100 cm, which is about what is needed for adequate penetration to the magnetic axis. For NET with D-^{3}He parameters, it appears that this depolarization process is more important than the one apparently involved in the Tokapole II experiment.

6.4.2 Compact Toroid Injection

Refuelling of tokamaks by the injection of plasma in the form of compact toroids has been proposed[7]. The compact toroid injectors offer very high injection velocities with a sizable amount of plasma injected per shot. Compact toroids with a mass of .5 mg have been accelerated to about 400 km/s in the RACE experiments at LLNL, while velocities over 2500 km/s have been achieved.[8] The lifetime of the compact toroid can be greater than a millisecond, depending on the electron temperature; this allows adequate time for acceleration of the plasma to high velocity. These results are very encouraging for the refuelling of large tokamak plasmas. Furthermore, the compact

toroid should be insensitive to the nuclear composition of the plasma of which it is composed and should therefore be suitable for injecting a D-^{3}He fuel mixture.

A compact toroid is a toroidally shaped plasma containing poloidal and magnetic fields generated by currents in the plasma, as shown in Fig. 6.4-3. The compact toroid is formed by firing a magnetized Marshall gun.[9] The toroidal field is produced by the current in the central conductor of the Marshall gun and gets trapped in the compact toroid upon reconnection. The compact toroid is formed when the plasma from the Marshall gun reaches the X-point of the guide field and reconnection occurs, as illustrated in Fig. 6.4-4. After reconnection, the compact toroid has a magnetic dipole and can be accelerated magnetically as a self-contained entity.

The interaction of the compact torus with the magnetic field of the tokamak is believed to occur as illustrated in Fig. 6.4-5. The compact toroid, upon entering the toroidal field of the tokamak, tilts its axis to align along the toroidal field direction. At the same time it is slowing down because of the rising toroidal field seen by the compact toroid. Because of the moment of inertia of the compact toroid, this takes a finite amount of time. After this alignment occurs, the poloidal field of the compact toroid reconnects with the poloidal field of the tokamak. In the analysis done at LLNL[8,10], it is assumed that the compact toroid rapidly disintegrates at this point, because of diffusion of the magnetic field, and deposits its fuel charge. Consequently, one estimate of the penetration depth for the purpose of refuelling is the distance travelled during the time for the compact toroid to tilt by 90 degrees. The fuel still has directed momentum at this point and should travel somewhat further into the plasma, depending on the degree to which depolarization currents and the emission of Alfven waves dissipate the directed kinetic energy of the fuel mass. In order to avoid excessively disturbing the tokamak plasma, the injection velocity was chosen to be less than the Alfven speed in the tokamak plasma.

The compact toroid refuelling scheme considered for TIBER[10] is applicable to D-^{3}He refuelling in NET because the slowing down and tilting of the compact toroid is determined by the toroidal field of the tokamak and not by the properties of the tokamak plasma. The NET device is somewhat larger, but this is compensated by the higher toroidal field, and field gradient, in TIBER. Consequently, the interaction and refuelling properties of the compact toroids should be pretty much the same.

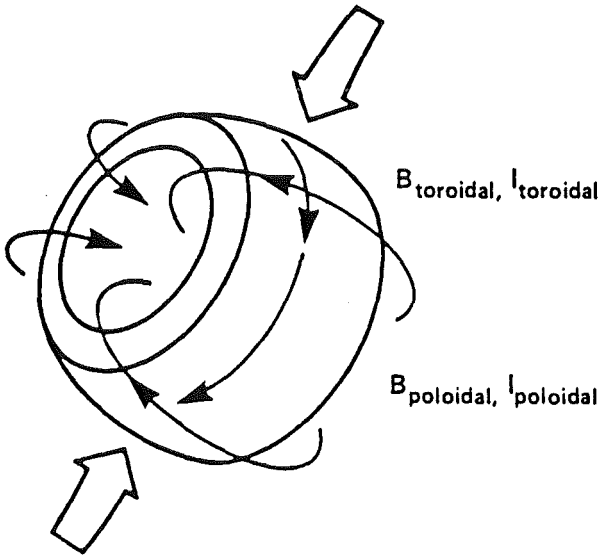

Fig. 6.4-3. Compact Torus

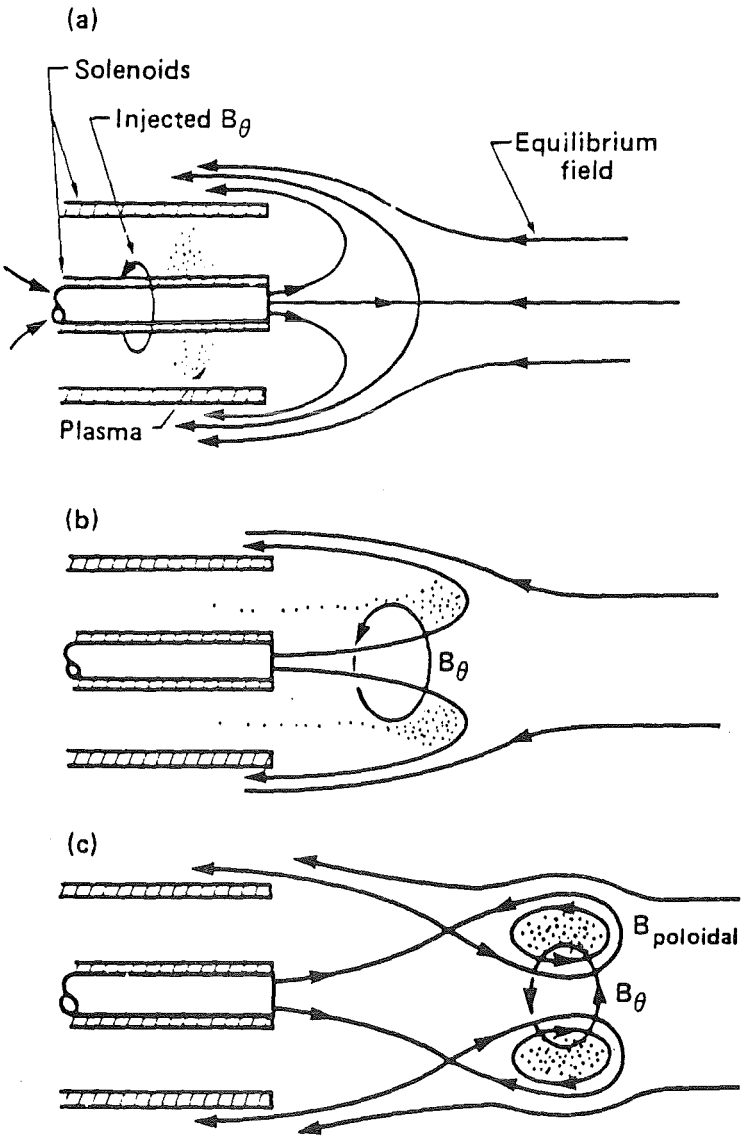

Fig. 6.4-4. Formation of compact torus. (a) Initial injection of toroidal flux. (b) Elongation. (c) Reconnection. (Taken from Ref. 9)

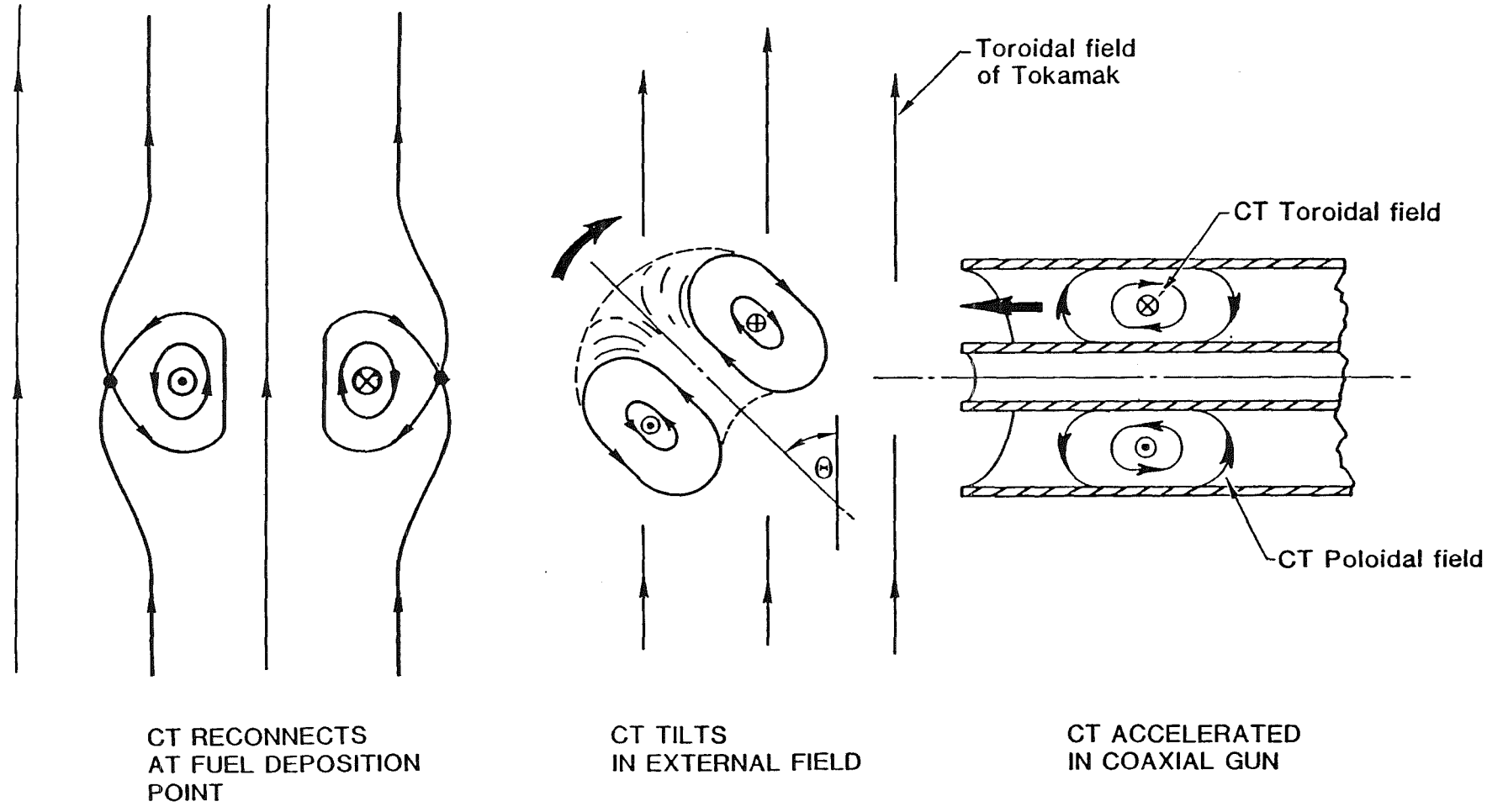

Fig. 6.4-5. Schematic of compact-toroid (CT) acceleration and interaction with the external tokamak toroidal field. As it traverses the external field, the CT rotates through a 90° angle due to the torque on its internal magnetic moment. Alignment of the CT poloidal field with the external field results in field-line reconnection and fuel deposition. (Taken from Ref. 10)

The proposed compact toroid fuel injector for TIBER used an injection velocity of 750 km/s with an injected mass per shot of 5 mg and a repetition rate of .9 Hz. The estimated time-averaged "wall-plug power" for refuelling was 2.5 MW, which is low considering the output of the plant. This system could be used on a D-^{3}He NET without any major changes. Because of the lower ion density in a D-^{3}He NET, compared with TIBER, the Alfvén velocity is higher. Consequently, the injection velocity could be increased if this were desirable. The estimated capital cost of the compact toroid injector system for TIBER was 15 million dollars. It should also be noted that the same system can be used for refuelling both D-^{3}He experiments and D-T experiments.

References for Section 6.4

1. D.A. Dory, D.W. Kerst, D.M. Meade et al., Phys. Fluids 9, 997 (1966).
2. J.H. Adam, Proc. of the 3rd I.A.E.A. Conf. on Plasma Phys. and Cont. Fusion, Novosibirsk, USSR, 1968.
3. G. Schmidt, Phys. Fluids 3, 961 (1960).
4. D.A. Baker and J. Hammel, Phys. Fluids 8, 713 (1965).
5. A.W. Leonard, R.N. Dexter, and J.C. Sprott, Phys. Rev. Lett. 57, 333 (1986).
6. A.W. Leonard, R.N. Dexter, and J.C. Sprott, Phys. Fluids 30, 2877 (1987).
7. C.W. Hartman and J.H. Hammer, Phys. Rev. Lett. 48, 929 (1982).
8. L.J. Perkins, S.K. Ho, and J. Hammer, "Deep Penetration Fueling of Reactor-Grade Plasmas with Accelerated Compact Toroids", LLNL Rept. UCRL-96894 (1987).
9. C.W. Hartman and J.H. Hammer, "Acceleration of a Compact Torus Ring" LLNL Rept. LLL-PROP-191 (1984).
10. "TIBER II/ETR Final Design Report", ed. by J.D. Lee, LLNL Rept. UCID-21150 Vol. 1, 1987.

6.5 Summary

It has been shown in the previous sections that pellet fueling for a D-^{3}He NET experiment is complicated by the difficulty in making ^{3}He pellets. We have presented a concept for encapsulating liquid ^{3}He in a thin polymeric shell, which is overcoated with deuterium; this composite pellet can then be injected into the plasma. Because of the high electron temperature associated with D-^{3}He, the ablation rate of the pellet is high and injection into the center of the discharge requires enormous pellet velocities. Surface fuelling, because of the shorter distance and lower electron temperature at the edge requires injection velocities above that currently available in gas gun injectors, but may be within the reach of what is considered for pellet refuelling in reactor-grade D-T plasmas.

Neutral beam fuelling of the core plasma requires 300 keV ^{3}He and D neutral beams for the cases considered. If one considers only fuelling the center using NBI and not the entire plasma, then the power delivered to the plasma is low enough that the plasma power balance is not upset. Deuterium NBI systems with 300 keV energy are beyond the range of the positive ion source technology currently used, but may be feasible with the development of a negative ion sources. The combination of NBI fuelling of the plasma center with pellet fuelling of the plasma edge is a possible solution to the fuelling problem for driven experiments near $Q = 1$, but may not be suitable in an ignited plasma because of the problem of upsetting the plasma power balance.

A more speculative approach to fuelling is plasma injection. This approach does not suffer from the difficulty of making ^{3}He pellets or the very large required pellet velocity, nor does it upset the plasma power balance. Furthermore, this approach appears to scale favorably to a reactor. Injection of plasma from a Marshall gun has been tried in only one small tokamak experiment, but the results were favorable. Applying the model developed for this experiment to a NET-like device indicated that adequate penetration to the plasma center could be obtained. There remains considerable uncertainty concerning possible depolarization processes which would reduce the penetration. Experimental investigation of plasma injection in larger experiments is very desirable. Injection using Marshall guns has the advantage that it uses basically off-the-shelf technology.

Another related plasma fuelling process is injection of accelerated compact toroid plasmas. The required injection velocity has been attained in current experiments, but the accelerated mass per toroid is about a factor or 10 less than that needed for

refuelling of a NET-like tokamak plasma. The interaction of a compact toroid with a tokamak plasma has not yet been tested experimentally, although some proposals are under study.

7. ICRF HEATING OF NET

7.1 Introduction

We examine ICRF D-^{3}He heating and fusion scenarios for the NET Enhanced Physics (NET-EP) and NET A-3 cases. Issues include: 1) review of previous ICRF D-^{3}He experiments, 2) the single pass NET-EP and NET A-3 minority ^{3}He and second harmonic absorption at concentrations ranging from 2-25%, 3) deuterium and fusion proton ICRF absorption in the machine and 4) the fusion Q factor in the subignited state when compared to the Maxwellian equivalent energy content.

The concept of ICRF enhanced fusion Q (fusion power out/auxiliary power in) was first examined by Scharer, Jacquinot, Lallia and Sand[1] for a modest ICRF power level near breakeven for D-T operation in JET. It was found that minority deuterium fundamental ion resonance non-Maxwellian tail heating produced fusion Q enhancements of factors of two compared to a Maxwellian equivalent. Majority deuterium second harmonic heating was also found to produce Q enhancements for D-T reactors by the same order of magnitude by Harvey, Kerbel and McCoy.[2] We examine ICRF induced tail formation Q factors for the high energy reactivity peak E ≈ 400 keV in D-^{3}He fusion scenarios. In recent JET[3] and earlier PLT[4] D-^{3}He ICRF ^{3}He minority ion heating experiments 3-5 keV majority deuterium ion temperatures have been achieved with strong tail formation. The γ-ray detection measurements on JET[5] have inferred 9 kW of D-^{3}He fusion power and a $Q = P_{FUSION}/P_{RF} = 2 \times 10^{-3}$. Current experiments underway planned for up to 20 MW of ICRF power anticipate a good fraction of a megawatt of D-^{3}He fusion power and a fusion Q of several percent.

7.2 JET D-^{3}He ICRF Fusion Results

The ICRF heating and confinement program on JET has concentrated recently on ^{3}He minority fundamental cyclotron resonant heating with a concentration of 2-5% averaged over the cross section. The remainder is majority deuterium with a typical Z_{eff} of 4 and a dominant carbon impurity. These experiments are similar to previous PLT experiments[4] in which comparable coupled power yielded a somewhat cooler majority temperature. The experiments have concentrated on this regime to examine the confinement of high energy fusion products without the use of tritium and neutron activation of the vessel. The proton is born at 14.7 MeV with the alpha particle at 3.6 MeV. These species do not resonate at the position corresponding to the ^{3}He cyclotron resonance unless the Doppler shift corresponding to their high energies causes

a sufficient overlap. This is a potential advantage over D-T ICRF heating scenarios in which the unshifted deuterium and alpha particle cyclotron resonances occur at the same position.

The best JET experimental results have been done at 5.5 MW of radiofrequency power coupled at a frequency of 33 MHz and several megamp discharges at electron densities of $3 \times 10^{13}/cm^3$. The deuterium ion temperatures are heated to the neighborhood of 4 keV with hotter electron sawteeth phenomena and with average central temperatures of 5-6 keV. The diagnostic of the ^3He tail temperature is difficult to measure and Sadler et al.[5] have used gamma ray detection coming from a separate branch of the fusion reaction and helium reactions with carbon have been used to determine the fusion production and tail temperature of the minority helium tail temperature. They find that the spectral shape of the gamma rays corresponds to a fusion power output of 9 kW and that the energy of typical helium ions in the tail of the distribution corresponds to 200 keV. The coupled ICRF power of 5.5 MW corresponds to a fusion Q of 2×10^{-3}.

Hellsten[6] has used an isotropic steady state Fokker-Planck code to estimate the fusion Q that is achievable on JET. The case of ^3He-D fusions is compared to second harmonic deuterium radiofrequency waves interacting with 80 keV deuterium beam ions with a 50/50 mix of helium and deuterium background and to second harmonic heating of helium with a 50/50 mix of helium and deuterium with beams. The background temperature and density is an input to the code and no accounting for losses or synchrotron radiation is considered in the code. The results are plotted versus the absorbed radiofrequency power in the core region in MW/m^3 and are shown in Fig. 7.2-1. The maximum fusion Q of 0.05 occurs for the minority helium case with the minimum RF absorbed power density corresponding to about 0.25 MW/m^3. These curves should be taken as an estimate and a more detailed calculation taking into account the self-consistent equilibration between the tail formation and the electron and background ion temperatures as well as energy and confinement losses should be made. Yet for these cases factors of 10-100 times the Q value for an equivalent Maxwellian tail temperature are obtained with large thermal anisotropies in the heated ion velocity distribution. For purposes of the NET-EP and NET A-3 cases it would be interesting to carry these calculations out for Q values near and above breakeven to see if substantial Q enhancement can be obtained.

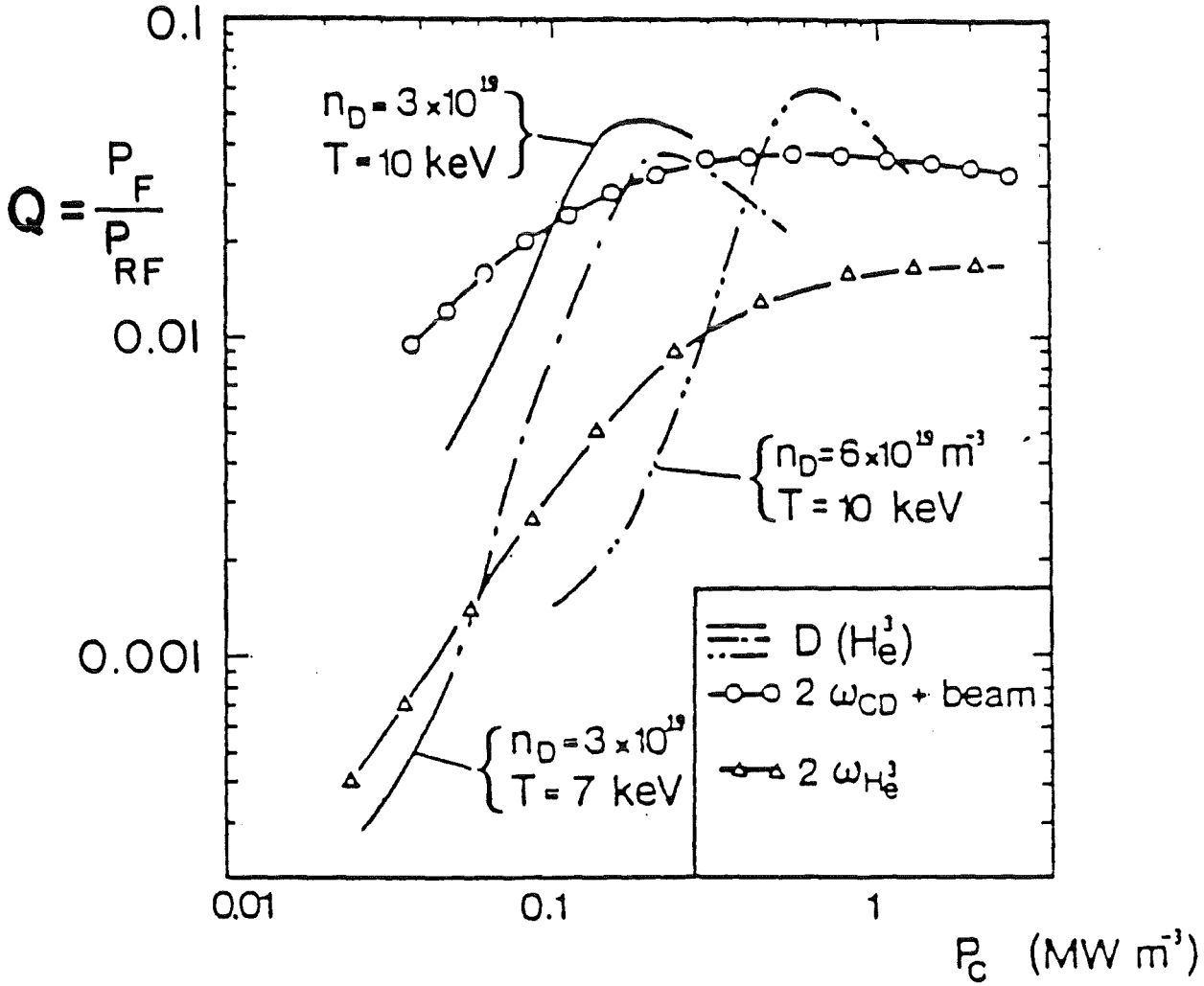

Fig. 7.2-1. Fusion amplification factor for D-^{3}He reaction versus the power damped in the resonating species. Three scenarios are considered: (i) D(^{3}He), ^{3}He resonating minority with n_{He}/n_D = 0.02, (ii) $2\omega_{CD}$, harmonic resonance with deuterium beam ions, E_{inj} = 80 keV, n_{He}/n_D = 1, (iii) $2\omega_{C\,He}$, harmonic resonance with helium-3, n_{He}/n_D = 0.5. In all cases Z_{eff} = 1. From Ref. 6.

7.3 Single Pass Fast Wave Absorption for NET-EP and NET (A-3 case) D-^{3}He Plasmas

To examine the efficiency of absorption for NET-EP parameters we use a computer code corresponding to a definition power absorption and the associated conservation relation for inhomogeneous plasmas developed by McVey, Sund and Scharer.[7] The code correctly solves the propagation and coupling of incident fast magnetosonic waves from the low field side of the machine to ion Bernstein waves in the resonant core region. It has also been checked with good agreement with a PLT data set and range of parallel wavelengths with other groups at Princeton, ORNL and NYU.

We take parameters corresponding to NET-EP startup of a 7 keV temperature for all species with an electron density of $1.78 \times 10^{14}/cm^3$, a toroidal field on axis of 5.6 T and a minor radius of 1.7 m. The helium fraction is taken to be 2% initially to achieve an optimum single pass absorption at lower temperatures. Figure 7.3-1 shows the dispersion relation near the core helium resonance for the incident and reflected fast wave (F) at a frequency of 115 MHz and incoming and outgoing Bernstein (B) wave, which is a backward wave in a tokamak. The solid lines correspond to the real part of the wavenumber and the dashed lines correspond to the imaginary parts which indicate absorption or mode conversion.

The real and imaginary parts of the left hand polarization of the composite field solution are shown on Fig. 7.3-2. Note the peaking of this heating component on the high field side near resonance at $x = 0$. Finally, the local absorbed power and Poynting and kinetic flux for the incoming wave are shown in Figs. 7.3-3a and 7.3-3b. The electron absorption is a small part of the heating (7%) corresponding to the cross-hatched region with the majority of the 65% single pass total absorption done by the helium species. The production of ion tails should broaden this absorption curve and increase the single pass absorption values.

The previous case, which has a very low helium concentration of 2%, achieves good single pass absorption at lower startup temperatures. As the plasma heats up, the helium concentration can be raised to 35% although an absorption description at elevated temperatures $T_{eff} \approx 50$ keV at this high density is more complex. An alternative heating scenario uses second harmonic helium absorption at a frequency of 230 MHz. This would make the single pass absorption less sensitive to the helium concentration but would yield a lower single pass absorption and reactivity enhancement during startup.

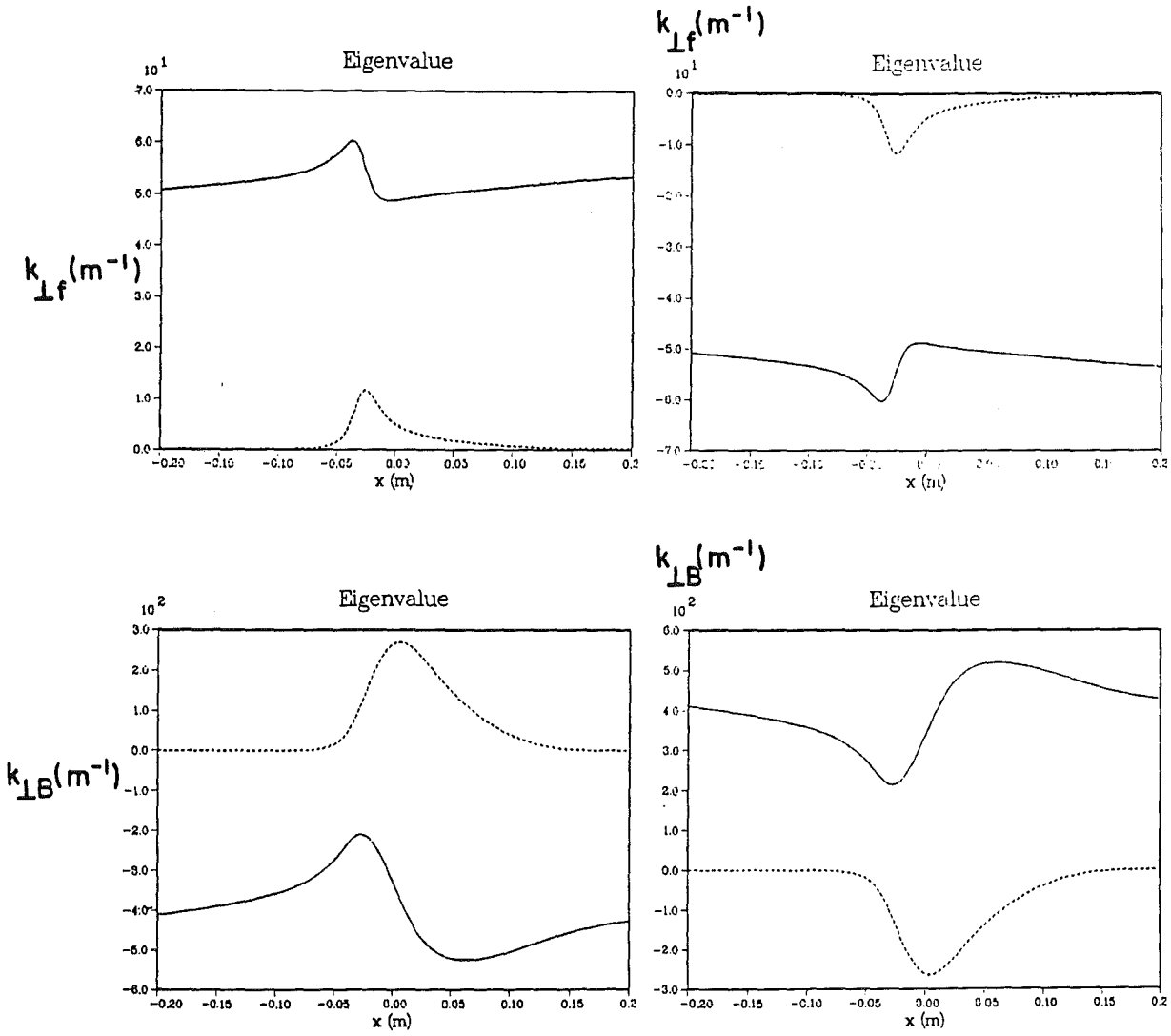

Fig. 7.3-1. Fast (F) and ion Bernstein wave (P) dispersion for fundamental ^3He heating in NET-EP.

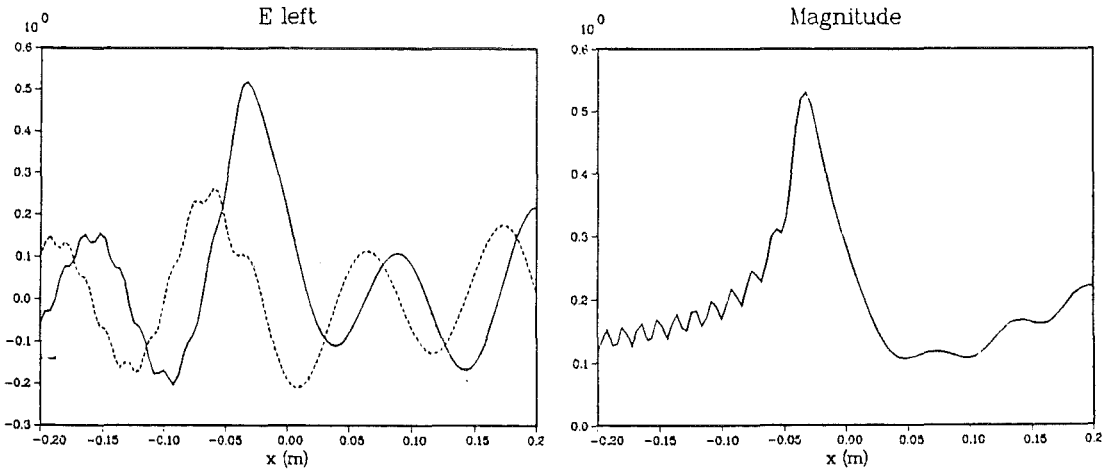

Fig. 7.3-2. Left hand wave polarization for NET-EP parameters.

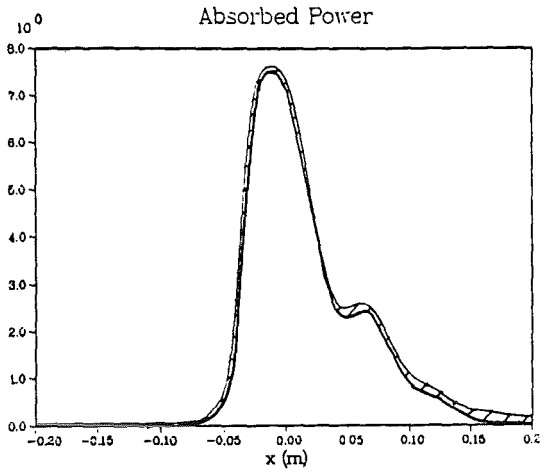

Fig. 7.3-3a. Helium and electron (hatched) fast wave absorption for NET-EP parameters.

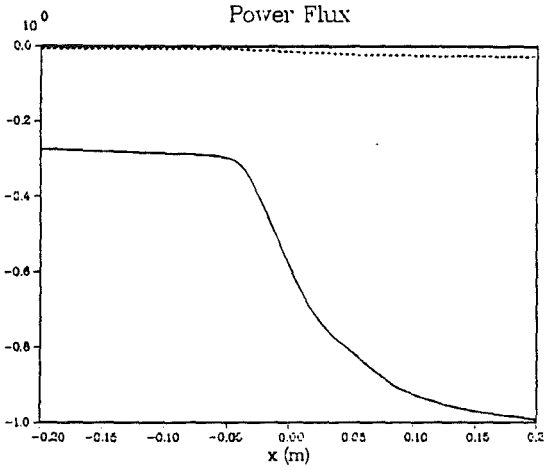

Fig. 7.3-3b. Poynting (solid) and kinetic flux for a fast wave incident from the right for NET-EP parameters.

Next we consider NET operated as a D-^{3}He machine at (NET A-3 case) higher concentrations of helium to increase the fusion power output. The magnetic field is 5.0 T at a major radius of 5 m with a core electron density of 1.4 x $10^{14}/cm^3$. At a frequency corresponding to the helium fundamental at the core, a helium temperature of 80 keV with a deuterium temperature of 40 keV and an electron temperature of 20 keV with a helium concentration of 14% and a $k_{\|}$= 8 m^{-1} yields 87% helium and 12% electron absorption in the 20 cm core region. At an ion temperature of 40 keV with 33% of the helium distribution having a tail temperature of 200 keV and all other parameters the same, 50% of the fast wave incident power goes to the bulk helium ions and 29% to the tails with 19% going to the electrons. This means that a radiofrequency generator set designed for fundamental minority helium absorption in a D-T plasma could provide reasonable absorption at these higher concentrations when the plasma temperature is increased. The results for fast wave absorption by species and the power flux for an 80 keV deuterium temperature tail of 4% concentration and with 11% bulk helium at 40 keV, a deuterium concentration for the remainder of the ions at a temperature of 40 keV and the electrons at 30 keV were studied next. The helium ion tails absorb 30% of the incident wave power, the bulk helium absorbs 47% and the electrons absorb 21% of the wave power at an incident $k_{\|}$ of 8 m^{-1}.

At still higher concentrations of helium, the fundamental absorption degrades but the second harmonic absorption on the helium-3 is quite efficient. At a helium concentration of 25% and 50% deuterium with 10 keV plasma temperatures and a $k_{\|}$= 8 m^{-1}, the helium second harmonic single pass absorption is 85% with a 7% electron absorption. At more elevated ion temperatures of 50 keV with 40 keV electrons and 25% helium concentrations, a parallel wavelength of $k_{\|}$= 4 m^{-1} yields 75% absorption by the helium and 25% by the electrons in the 20 cm core. Table 7.3-1 summarizes the cases that were studied for NET ICRF absorption.

The following statements can be made about the fundamental and second harmonic full wave absorption studies and the use of ICRF generators and antennas designed for D-T heating for use in D-^{3}He fusion reactors:

1. Fundamental $\omega = \omega_{CHe^3}(0)$ at low concentrations (n_{He3}/n_e = 2-4%) would work well during ohmic startup and one could use the same RF generators and antennas as the D-T (He^3) ICRF heating scenario.

Table 7.3-1
Summary of NET D-He^3 ICRF Absorption Cases

MACHINE CASE 1: B_o = 5.6 T, R = 4.6 m, $n_{eo} = 1.76x10^{14}/cm^3$

$\omega/\omega_{CHe3(o)}$	T_{He3} (tails) (keV)	T_D	T_e	n_{He3}/n_e (tails) %	k_z (m^{-1})	$\Sigma_l P_a$ (%)	P_{He} (tails)	P_D	P_e
Startup 1	4	4	4	2	6	72	64	0	8
2	8	8	8	25	6	89	88	0	1

MACHINE CASE 2: B_o = 5.0 T, R = 5.0 m, $n_{eo} = 1.4x10^{14}/cm^3$

$\omega/\omega_{CHe3(o)}$	T_{He3} (tails) (keV)	T_D	T_e	n_{He3}/n_e (tails) %	k_z (m^{-1})	$\Sigma_l P_a$ (%)	P_{He} (tails)	P_D	P_e
1	50	25	25	25	4	34	5	0	29
1	40 (80)	40	30	11 (4)	8	98	47 (30)	0	21
1	40 (200)	40	30	11 (4)	8	99	50 (29)	0	19
1	40 (200)	40	20	11 (4)	4	96	13 (38)	0	48
1	80	40	20	14	8	99	87	0	12
1	80	40	20	14	16	85	72	4	8
2	50	25	25	25	4	100	87	0	12
2	10	10	10	25	4	92	92	0	0
2	10	10	10	25	8	91	85	0	7
2	10	10	10	25	14	87	74	0	13
2	50	50	40	25	4	100	75	0	25

2. Fundamental $\omega = \omega_{CHe^3}(0)$ heating at higher He^3 concentrations (n_{He3}/n_e = 15%) near NET case A-3 operating conditions would also work well but the heating zone is shifted 30 cm off axis to the high field side for the same operating frequency as the D-T (He^3) scenario.
3. Fundamental $\omega = \omega_{CHe^3}(0)$ at n_{He3}/n_e = 25% does not appear attractive due to weaker single pass absorption and weak helium-3 heating relative to electrons. This is because the high helium-3 concentration shields the desirable wave polarization and a large circulating power in the machine would result in dominant electron heating.
4. If higher concentrations of n_{He3}/n_e = 25% are desired for NET A-3 operating conditions, second harmonic $\omega = 2\omega_{CHe^3}(0)$ heating on axis is quite attractive with dominant helium absorption in a single wave pass. This would, however, require both RF generator and antenna modifications from the D-T (He^3) fundamental minority heating scenario.

7.4 Estimates of Core Fusion Reactivity and Fusion Q from ICRF Produced ^{3}He Tails

In this section we make estimates of the core fusion reactivity and Q produced by making non-Maxwellian tails in a D-^{3}He NET. Earlier studies[1,2] for D-T machines have shown that fusion Q = fusion power per unit volume/ICRF power per unit volume needed to sustain plasma heating and ion tails > 1 can be obtained. In this work we use a formalism developed by Stix[8] which assumes a minority isotropic tail temperature T_{eff} heated at its fundamental ion cyclotron frequency with a Maxwellian background majority ion and electron distribution at a lower temperature. Both ion and electron background drag processes on the minority tail distribution are taken into account. The power balance calculation yields [Stix - Ref. 8, Eq. (34)]

$$\frac{1}{kT_{eff}} = \frac{1}{kT_e(1+\xi)}\left[1 + \frac{R_j(T_e - T_j + \xi T_e)}{T_j(1 + R_j + \xi)}\,\frac{1}{(1 + (\frac{E}{E_j})^{3/2}}\right]$$

where $kT_{eff} = -\left[\frac{d(\ln f)}{dE}\right]^{-1}$, $\xi = \frac{P_{RF}}{P_{t\to e}}$, $R_j = \sum_j \frac{n_j Z_j^2 l_j}{n_e l_e}$,

$$l_j = \left(\frac{m_j}{2\kappa T_j}\right)^{+1/2} \text{ and } E_j(\xi) = T_j \left|\frac{1 + R_j + \xi}{(0.75)(1+\xi)}\right|^{2/3}$$

where P_{t+e} represents the electron drag on the ion tail particles.

We take the NET A-3 case where $T_j = T_e$ for the background, $n_e = 1.4 \times 10^{20}/cm^3$ and the $D/^3He$ is in a 0.65/0.35 ratio with a 7% ion ash dilution. The power balance relation then becomes

$$\frac{T_{eff}}{T_e} = \frac{1 + \xi}{1 + \left(\frac{R_j \xi}{1 + R_j + \xi}\right) \frac{1}{\left|1 + \left(\frac{E}{E_j}\right)^{3/2}\right|}}$$

where $E_j = 60\left(\frac{98 + \xi}{1 + \xi}\right)^{2/3}$.

We solve this for different values of T_{eff} vs. ξ, the ratio of ICRF power density applied to sustain the tails to the power density of electron drag on the tail ions. We chose E = 500 keV corresponding to the peak in the $D-^3He$ reactivity. The solution depends critically on the slope in the tail distribution at the test particle energy. Solutions range from $\xi = 145$ at $E = T_{eff} = 500$ keV to $\xi = 10$ at $T_{eff} = 120$ keV. The lower limit is obtained by noting recent work by Anderson et al.[9] who examine analytic methods and compare them with computational results for ICRF tail production. They find that the T_{eff} at higher energies comparable to what we examine can be as small as 1/5 of the test particle energy.

The tail fusion power production in the core using $\langle\sigma v\rangle = 3 \times 10^{-22}$ m^3/s and $Q_F = 18.3$ MeV corresponds to

$$\Delta P_F = n_D n_{tHe} \langle\sigma v\rangle Q_F = 0.22 \text{ watts/cm}^3 .$$

Thus the core tail fusion Q for our case lies in the range of 0.06 - 0.5. These are to be taken as estimates. However, note that tail production at these densities requires power levels of the order of several watts/cm^3. Note that Q from the tails might reach several tenths in the core region but that it would have a minor effect on the overall Q of the machine. It is undesirable to produce tails at this high temperature in a D-^{3}He reactor plasma. However, at moderate power levels, the use of ICRF heating to produce desirable NET operating conditions at the fundamental or second harmonic does appear attractive.

References for Chapter 7

1. J. Scharer, J. Jacquinot, P. Lallia and F. Sand, "Fokker-Planck Calculations for JET ICRF Heating Scenarios," Nuclear Fusion 25, 435 (1985).

2. Harvey, Kerbel, McCoy, and Chiu, "ICRF Fusion Reactivity Enhancement in Tokamaks," Nuclear Fusion 26, 43 (1986).

3. JET Team, "RF Heating on JET," International Conference on Plasma Physics and Controlled Fusion Research, IAEA-CN-47/F-I-1 (1986) Kyoto, Japan.

4. J. Hosea et al., 12th European Conference on Controlled Fusion and Plasma Physics, 9F Part II, 120 (1985) Budapest, Hungary.

5. G. Sadler, O. Jarvis, P. Belle, N. Hawkes and B. Syrne, "Observation of Fusion Reaction γ-Rays in JET," Proc. of European Conference on Plasma Physics and Controlled Fusion, 1232 (1987) Madrid.

6. Hellsten, part of invited paper presented by J. Jacquinot, "Results of RF Heating on JET and Future Prospects," Seventh APS Topical Conference on Applications of Radiofrequency Power to Plasmas, Kissemmee, FL (May 1987) to be published.

7. B. McVey, R. Sund and J. Scharer, "Local Power Conservation for Linear Wave Propagation in an Inhomogeneous Plasma," Phys. Review Letters July 29, 507 (1985).

8. T. Stix, "Fast Wave Heating of a Two-Component Plasma," Nuclear Fusion 15, 737 (1975).

9. D. Anderson, L.-G. Eriksson and M. Lisak, "Analytical Models for Predicting the Ion Velocity Distributions in JET in the Presence of ICRF Heating," CTH-IEFT/PP-1986-16, Institute for Electromagnetic Field Theory and Plasma Physics, Chalmers University of Technology, Gothenburg, Sweden.

8. OTHER RELATED ISSUES

8.1 MHD Equilibrium and the Poloidal Field Coil System

This study shows the feasibility of using the R = 5.18 m NET-DT poloidal field (PF) coil system to position and shape the D^3He plasma of case A-3. The PF coil system developed for the NET design consists of 4 coil groups, labeled P1 through P4. The OH central solenoid is split into 3 sections: P1B, P1C, and P1D. There is a total of 12 coils symmetric about the horizontal midplane. The PF coil configuration is shown in Fig. 8.1-1 and the coil locations are listed in Table 8.1-1. All coils are superconducting and are positioned external to the TF coils for maintenance and machine access considerations.

The purpose of this analysis is to determine, for given PF coil positions, the PF coil currents that are consistent with MHD equilibrium and satisfy the plasma shape and volt-second requirements for case A-3 of NET-D^3He. We used the tokamak MHD equilibrium code NEQ developed by Strickler[1] to define the PF coil currents. A complete PF coil current scenario over the startup and burn cycle of the plasma cannot be done due to the limited time of this study. Instead, the PF coil currents required for MHD equilibrium at the end of the burn cycle will be calculated using the plasma parameters given in Chapter 3.

The MHD equilibrium code requires an initial guess for the PF coil currents. The code provides the option of fixing the currents in some of the coils to the input values and solves for the other coil currents that satisfy the desired properties. It usually takes several equilibrium calculations to converge to a solution that satisfies prescribed plasma parameters such as major radius, minor radius, elongation, triangularity, volume average beta, field on axis, and plasma current. The last two parameters remain fixed during iteration and the code generates a set of optimal plasma parameters consistent with the MHD equilibrium. During iterations, the maximum field at the PF coils is constrained to 8 T.

The first set of calculations used the NEQ code to reproduce the NET-DT reference case (as represented by the 1985 NET report) with plasma major radius R = 5.18 m, minor radius a = 1.35 m, field on axis B = 5.6 T, and plasma current I_p = 10.8 MA. The first column of Table 8.1-2 lists representative parameters of the NET-DT reference case. The second column represents results from the equilibrium analysis in which the P1D coil current was fixed at -25 MA (opposite to the plasma current). Differences noted are in the P1C and P3 current directions. The equilibrium parameters differ slightly from the reference parameters.

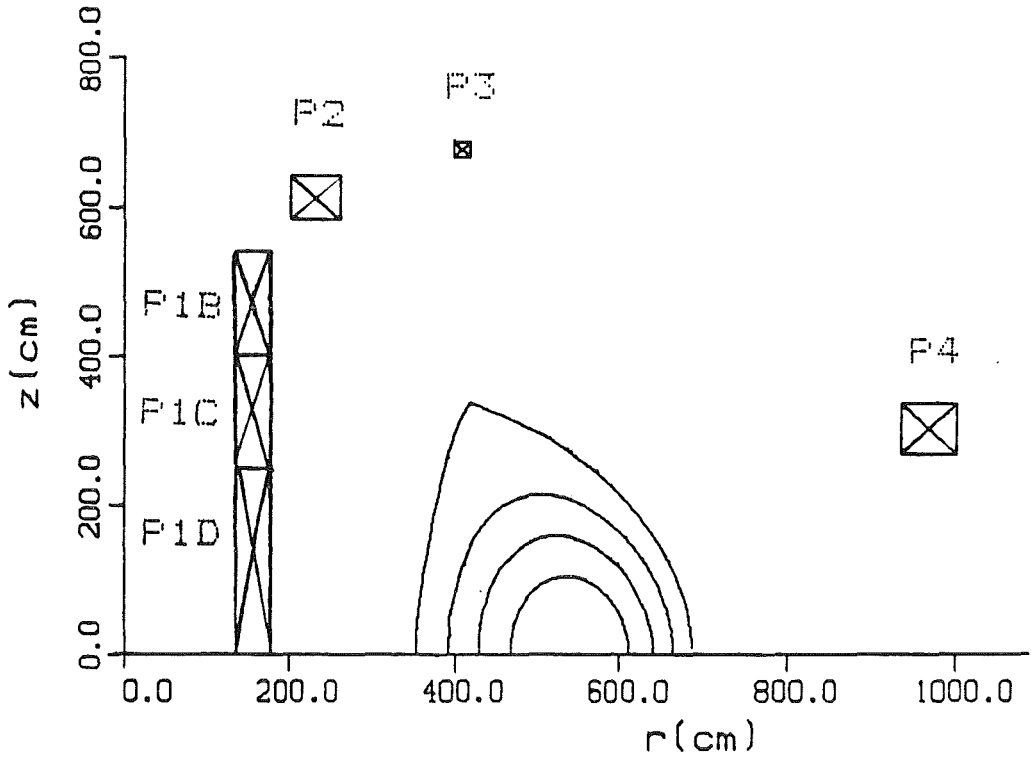

Fig. 8.1-1. PF coil configuration.

Table 8.1-1. NET PF Coil Locations

Coil	r*(m)	Z*(m)
P1D	1.55	± 1.25
P1C	1.55	± 3.25
P1B	1.55	± 4.75
P2	2.275	± 6.12
P3	4.05	± 6.75
P4	9.65	± 3.0

*at coil center

Table 8.1-2. Plasma Parameters and End-of-Burn

PF Coil Currents for NET-DT

	Physics Parameters	Equilibrium Parameters
R (m)	5.18	5.25
a (m)	1.35	1.4
Elongation	2.18	2.0
Triangularity	0.65	0.69
$\langle\beta\rangle$ (%)	5.6	5.5
B_{axis} (T)	5.0	5.0
I_p (MA)	10.8	10.8
Plasma Self-Inductance (10^{-6}H)	10	11.9
Plasma Magnetic Flux (volt$_+$s)	108	128
PF Volt-Seconds		104
PF Coil Currents:		
P1D (MA)	-25	-25
P1C (MA)	2	-2
P1B (MA)	10.4	11
P2 (MA)	5	5
P3 (MA)	-1.4	2.6
P4 (MA)	-6.5	-7.3

The results of case A-3 are given in Table 8.1-3. In this case, the plasma current was required to be 16.2 MA. The operating parameters, listed in the first column of Table 8.1-3, were specified in the input to the MHD code and the P1D coil current was fixed at -25 MA. An examination of the results indicates that the equilibrium parameters match the physics parameters to a good extent. Figures 8.1-2 - 8.1-4 show the equilibrium flux surfaces, plasma profiles, and PF coil configuration for this case. It should be pointed out that the PF coil currents are well within the range of values shown in Fig. III.4-12 of the 1985 NET report (for the time-dependence of the currents during the burn cycle of the NET-DT reference case) with the exception being an increase in the P4 coil current of about 37%.

The volt-seconds provided by the PF coils are computed to determine if the PF coil system satisfies the plasma flux requirements. The output of the equilibrium code indicates that the PF coils contribute only 77% of the plasma volt-seconds. The main contribution (57%) is provided by the P4 coil due to the strong mutual coupling between it and the plasma. The central OH solenoid P1D provides 25% of the volt-seconds. The remainder of the volt-seconds could be provided by an OH solenoid swing. This is practically feasible by starting the central solenoid P1D at the initiation of burn with the same current but in the reverse direction (+ 25 MA) and ramping it down to -25 MA.

To conclude, the present design of the NET-DT PF coil system is able to control the plasma of NET-D^{3}He with minor modifications to the coil currents. The volt-seconds provided by the PF system satisfy the plasma flux requirements with some OH solenoid swing.

Reference for Section 8.1

1. D.J. Strickler et al., "Equilibrium Modeling of the TFCX Poloidal Field Coil System," ORNL/FEDC-83/10, Oak Ridge National Laboratory, April 1984.

Table 8.1-3. Plasma Parameters and End-of-Burn PF Coil Currents for Case A-3 of NET-D^3He

	Physics Parameters	Equilibrium Parameters
R (m)	5.14	5.17
a (m)	1.69	1.67
Elongation	2.17	2.01
Triangularity		0.65
$\langle\beta\rangle$ (%)	6.7	6.73
B_{axis} (T)	5.01	5.01
I_p (MA)	16.2	16.2
Plasma Self-Inductance (10^{-6}H)		10.4
Plasma Magnetic Flux (Wb)		168
PF Volt-Seconds		130
PF Coil Currents:		
P1D (MA)		-25
P1C (MA)		-8
P1B (MA)		8.4
P2 (MA)		5
P3 (MA)		1.6
P4 (MA)		-8.9

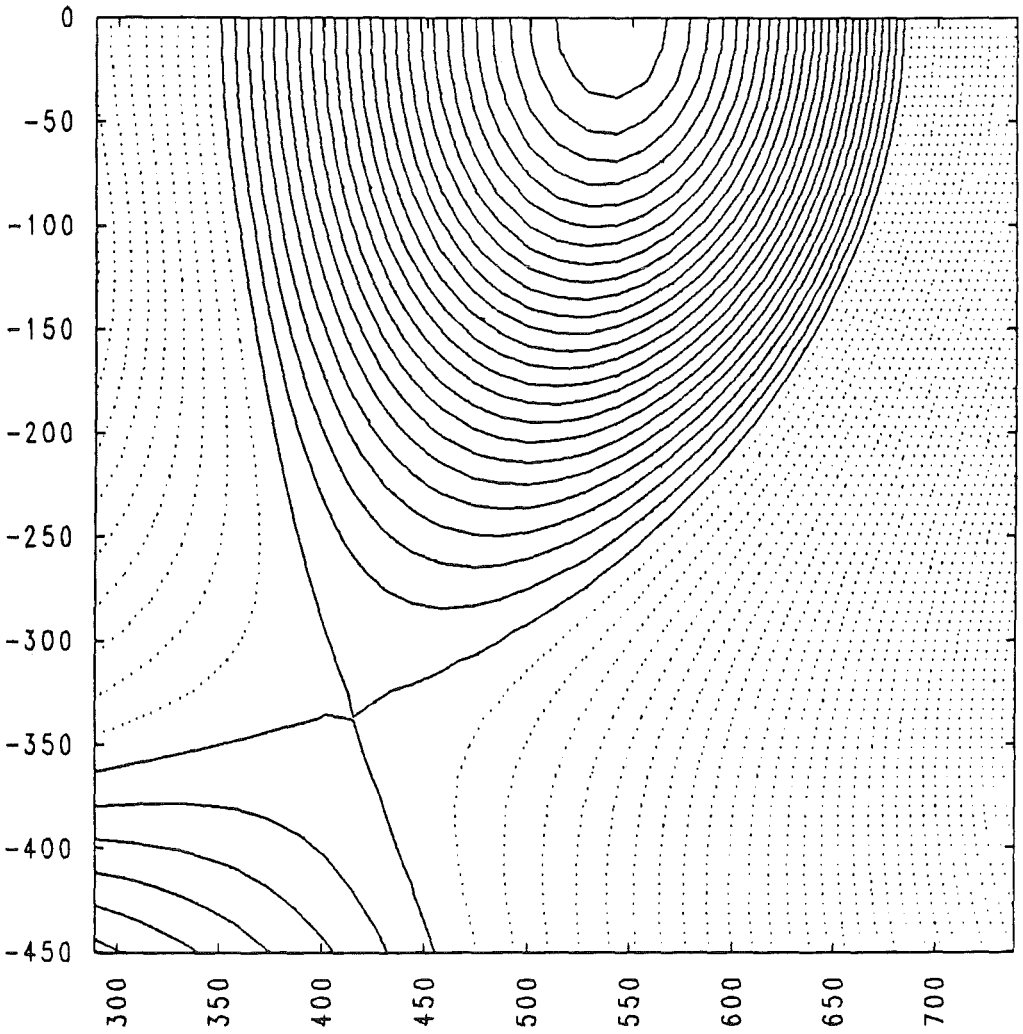

Fig. 8.1-2. Equilibrium flux surfaces for case A-3.

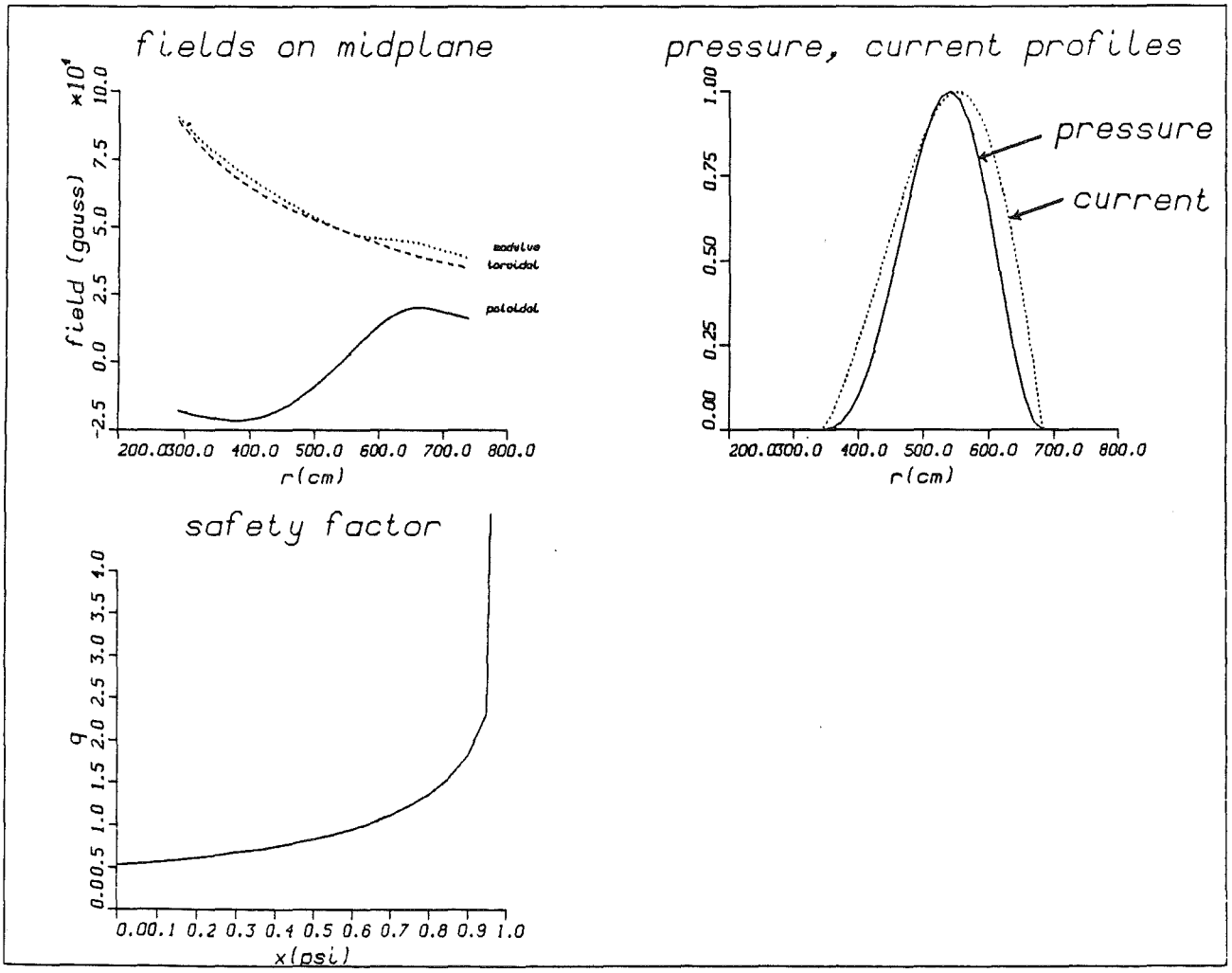

Fig. 8.1-3. Plasma profiles for case A-3.

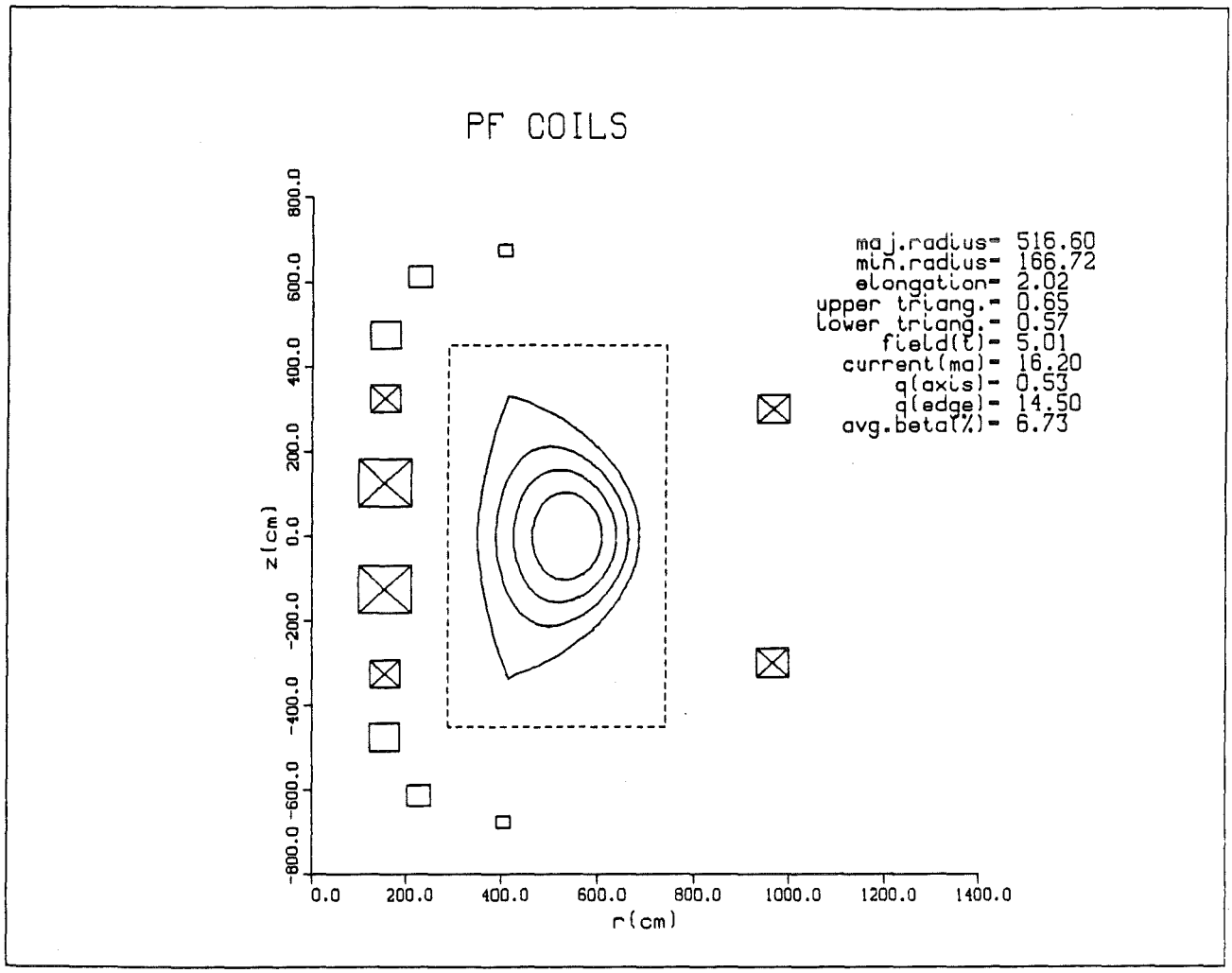

Figure 8.1-4. PF coil system for case A-3.

8.2 Heat Loads on the First Wall and Divertor

8.2.1 Heat Load on the First Wall

In this section we consider the heat load on the first wall in NET with D-^{3}He operation. The heat load on the first wall is composed primarily of three parts. First, there is the load from synchrotron and bremsstrahlung radiation emitted by the plasma. Next, there will be a neutral particle flux incident on the first wall. Finally, there will be energetic ions striking the wall because of finite orbit effects and trapping in the magnetic field ripple. This latter loss is discussed in Chapter 5.

Bremsstrahlung is radiation emitted during Coulomb collisions of the electrons with ions; the photons emitted have a broad energy spectrum extending up to about 2 or 3 times the mean electron energy. For a D-^{3}He plasma the electron temperature is generally about 30 - 60 keV in the center of the discharge, so one can expect the spectrum to extend up to about 200 keV. The photons don't penetrate far into the walls so this appears primarily as a surface heat load. There will be a poloidal variation of the heat load with a profile similar to the poloidal variation of the neutron wall loading (see Chapter 4) since, for both forms of radiation, the plasma acts like a volume emitter.

Synchrotron radiation is microwave radiation emitted at harmonics of the electron cyclotron frequency. Because of relativistic and doppler broadening and the variation of the magnetic field strength in the plasma, the frequency spectrum becomes smeared out. The poloidal variation is a little harder to deduce since the plasma is optically thick for synchrotron radiation. Consequently, one expects the escaping photons to have come from near the surface of the plasma. Due to the variation of the magnetic field strength, one might expect the radiation to be stronger on the inboard side where B is higher, since the radiation is proportional to $B^{2.5}$.

For D-^{3}He operation in NET, the average surface heat load due to radiation is not large. For NET-DT and NET-EP the average heat load is about 5 W/cm^2. The Q = 2.5 - 3 cases have an average surface heat load of about 15 W/cm^2, and the ignition cases have an average surface heat load of 30-50 W/cm^2, depending on the plasma elongation. These values are shown in Table 3.4-1 and Table 8.2-1.

If we assume the bremsstrahlung radiation has the same poloidal variation as the neutron wall loading and the synchrotron radiation varies poloidally as $B^{2.5}$, where B is the magnetic field strength at the edge of the plasma, then the inboard and outboard peaks in the first wall heat flux can be estimated. The results are shown in Table 8.2-1. For the neutron wall load variation, the profile shown in Fig. 4.2-3 was used for cases

Table 8.2-1. First Wall Heat Flux

	CASE							
	A-1	A-2	A-3	B-1	B-2	C-1	D-1	D-2
Major Radius, m	5.18	5.41	5.14	4.61	4.61	5.41	4.61	4.61
Minor Radius, m	1.35	1.69	1.69	1.69	1.69	1.69	1.69	1.69
Plasma Area, m^2	362	475	450	405	405	475	472	431
Synchrotron Power, MW	9.1	16	17	37	29	47	54	90
Bremsstrahlung, MW	7.3	12	29	22	56	24	92	124
Neutron Wall Load Peaking								
Inboard	1.1	1.1	1.5	1.7	1.7	1.7	1.7	1.7
Outboard	1.5	1.5	1.4	1.3	1.3	1.3	1.3	1.3
Heat Flux								
Average, W/cm^2	4.5	5.9	10	15	21	15	31	50
Peak Inboard, W/cm^2	7.6	11	20	38	46	34	69	114
Peak Outboard, W/cm^2	4.4	5.5	11	11	21	12	31	47

A-1 and A-2; the profile shown in Fig. 4.2-4 was used for cases B through D. The neutron wall load profile for case A-3 is shown in Fig. 4.3-1. We see that the peak heat flux occurs on the inboard side and is less than 20 W/cm^2 for cases A-1, A-2, and A-3. The present NET-DT design value for the total peak heat flux on the first wall is 40 W/cm^2 and is set by the stainless steel-graphite design concept. We see that the A cases leave an allowance of at least 20 W/cm^2 and cases B-1 and C-1 are acceptable by this criteria. Cases B-2, D-1, and D-2 exceed this criteria and would require a different design concept. The peak heat flux on the outboard side is considerably less than 40 W/cm^2, except for case D-2. These estimates for the peak heat flux are conservative since synchrotron radiation transport in the vacuum chamber will reduce somewhat the peaking from that used in this analysis. Furthermore, the heat flux here has been calculated using the plasma surface area, and not the true wall area, since the location of the wall is not determined in all cases.

The above estimates do not include fast ion losses, which is a poorly determined loss and depends sensitively on the magnetic field ripple. The fast ion loss is expected to impinge on the wall on the outboard side, where the heat flux is much less than that on the inboard side. Furthermore, the fast ion heat flux is sensitive to the location and shape of the first wall on the outboard side. One can use Table 8.2-1 as an indication of what fast ion heat flux can be tolerated within a given design concept.

The neutral particle flux emitted from a D-^{3}He plasma has not been analyzed in detail, but some conclusions based on atomic processes and cross-sections can be made. The charge exchange processes leading to escaping neutral atoms are present in a D-^{3}He plasma, but will be reduced in magnitude in comparison to a D-T plasma since helium does not charge exchange well with hydrogen isotopes. Helium can undergo resonant charge exchange with itself, but the cross-sections are smaller since a two-electron transfer is required to produce a neutral helium atom. It is difficult to be quantitative about the expected power loss due to charge exchange but the problem should be less severe than it is in a D-T plasma. Generally, the overall power loss due to charge exchange is small, but localized peaking near the divertor where the recycling occurs can be a problem as in D-T plasmas.

8.2.2 Heat Load on the Divertor

An upper limit to the heat load to the divertor is the total fusion power plus the injected power minus the power carried to the first wall by synchrotron and

bremsstrahlung radiation. For the NET-DT and NET-EP cases with D-^{3}He, this power is about 55-60 MW. For the Q = 2.5 - 3 cases, this power is about 75 MW, and for ignition it is about 95 - 100 MW. This number should be compared to the alpha heating power of 120 MW in NET using D-T. Consequently, one can expect the power to the divertor with D-^{3}He to be less than, or comparable to, that with D-T. The NET-DT divertor is designed for 80 MW (135 MW in NET-EP) using the assumption that the remaining 40 MW (65 MW in NET-EP) is radiated from the scrape-off layer plasma and is distributed over a larger area than the target plates. Plasma transport and recycling in the scrape-off layer and divertor has not been analyzed with D-^{3}He operation, but there is no reason to expect that the plasma scrape-off layer will be thinner with D-^{3}He than it is with D-T. Consequently, the power density on the divertor target plates will be similar to, or less than, that already designed for in the D-T version of NET. (Note: values in Table 3.3-2 are maximum heat fluxes to the divertor with no allowances for charge exchange or radiation losses.)

8.3 He-3 Vacuum Pumping

The December 1985 NET status report lists the α-generation rate as 2.4×10^{20} particles/s and assumes a 5% ratio of He to DT atoms incident on the divertor target. The combined form of DT molecules will amount to a flux of 2.4×10^{21} particles/s. Using room temperature (300 K) we obtain a throughput of 7.4 torr ℓ/s for He and 74 torr ℓ/s of DT. The effective pumping speed at the torus of 2.5×10^5 ℓ/s is used overall for He and DT. Using these values, the equilibrium pressure at the divertor throat will be

$$P_{eq.\ He} = 3 \times 10^{-5} \text{ torr}$$

$$P_{eq.\ DT} = 3 \times 10^{-4} \text{ torr} .$$

Depending on the He behavior in the divertor, the throughput could be higher but this is an uncertainty at the present.

For D-^{3}He operation, the vacuum pumping throughput of helium is determined by its fuelling rate. As discussed in Chapter 6, the fusion power density is very low at the edge of the plasma; 95% of the fusion power is produced at radii less than 60% of the minor radius of the plasma. Consequently, fuelling the outer 40% of the plasma with helium is unnecessary. The total amount of helium injected to maintain the required

helium concentration in the plasma center depends on the fuelling mechanism adopted. If the helium is fuelled by neutron beam injection, then the injection rate of helium is 2×10^{20} particles/s for case A-3. If plasma injection is used for refuelling, then the helium injection rate could rise to about 4×10^{20} particles/s assuming that the entire plasma (not including edge recycling) was fuelled from the same plasma stream with a 35% helium concentration. The lower value is the same as the helium generation rate in NET-DT and consequently both systems have the same helium throughput and the equilibrium partial pressure of helium at the divertor throat would be 3×10^{-5} torr. The higher value would mean that the helium throughput would increase by a factor of 2 over that in NET-DT. With no change in the vacuum system, the helium partial pressure would be 6×10^{-5} torr in this case.

The required deuterium refuelling rate, and vacuum pumping rate, is difficult to establish since it depends sensitively on the transport processes in the center of the plasma and the recycling processes at the plasma edge. The plasma density in NET with D-^{3}He operation is a factor of 3 or so less than that in NET with DT operation because of the higher operating temperature with D-^{3}He. Consequently, it is reasonable to conclude that the required fuelling and vacuum pumping rates will also be a factor of about three lower. As a result the NET-DT vacuum system, if it is able to handle the gas throughput with D-T operation, should also be able to handle it with D-^{3}He operation.

From this brief analysis it would appear that He pumping for D-^{3}He operation in NET is possible using the effective pumping speed intended for DT operation and will result in equilibrium pressures comparable or lower than for DT operation. If the recycling at the divertor as assumed for DT operation in NET is too optimistic, then the He equilibrium pressure would be higher for both D-^{3}He as well as DT operation.

9. SUMMARY AND CONCLUSIONS

A preliminary study of the feasibility of achieving significant energy multiplication, Q, with D-^{3}He fuel in NET, and variations of it, has been performed. The starting point for this study is the reference NET design for D-T operation,[1] referred to here as NET-DT, and an enhanced plasma case,[2] NET-EP, also developed by the NET team for D-T operation.

A physics model based on a power balance of the plasma, with consideration of MHD equilibrium and stability, fusion product charged particle heating, fast ion pressure, bremsstrahlung and synchrotron radiation losses, and energy transport across the magnetic field has been developed and used for a parametric study of the energy multiplication and ignition margin expected with D-^{3}He operation. Neutronics calculations have been performed for the present NET-DT stainless steel shield and to estimate the thinnest possible shield for the neutron spectrum expected with D-^{3}He fuel; the reduced shield thickness allows a much better utilization of the magnetic field generated by the toroidal field magnets. Shield thicknesses of about 25-30 cm, depending on the neutron power level, are feasible.

Using the above physics model and neutronics results, a parametric study of D-^{3}He operation in NET-DT, NET-EP, and possible modifications to NET-EP to improve the energy multiplication and/or achieve ignition has been performed. From this parametric survey the following general conclusions may be drawn.

Breakeven (Q = 1) may be obtained in the present NET-DT design if ASDEX H-mode scaling is applicable. In addition, the required injection power is less than that planned for startup in NET-DT. If Kaye-Goldston scaling continues to plague tokamaks, then the Q-values obtained are much lower (Q = .4) and the injection power is much higher (P_{inj} = 120 MW). The enhanced plasma size NET case (NET-EP) can achieve a Q-value of about 1.4 using ASDEX H-mode scaling with no changes in the machine parameters except for the fuel and the operating temperature.

The Q-value can be increased in many ways in NET because of the low neutron production with D-^{3}He fuel. Reduction of the major plasma radius to 4.61 m increases the Q-value to about 3. This improvement in Q is due to the increase in magnetic field at the plasma and to the reduced aspect ratio which leads to higher plasma current, energy confinement times, and beta. The reduction in major radius can be achieved by removing the inboard blanket designed for DT operation and using a much thinner shield designed for the low DD and DT neutron exposure.

An alternative approach is to increase the magnetic field at the toroidal field magnets without changing the plasma dimensions from the NET-EP case. Q values of about 2.5 - 3 can be obtained by a 20% increase in the magnetic field strength at the TF coil.

Ignition with D-^{3}He in NET may be obtained if the plasma major radius is reduced in conjunction with an increase in the toroidal field and in the plasma elongation. The required elongation for ignition is about 2.4 at B_c = 13 T and 2.7 at B_c = 10.5 T. (B_c is the toroidal field at the TF magnet.) Present understanding of MHD limits on elongation restrict the elongation to about 2.2. In addition, a 13 T toroidal field magnet is infeasible for NET within the context of the present design guidelines.

The above predictions are obtained using the ASDEX H-mode scaling law. Break-even in NET is possible with the Kaye-Goldston scaling law for an H-mode factor of about 2.5, but the required injection power is about 120 MW. This assumes the major radius of the plasma has been reduced to 4.61 m and the toroidal field at the magnet remains at the NET value of 10.4 T.

We have considered in more detail a minor revision to NET-EP. By removing the breeding blanket, but retaining the NET stainless steel shield, the major radius of the plasma can be decreased from 5.41 m to 5.14 m. The NET shield alone gives sufficient neutron attenuation for D-^{3}He operation such that the TF magnet is more than adequately protected. This configuration, referred to as case A-3, has been used for a more detailed study of issues related to D-^{3}He operation.

Using ASDEX H-mode confinement scaling, this case has a Q value of 1.6 if impurities are neglected. With a 1% oxygen impurity concentration and ash accumulation calculated assuming the particle confinement time in the center is four times longer than the energy confinement time, the Q value decreases to about 1.2.

Because of the reduced major radius of case A-3, the plasma current is increased to 16 MA. However, the coupling of plasma to the OH system is improved and there is no significant increase in the volt-s of the OH system required to establish the plasma current. Furthermore, the currents in the poloidal field coils required for MHD equilibrium of the plasma are not significantly increased.

The feasibility of heating a D-^{3}He plasma using ICRF has been investigated for NET-EP and case A-3. At low helium concentrations (n_{He}/n_e = 2-4%) the single pass RF absorption on the helium at the fundamental ion cyclotron frequency is good. This means that the same RF system needed for a D-T plasma with either second harmonic tritium

heating or fundamental minority ^{3}He heating would also work in the D-^{3}He plasma at low ^{3}He concentrations. ICRF heating at the fundamental frequency at higher helium concentrations (n_{He}/n_e = 25%) is not attractive for good single pass absorption on the helium. Second harmonic ICRF heating on the helium does give good single pass absorption, however, at these concentrations. The electron absorption is low, which is good, since it is desirable to keep the electron temperature low. Second harmonic heating on the helium would require a change in the RF generator and the antennas from those for a D-T system to accommodate the higher RF frequency.

ICRF heating produces an enhanced "tail" in the helium distribution function. This tail, if it is strong enough, gives a higher fusion power since there are more particles with energies in the range where the D-^{3}He fusion cross-section is largest. Estimates of the magnitude of this effect for case A-3 indicate that the fusion power density in the inner core ($r < 10 - 20$ cm) may be increased by roughly 30% over that obtained using Maxwellian distribution functions. The overall increase in Q due to the hot ion tails is small, although the local increase in fusion power density may be useful in investigating the physics of a burning plasma.

The loss of fast fusion-produced ions from the plasma is a concern because of the impact on the plasma power balance and the resulting heat load on the portion of the first wall that these ions strike. There are two sources of this loss; one is the prompt loss, which occurs because an ion is born with an orbit which intercepts the wall. The second is the loss that occurs during the slowing down phase of the fast ions because of local magnetic trapping and detrapping, and stochastic effects, caused by the non-zero magnetic ripple in the toroidal field.

The prompt loss of fast fusion-produced protons from the plasma has been modeled using a computer code provided by L.M. Hively; this treats a circular plasma, rather than the actual D shape, but includes the finite width of the scrape-off layer. The calculation also uses the same density and temperature profiles used in Chapter 3 for the plasma power balance modelling. For case A-3 the outboard scrape-off layer is rather wide because of the 27 cm inward shift of the plasma. The prompt loss of fast protons, and the resulting heat flux on the outboard side is very small. Treating the loss due to magnetic ripple is more difficult and, unfortunately, there is major disagreement in the field concerning ripple losses in D-T plasmas. This makes it impossible to provide a definitive estimate of the ripple loss in a D-^{3}He plasma, although the prompt-loss results

imply that the ripple-loss heat load is probably also small. Clearly, further work in this area is required, but this is beyond the scope of this study.

Fuelling of a D-^{3}He plasma has been investigated for the Q $\simeq$ 1 cases. Pellet injection is difficult because of the high injection ablation rate associated with the high electron temperature. Pellet fabrication is more complicated if the pellets are to contain ^{3}He. We have presented a concept for making such pellets; this concept utilizes a polymeric shell containing liquid ^{3}He and overcoated with D_2. The helium content in the center of the plasma can be fuelled by neutral beam injection using a 10 MW 300 keV NBI system. Helium fuelling of the outer regions is not required since the fusion power density is strongly peaked in the center and little fusion power is produced in the outer regions. Fuelling of the deuterium in the center can also be done, but the required injection energy is also 300 keV, which requires the development of negative ion sources.

Fuelling by plasma injection, either using guns, such as the Marshall gun, or injection of compact toroid plasmas is a more speculative concept. Initial modelling of the slowing down of an injected plasma in a tokamak environment indicates that this method may be feasible. However, the experimental database for fuelling by plasma injection is almost nonexistent. Experimental investigations on the larger present tokamaks is necessary before one can have confidence in the theoretical models. Fueling by plasma injection has the advantage that it is not isotope dependent and the fuelling process appears to extrapolate to a power producing reactor.

The vacuum pumping requirements for case A-3 have been assessed. The gas throughput for helium is about the same in case A-3 as the helium generation rate (and therefore the helium pumping rate) in NET-DT. This is because the ^{3}He concentration is only 35% in the center of the discharge and the average plasma density is about a factor of three less than with D-T operation because of the higher operating temperature with D-^{3}He. In addition, the deuterium gas throughput, which is more difficult to determine because of the uncertainties of recycling at the edge and transport of fuel to the center, should be less than that in NET-DT since the plasma volume is essentially the same and the average ion density is lower. Consequently, the vacuum pumping system considered for NET-DT will be sufficient for D-^{3}He operation.

The D-^{3}He fuel cycle produces almost all its energy in the form of charged particles; this could potentially lead to larger surface heat loads than are experienced in D-T fusion where 80% of the fusion energy is in the form of neutrons which heat the blanket and shield volumetrically. It turns out that, because of the lower fusion power

density with D-^{3}He, the surface heat loads on the first wall due to bremsstrahlung and synchrotron radiation for the Q $\simeq$ 1-3 cases are similar to, or less than, those encountered in the D-T version of NET. Under ignition conditions, the peak first wall heat flux will be about 100 W/cm^2, which requires a different first wall design concept. The power density on the divertor neutralizer plates due to charged particle impact is also similar to that designed for in the D-T version of NET.

From these results we see that significant energy multiplication in a mildly revised form of NET can be obtained if nature is not too perverse. Significant energy multiplication means that the fusion reactions are as important as the external heating power in determining the power balance of the plasma. Consequently, important questions regarding burn physics and the effects of a significant number of fast fusion produced ions in the plasma can be studied with such a machine. In addition, the much reduced neutron production makes the environment more hospitable to performing physics experiments on burning plasmas than is the case with DT fuel.

References for Chapter 9

1. The NET team, "NET Status Report 1985", NET Report 51, Commission of the European Communities (1985).

2. F. Engelmann, "Concept and Parameters of NET", NET Report 64, EUR-FU/XII-80/86/64, Commission of the European Communities (1986).

ACKNOWLEDGMENTS

This research was supported by Kernforschungszentrum Karlsruhe (KfK), West Germany. The authors gratefully acknowledge helpful discussions with the NET team and valuable comments and suggestions made by W. Heeringa, K. Kleefeldt, W. Maurer, and R.A. Mueller of KfK.